Development of Targeted, Polymeric Delivery Vehicles for Camptothecin and siRNA via Boronic Acid-Diol Complexation

Thesis by

Han Han

In Partial Fulfillment of the Requirements

for the degree of

Doctor of Philosophy

California Institute of Technology

Pasadena, California

2013

(Defended December 7, 2012)

Acknowledgments

As a child, I have always wanted to know the reasons behind why and how things work. To this end, I have taken apart and broken many things, and wherever I went the path of destruction seemed to follow. I thank my parents for putting up with me during these years and for still always encouraging me to pursue and satisfy my curiosities. I am grateful that they have given me many siblings to grow up with, having a large family means that laughter and warmth are never in shortage.

I would like to thank all the professors from the University of Melbourne who have taught me and have helped in developing me scientifically including Professors Michelle Gee, George Franks, Sandra Kentish and Andrea O'Connor. I am greatly indebted to Professor Dave Dunstan for mentoring me during my first research project and for giving me the freedom to ask questions and seek answers. It was this research experience that led to my desire to pursue graduate studies. Special thanks to Professor Peter Scales who has made the lectures especially enjoyable and has helped in guiding me on my career path.

I would like to thank the staff at Caltech who has helped me throughout the years including Martha Hepworth, Kathy Bubash, Suresh Guptha and Steve Gould. To the professors who have taught me, including Professors John Brady, Zhen-Gang Wang, Bob Grubbs, Scott Virgil, Judith Campbell and Carl Parker – I thank you. I am indebted to Doctors David VanderVelde, Alasdair McDowall and Mona Shahgholi for training me on the usage of NMR, TEM, and mass spectroscopy, respectively, and for always being available when I needed assistance. I am grateful to Professor Jeremiah Johnson and Doctor Janek Szychowski for their invaluable discussions in organic synthesis. I would

like to thank Professors Dave Tirrell, Zhen-Gang Wang and Bob Grubbs for taking their time to be on my thesis committee.

I appreciate everyone in the Davis group who has helped me and has made my time more enjoyable. I am grateful to Chris Alabi for teaching me lab work and for answering my endless questions. I am thankful to Jonathan Choi for helping me in getting started in the lab and for being a great friend. I am glad to have worked with Fanny Eriksen and thankful for the continued friendship. A big thanks to Leonard Medrano for assisting me with lab work whenever needed. I am thankful to Yasho Bhawe for helping me both in and outside the lab, and for being a great friend. I am grateful to Devin Wiley and Aaron Gale for always being willing to assist me with lab work.

I would like to thank all the friends whom I have made while cycling. I am grateful for their patience in helping me in getting started in this sport and look back fondly on the adventures we have had.

All that I have learnt and achieved in the past few years would not have been possible without my advisor, Professor Mark Davis. The reason I chose to come to Caltech was to work with Mark. I am especially appreciative of all the flexibility he has given me, the interesting discussions we have had and for the guidance he has provided. Mark's mentoring style has helped me to grow and mature scientifically. I couldn't have asked for more.

Abstract

Our research lab has developed polymer-based nanoparticle delivery systems for the anticancer drug, camptothecin (CPT), CRLX101; and for the small interfering RNA (siRNA), CALAA-01. CRLX101 has shown great success in both animal studies and clinical trials. However, it is incapable of achieving targeted delivery. CALAA-01 has demonstrated effectiveness in a phase I clinical trial. However, it suffers from its rapid *in vivo* clearance. To address the issues of targeting in the anticancer drug delivery system and the short circulation time in the siRNA delivery system, we have created a new delivery platform involving the use of boronic acid-diol complexation. This thesis is divided into two parts to discuss CPT delivery and siRNA delivery separately.

In Part I, the targeted delivery of CPT via boronic acid-diol complexation is described. CPT was conjugated to a copolymer of mucic acid and PEG (MAP) and self-assembled into MAP-CPT nanoparticles. The targeting agent, Herceptin antibody was attached to boronic acid (BA), this was then complexed with the diol-containing MAP to form a targeted nanoparticle carrying ca. 60 CPT, with a 40 nm diameter and a slightly negative surface charge. The attachment of a single Herceptin per nanoparticle was sufficient to enhance cellular uptake of nanoparticles into BT-474, a HER2 overexpressing cell line by 70% compared to the non-targeted version. Nude mice bearing BT-474 xenograft tumors treated with targeted MAP-CPT nanoparticles resulted in all mice revealing complete tumor regression.

In Part II, the boronic acid-diol complexation delivery platform is applied for the delivery of siRNA. First, the CALAA-01 delivery system for siRNA was further characterized and optimized. Then, a copolymer of mucic acid and dimethylsuberimidate

(MAD) was synthesized and used in condensing the anionic siRNA into nanoparticles. Nanoparticles were stabilized by placing a surface PEG layer through boronic acid-diol complexation. Targeting was achieved by conjugating the distal end of the BA-PEG with a targeting agent, Herceptin antibody. MAD/siRNA nanoparticles effectively entered cells and demonstrated low cellular toxicity. MAD/siRNA nanoparticles stabilized with nitroPBA-PEG resulted in a diameter of 130 nm with a slightly negative surface charge. Pharmacokinetic studies in mice demonstrated improved circulation compared to CALAA-01.

Table of Contents

List of Schemes

List of Figures

List of Tables

Chapter 1

Introduction

Cancer is a leading cause of death worldwide. In the United States, one in two men and one in three women would develop cancer within their lifetimes. Recently, death due to cancer has surpassed heart diseases in Hispanic/Latino populations (*1, 2*). Current cancer treatments for solid tumors include surgical removal, radiation therapy and chemotherapy involving cytotoxic drugs. Chemotherapies are commonly administered especially in patients with metastasized cancers. However factors including rapid systemic clearance, multidrug resistance and nonspecific toxicity result in low efficacy and numerous side effects. To improve efficacy and minimize side effects, a delivery vehicle is desired to protect and transport the payload to the solid tumor site. One of the most promising approaches to achieve this is the targeted delivery of therapeutics via nanoscaled vehicles due to their ability to protect their payload and enhance its delivery to cancerous cells by passive and active targeting; and their ability to bypass multidrug resistance (*3, 4*).

Solid tumors are characterized by irregular and leaky vasculature with 200 nm to 600 nm pore sizes (*5, 6*) and impaired lymphatic drainage, these features result in the preferential accumulation of macromolecules in the tumor site in a process known as the enhanced permeability and retention (EPR) effect (*7*). To take advantage of this phenomenon and in the process achieve passive targeting, nanoparticles are designed to be between 10 and 100 nm in size. 10 nm is chosen as the lower size limit to avoid first pass kidney clearance (*8*), while 100 nm is set as the upper limit to minimize recognition and clearance by the mononuclear phagocyte system (MPS). Recently it has been shown that nanotherapeutics of ca. 100 nm are effective in highly permeable tumors such as Kaposi's sarcoma (*9*) but not in poorly permeable tumors due to limited penetration.

Nanoparticles smaller than 50 nm is necessary for tumor penetration in poorly permeable tumors such as human pancreatic adenocarcinoma BxPC-3 (*10*). To take full advantage of the EPR effect, nanoparticles should circulate for a long period of time to allow for accumulation at the tumor site. Therefore, in addition to size considerations, nanoparticles with slightly negative surface charges are desired to evade the electrostatic interactions with blood components and to reduce the clearance by the MPS (*11*). As well, polyethylene glycol (PEG), a biocompatible polymer is often used as a 'stealth' layer on the surface of nanoparticles to shield against self-self interactions that lead to aggregation and to shield against self-non-self interactions such as opsonin adsorption that result in removal by the MPS (*12, 13*).

Once the nanoparticles have reached the solid tumor site by the EPR effect, it is advantageous to actively target the nanoparticles to the cancerous cells for enhanced cellular uptake (*14, 15*). This can be achieved by functionalizing the surface of nanoparticles with ligands against over-expressed or specific receptors on tumor cell surfaces. Studies have shown that nanoparticles with and without targeting resulted in similar biodistribution and amount reaching tumor site (*14, 16, 17*). However, the same studies found that targeted nanoparticles show significant tumor reduction efficacy compared to their non-targeted counterparts. This suggests that the targeted delivery of nanoparticles enhances cellular internalization of nanoparticles via receptor mediated endocytosis rather than by increasing the accumulation of the nanoparticles at the tumor site.

In the past years, our research lab has developed polymer-based nanoparticle delivery systems for the anticancer drug, camptothecin (CPT), named CRLX101

(formerly IT-101); and for the small interfering RNA (siRNA), named CALAA-01. The basis of these systems involves the use of β-cyclodextrin-containing polymers (CDP). IT-101 is composed of CPT conjugated to CDP and is self-assembled into nanoparticles by hydrophobic interactions (*18, 19*). This drug delivery system has shown great success in both animal studies (*20, 21*) and clinical trials (*22*). However, it is incapable of achieving targeted delivery. We expect that with targeting, the efficacy of this type of delivery system would be enhanced. CALAA-01 is composed of anionic siRNA condensed by cationic CDP to form nanoparticles via electrostatic interactions (*23, 24*). This nanoparticle system is stabilized by the presence of a steric PEG layer on its surface. The attachment of PEG onto the nanoparticles is attained by the formation of inclusion complexes of adamantine (AD) with the cyclodextrins in the polymer via an adamantane PEG conjugate (AD-PEG). Targeting is achieved by attaching ligands, such as human transferrin protein on the AD-PEG conjugate to form AD-PEG-Transferrin. This siRNA delivery system has shown rapid clearance rate in *in vivo* imaging and in non-human primate plasma studies (*25, 26*). This is likely due to the weak non-covalent interactions between the AD-PEG and the β-cyclodextrin in the stabilization process. Nevertheless, this siRNA therapy route has recently been shown to be effective in human during a phase I clinical trial (*24*). Thus with a more stable and long circulating delivery system we expect to achieve better therapeutic efficacy by allowing more particles to reach the tumor site via the EPR effect.

To address the issues of targeting in the anticancer drug delivery system and short circulation time in the siRNA delivery system, we have created a new targeted delivery platform involving the use of boronic acid-diol complexation (Scheme 1.1).

Boronic acids have been used in a variety of pharmaceutical agents such as in the FDA approved proteasome inhibitor, Bortezomib (*27*), in glucose sensing by the formation of boronic acid-diol complexes (*28, 29*), in boron neutron capture therapy (BNCT) for localized radiation therapy (*30, 31*) and in compounds to create drug delivery systems such as the recent complexation of boronic acids with diols to form cross-linked micelles (*32, 33*).

We demonstrate a new assembly of targeted nanoparticles that employs boronic acid complexation with diols. That is, nanoparticles are assembled using polymers that have sugars in their backbone, e.g., mucic acid, to provide a repeating unit that contains vicinal diols. Nanoparticle targeting agents are conjugated with flexible spacing groups, e.g., polyethylene glycol (PEG), and terminated with a boronic acid. These targeting moieties are then assembled onto the surface of the nanoparticle via the reversible, covalent bonding between the boronic acid and the surface vicinal diols of the polymer. This complexation system can have numerous functionalities that allow for assembly with a wide variety of therapeutic and imaging agents (*34*).

For the targeted delivery of anticancer drugs, for instance, the small hydrophobic drug CPT, the complexation between boronic acids on the targeting moiety and vicinal diols on the polymer can be used to form a targeted nanoparticle delivery system. Specifically, CPT is conjugated onto a biocompatible hydrophilic copolymer backbone of mucic acid and PEG (MAP). This conjugate, when placed in water can self-assemble into nanoparticles. The addition of the targeting agent of choice is achieved by exploiting the complexation between boronic acids in the targeting moiety and the mucic acid repeats in the polymer backbone (Scheme 1.1). This will be described in Part I of this thesis.

For the targeted delivery of siRNA, the same boronic acid-diol complexation platform can be exploited. A cationic biocompatible hydrophilic copolymer backbone of mucic acid and dimethylsuberimidate (MAD) is used to condense anionic siRNA into nanoparticles. PEG and targeting agent terminated with boronic acid are used for stabilization and targeting purposes respectively via the complexation of boronic acid with the mucic acid repeats in the polymer backbone (Scheme 1.1). This will be described in Part II of this thesis.

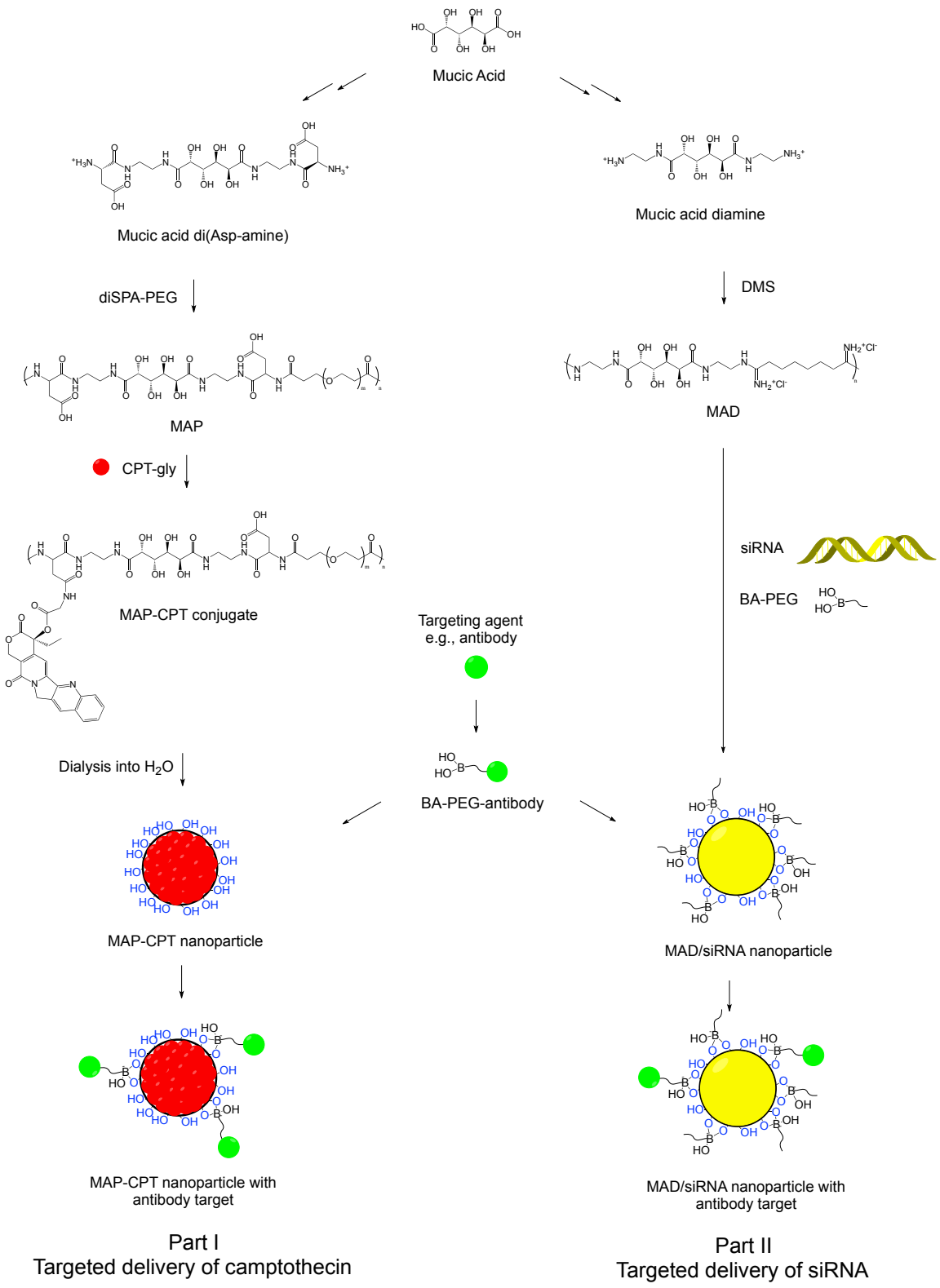
Mucic Acid
Mucic acid di(Asp-amine)
Mucic acid diamine
diSPA-PEG
DMS
MAP
MAD
CPT-gly
MAP-CPT conjugate
siRNA
BA-PEG
Targeting agent
e.g., antibody
Dialysis into H2O
BA-PEG-antibody
MAP-CPT nanoparticle
MAD/siRNA nanoparticle
MAP-CPT nanoparticle with
antibody target
MAD/siRNA nanoparticle with
antibody target
Part I
Targeted delivery of camptothecin
Part II
Targeted delivery of siRNA

Scheme 1.1 Delivery platform involving boronic acid-diol complexation for the (I) targeted delivery of anticancer drug, camptothecin (CPT) and the (II) targeted delivery of small interfering RNA (siRNA). Abbreviations: CPT-gly, CPT with glycine linker; DMS, dimethylsuberimidate; MAP, mucic acid and PEG copolymer; MAD, mucic acid and dimethylsuberimidate copolymer; BA, boronic acid.

1.1 References

(1) Siegel, R., Naishadham, D., and Jemal, A. (2012) Cancer Statistics, 2012. *CA Cancer J Clin 62*, 10-29.

(2) Siegel, R., Naishadham, D., and Jemal, A. (2012) Cancer statistics for Hispanics/Latinos, 2012. *CA Cancer J Clin 62*, 283-298.

(3) Peer, D., Karp, J. M., Hong, S., FaroKHzad, O. C., Margalit, R., and Langer, R. (2007) Nanocarriers as an emerging platform for cancer therapy. *Nature Nanotechnology 2*, 751-760.

(4) Schroeder, A., Heller, D. A., Winslow, M. M., Dahlman, J. E., Pratt, G. W., Langer, R., Jacks, T., and Anderson, D. G. (2012) Treating metastatic cancer with nanotechnology. *Nat Rev Cancer 12*, 39-50.

(5) Yuan, F., Dellian, M., Fukumura, D., Leunig, M., Berk, D. A., Torchilin, V. P., and Jain, R. K. (1995) Vascular-Permeability in a Human Tumor Xenograft - Molecular-Size Dependence and Cutoff Size. *Cancer Research 55*, 3752-3756.

(6) Hobbs, S. K., Monsky, W. L., Yuan, F., Roberts, W. G., Griffith, L., Torchilin, V. P., and Jain, R. K. (1998) Regulation of transport pathways in tumor vessels: Role of tumor type and microenvironment. *Proceedings of the National Academy of Sciences of the United States of America 95*, 4607-4612.

(7) Maeda, H., Wu, J., Sawa, T., Matsumura, Y., and Hori, K. (2000) Tumor vascular permeability and the EPR effect in macromolecular therapeutics: a review. *Journal of Controlled Release 65*, 271-84.

(8) Venturoli, D., and Rippe, B. (2005) Ficoll and dextran vs. globular proteins as probes for testing glomerular permselectivity: effects of molecular size, shape, charge, and deformability. *Am J Physiol-Renal 288*, F605-F613.

(9) Northfelt, D. W., Dezube, B. J., Thommes, J. A., Miller, B. J., Fischl, M. A., Friedman-Kien, A., Kaplan, L. D., Du Mond, C., Mamelok, R. D., and Henry, D. H. (1998) Pegylated-liposomal doxorubicin versus doxorubicin, bleomycin, and vincristine in the treatment of AIDS-related Kaposi's sarcoma: Results of a randomized phase III clinical trial. *Journal of Clinical Oncology 16*, 2445-2451.

(10) Cabral, H., Matsumoto, Y., Mizuno, K., Chen, Q., Murakami, M., Kimura, M., Terada, Y., Kano, M. R., Miyazono, K., Uesaka, M., Nishiyama, N., and Kataoka, K. (2011) Accumulation of sub-100 nm polymeric micelles in poorly permeable tumours depends on size. *Nature Nanotechnology 6*, 815-23.

(11) Xiao, K., Li, Y., Luo, J., Lee, J. S., Xiao, W., Gonik, A. M., Agarwal, R. G., and Lam, K. S. (2011) The effect of surface charge on in vivo biodistribution of PEG-oligocholic acid based micellar nanoparticles. *Biomaterials 32*, 3435-3446.

(12) van Vlerken, L. E., Vyas, T. K., and Amiji, M. M. (2007) Poly(ethylene glycol)-modified nanocarriers for tumor-targeted and intracellular delivery. *Pharmaceutical Research 24*, 1405-1414.

(13) Jokerst, J. V., Lobovkina, T., Zare, R. N., and Gambhir, S. S. (2011) Nanoparticle PEGylation for imaging and therapy. *Nanomedicine 6*, 715-728.

(14) Kirpotin, D. B., Drummond, D. C., Shao, Y., Shalaby, M. R., Hong, K. L., Nielsen, U. B., Marks, J. D., Benz, C. C., and Park, J. W. (2006) Antibody targeting of long-circulating lipidic nanoparticles does not increase tumor localization but does increase internalization in animal models. *Cancer Research 66*, 6732-6740.

(15) Wang, X., Li, J., Wang, Y. Q., Cho, K. J., Kim, G., Gjyrezi, A., Koenig, L., Giannakakou, P., Shin, H. J. C., Tighiouart, M., Nie, S. M., Chen, Z., and Shin, D. M. (2009) HFT-T, a Targeting Nanoparticle, Enhances Specific Delivery of Paclitaxel to Folate Receptor-Positive Tumors. *ACS Nano 3*, 3165-3174.

(16) Choi, C. H. J., Alabi, C. A., Webster, P., and Davis, M. E. (2010) Mechanism of active targeting in solid tumors with transferrin-containing gold nanoparticles. *Proceedings of the National Academy of Sciences of the United States of America 107*, 1235-1240.

(17) Bartlett, D. W., Su, H., Hildebrandt, I. J., Weber, W. A., and Davis, M. E. (2007) Impact of tumor-specific targeting on the biodistribution and efficacy of siRNA nanoparticles measured by multimodality in vivo imaging. *Proceedings of the National Academy of Sciences of the United States of America 104*, 15549-15554.

(18) Cheng, J. J., Khin, K. T., Jensen, G. S., Liu, A. J., and Davis, M. E. (2003) Synthesis of linear, beta-cyclodextrin-based polymers and their camptothecin conjugates. *Bioconjugate Chemistry 14*, 1007-1017.

(19) Davis, M. E. (2009) Design and development of IT-101, a cyclodextrin-containing polymer conjugate of camptothecin. *Adv Drug Deliver Rev 61*, 1189-1192.

(20) Schluep, T., Hwang, J., Cheng, J. J., Heidel, J. D., Bartlett, D. W., Hollister, B., and Davis, M. E. (2006) Preclinical efficacy of the camptothecin-polymer conjugate IT-101 in multiple cancer models. *Clinical Cancer Research 12*, 1606-1614.

(21) Numbenjapon, T., Wang, J. Y., Colcher, D., Schluep, T., Davis, M. E., Duringer, J., Kretzner, L., Yen, Y., Forman, S. J., and Raubitschek, A. (2009) Preclinical Results of Camptothecin-Polymer Conjugate (IT-101) in Multiple Human Lymphoma Xenograft Models. *Clinical Cancer Research 15*, 4365-4373.

(22) Svenson, S., Wolfgang, M., Hwang, J., Ryan, J., and Eliasof, S. (2011) Preclinical to clinical development of the novel camptothecin nanopharmaceutical CRLX101. *Journal of Controlled Release 153*, 49-55.

(23) Davis, M. E. (2009) The First Targeted Delivery of siRNA in Humans via a Self-Assembling, Cyclodextrin Polymer-Based Nanoparticle: From Concept to Clinic. *Molecular Pharmaceutics 6*, 659-668.

(24) Davis, M. E., Zuckerman, J. E., Choi, C. H. J., Seligson, D., Tolcher, A., Alabi, C. A., Yen, Y., Heidel, J. D., and Ribas, A. (2010) Evidence of RNAi in humans from systemically administered siRNA via targeted nanoparticles. *Nature 464*, 1067-1071.

(25) Bartlett, D. W., Su, H., Hildebrandt, I. J., Weber, W. A., and Davis, M. E. (2007) Impact of tumor-specific targeting on the biodistribution and efficacy of siRNA nanoparticles measured by multimodality in vivo imaging. *Proceedings of the National Academy of Sciences of the United States of America 104*, 15549-15554.

(26) Heidel, J. D., Yu, Z. P., Liu, J. Y. C., Rele, S. M., Liang, Y. C., Zeidan, R. K., Kornbrust, D. J., and Davis, M. E. (2007) Administration in non-human primates of escalating intravenous doses of targeted nanoparticles containing ribonucleotide reductase subunit M2 siRNA. *Proceedings of the National Academy of Sciences of the United States of America 104*, 5715-5721.

(27) Richardson, P. G., Mitsiades, C., Hideshima, T., and Anderson, K. C. (2006) Bortezomib: Proteasome inhibition as an effective anticancer therapy. *Annu Rev Med 57*, 33-47.

(28) Springsteen, G., and Wang, B. H. (2002) A detailed examination of boronic acid-diol complexation. *Tetrahedron 58*, 5291-5300.

(29) Fang, H., Kaur, G., and Wang, B. H. (2004) Progress in boronic acid-based fluorescent glucose sensors. *J Fluoresc 14*, 481-489.

(30) Barth, R. F., Coderre, J. A., Vicente, M. G. H., and Blue, T. E. (2005) Boron neutron capture therapy of cancer: Current status and future prospects. *Clinical Cancer Research 11*, 3987-4002.

(31) Wittig, A., Michel, J., Moss, R. L., Stecher-Rasmussen, F., Arlinghaus, H. F., Bendel, P., Mauri, P. L., Altieri, S., Hilger, R., Salvadori, P. A., Menichetti, L., Zamenhof, R., and Sauerwein, W. A. G. (2008) Boron analysis and boron imaging in biological materials for Boron Neutron Capture Therapy (BNCT). *Crit Rev Oncol Hemat 68*, 66-90.

(32) Chen, W. X., Cheng, Y. F., and Wang, B. H. (2012) Dual-Responsive Boronate Crosslinked Micelles for Targeted Drug Delivery. *Angew Chem Int Edit 51*, 5293-5295.

(33) Li, Y. P., Xiao, W. W., Xiao, K., Berti, L., Luo, J. T., Tseng, H. P., Fung, G., and Lam, K. S. (2012) Well-Defined, Reversible Boronate Crosslinked Nanocarriers for Targeted Drug Delivery in Response to Acidic pH Values and cis-Diols. *Angew Chem Int Edit 51*, 2864-2869.

(34) Gottesman, M. M., Fojo, T., and Bates, S. E. (2002) Multidrug resistance in cancer: Role of ATP-dependent transporters. *Nat Rev Cancer 2*, 48-58.

Part I

Targeted Delivery of Camptothecin

Chapter II

Synthesis of Targeted MAP-CPT Delivery System

2.1 Abstract

The delivery of therapeutics via nanoscaled vehicles for solid cancer treatment can be enhanced by the incorporation of targeting capability. In here, the reversible covalent complexation between boronic acids and diols is used to achieve targeting for the delivery of small hydrophobic drug camptothecin (CPT). CPT is conjugated to a biocompatible hydrophilic copolymer of mucic acid and PEG (MAP). This when placed in water, self-assembles into MAP-CPT nanoparticles. The targeting agent of choice, Herceptin antibody is attached to boronic acid. This boronic acid-containing targeting moiety then complexes with the diol-containing MAP to form a targeted MAP-CPT nanoparticle. MAP polymer lengths of 20 kDa (short), 65 kDa (medium) and 102 kDa (long) are synthesized. Upon conjugation of CPT, nanoparticle sizes of ca. 30 nm and slightly negative surface charges are observed for all. The addition of Herceptin targeting agent to medium MAP-CPT nanoparticles to form targeted MAP-CPT nanoparticles increases nanoparticle size to ca. 40 nm with a slightly negative surface charge.

2.2 Introduction

Nanoparticles are finding application for the delivery of a broad range of therapeutic and imaging agents, some of which are currently being investigated in human clinical trials (*1, 2*). When nanoparticles are employed for the delivery of therapeutics to solid cancers, they rely upon the enhanced permeability and retention (EPR) effect to accumulate in the tumors (*3*). After reaching the tumor site by the EPR effect, nanoparticles containing targeting agents that can engage cancer cell surface receptors are shown to achieve uptake into cancer cells in amounts exceeding those of non-targeted nanoparticles with similar size and surface charge (*4-6*).

Our research group has been involved in translating two polymer-based nanoparticles from the laboratory to the clinic. The first, CRLX101 (previously known as IT-101) is a ca. 30 nm, non-targeted nanoparticle composed of a cyclodextrin-polymer conjugate of anticancer drug camptothecin (CPT) (*7*). The second, CALAA-01, is a ca. 70 nm human protein transferrin targeted nanoparticle comprised of cyclodextrin-polymer and siRNA (*8, 9*). The method of assembling the targeting moiety onto the CALAA-01 nanoparticle involves the formation of inclusion complexes of adamantane with the cyclodextrins in the polymer (*8*). Since the method of assembling CRLX101 utilizes inclusion complex formation between the cyclodextrins in the polymer with the conjugated CPT, the targeting methodology employed with CALAA-01 is not amenable for CRLX101. Because of this issue and others that were encountered as these nanoparticles were translated to the clinic, we have been exploring new ways of assembling targeted nanoparticles that could carry any type of payload. Here, we describe a methodology to create targeted nanoparticles that involves the use of boronic acid-diol

complexes.

Boronic acids have been used: (i) in a variety of pharmaceutical agents, (ii) in creating devices to sense sugars and (iii) in compounds to create drug delivery materials and devices (*10*). For example, the complexation of boronic acids with diols has recently been employed to assemble cross-linked micelles (*11, 12*). Here, we demonstrate a new assembly of targeted nanoparticles that employs boronic acid complexation with diols. That is, nanoparticles are assembled using polymers that have sugars in their backbone, e.g., mucic acid, to provide a repeating unit that contains vicinal diols. Nanoparticle targeting agents are conjugated with flexible spacing groups, e.g., polyethylene glycol (PEG), and terminated with a boronic acid. These targeting moieties are then assembled onto the surface of the nanoparticle via the reversible, covalent bonding between the boronic acid and the surface vicinal diols of the polymer (Scheme 2.1). This complexation system can have numerous functionalities that allow for assembly with a wide variety of therapeutic and imaging agents (*13*). For example, small hydrophobic drug molecules like CPT can be conjugated to the polymer backbone and self-assembled into nanoparticles.

In this chapter, an antibody (Herceptin) targeted, polymer-based nanoparticle system for the delivery of CPT that utilizes the complexation of boronic acids on the antibody targeting moiety and vicinal diols on the polymer for assembly of the targeted nanoparticle was synthesized. CPT was conjugated onto a biocompatible hydrophilic copolymer backbone of mucic acid and PEG (MAP). This conjugate, when placed in water self-assembled into nanoparticles. Addition of the antibody targeting agent was

achieved by exploiting the complexation between boronic acids in the targeting moiety and the mucic acid repeats in the polymer (Scheme 2.1).

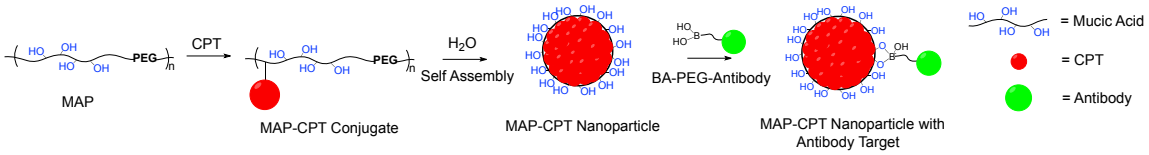

Scheme 2.1 Targeted MAP-CPT nanoparticle delivery system assembly. MAP, copolymer of mucic acid and polyethylene glycol; CPT, camptothecin; BA, boronic acid.

2.3 Experimental

2.3.1 General

All commercially purchased reagents and solvents including anhydrous and HPLC grade were used without further purification. Boc-L-aspartic acid 4-benzyl 1-(N-hydroxysuccinimide) ester (Boc-Asp(OBzl)-OSu) was purchased from Bachem (Bubendorf, Switzerland). Disuccinimidyl propionate poly(ethylene glycol) (diSPA-PEG, MW 3400) was purchased from Sunbio (South Korea). Camptothecin was obtained from Boehringer Ingelheim (Ingelheim, Germany). 3-carboxylphenylboronic acid and 3-carboxy 5-nitrophenylboronic acid were purchased from Alfa Aesar (Ward Hill, MA). Amine polyethylene glycol carboxylic acid (NH_2-PEG-CO_2H, MW 5000) was purchased from JenKem Technology USA (Allen, TX). Herceptin® (Trastuzumab) was obtained from Dr. Y. Yen at the City of Hope (Duarte, CA). All other reagents were purchased from Sigma (St Louis, MO).

^{1}H, ^{13}C and ^{19}F NMR spectra were recorded on either a 500 MHz or 600 MHz spectrometer (Inova, Varian). Mass spectrometry was carried out using a LCQ ion trap mass spectrometer (Finnigan, Thermo) by direct infusion electrospray ionization or MALDI-TOF mass spectrometer (Voyager DE^{TM}-PRO, Applied Biosystems).

Absorbance and fluorescence measurements were taken on a microplate reader (Infinite 200, Tecan).

2.3.2 Preparation and Characterization of MAP-CPT Nanoparticles

1. Mucic acid dimethyl ester

120 ml of methanol and 0.4 ml of concentrated sulfuric acid were added to 5 g (22.8 mmol) of mucic acid. This mixture was refluxed at 85 ^{o}C overnight under constant stirring. Solids were filtered, washed with methanol, recrystallized and dried under vacuum overnight to yield 8 g (71%) of mucic acid dimethyl ester. ^{1}H NMR ($(CD_3)_2SO$) δ 4.88-4.91 (d, 2H), 4.78-4.81 (m, 2H), 4.28-4.31 (d, 2H), 3.77-3.78 (d, 2H), 3.63 (s, 6H). ESI/MS (m/z): 261.0 $[M+Na]^{+}$.

2. Protected mucic acid diamine

60 ml of methanol, 5.25 g (32.7 mmol) of N-Boc-ethylenediamine and 5.7 ml (32.7 mmol) of N, N-diisopropylethylamine (DIPEA) were added to 3 g (12.6 mmol) of mucic acid dimethyl ester. This reaction mixture was refluxed at 85 ^{o}C overnight under constant stirring. Solids were filtered, washed with methanol, recrystallized and dried under vacuum to give 4.65 g (75%) of product. ^{1}H NMR ($(CD_3)_2SO$) δ 7.72 (t, 2H), 6.82 (t, 2H), 5.13-5.15 (d, 2H), 4.35-4.38 (d, 2H), 4.08-4.11 (d, 2H), 3.78-3.80 (d, 2H), 2.95-3.15 (m, 8H), 1.36 (s, 18). ESI/MS (m/z): 517.1 $[M+Na]^{+}$.

3. Mucic acid diamine

8 g (16.2 mmol) of protected mucic acid diamine was transferred to a flask containing 3 N HCl in methanol (160 ml) and reacted for 6 h at room temperature under constant stirring. Precipitate was filtered, washed with methanol and vacuum dried overnight to yield 5.69 g (96%) of mucic acid diamine. ^{1}H NMR ($(CD_3)_2SO$) δ 7.93-

7.99 (m, 8H), 5.31-5.34 (d, 2H), 4.57 (d, 2H), 4.10-4.17 (d, 2H), 3.82 (d, 2H), 3.32-3.38 (m, 4H), 2.82-2.86 (m, 4H). ESI/MS (m/z): 295.1 $[M]^+$.

4. Mucic acid di(Asp(OBzl)-Boc)

9.27 g (22.1 mmol) of Boc-Asp(OBzl)-OSu in 75 ml of acetonitrile and 2.88 ml (35.8 mmol) of pyridine was added to 2.7 g (7.35 mmol) of mucic acid diamine dissolved in 45 ml water. This reaction mixture was refluxed at 60 ^oC overnight under constant stirring. Acetonitrile was removed by rotavap and resulting precipitate was recrystallized from hot water and dried under vacuum to yield 2.03 g (31%) mucic acid di(Asp(OBzl)-Boc). ^1H NMR ($(CD_3)_2SO$) δ 7.93 (t, 2H), 7.75 (t, 2H), 7.29-7.35 (m, 10H), 7.05 (d, 2H), 5.11 (t, 2H), 5.06 (s, 4H), 4.34-4.39 (d, 2H), 4.25-4.30 (d, 2H), 4.10-4.12 (d, 2H), 3.77-3.79 (d, 2H), 3.11-3.15 (m, 8H), 2.53-2.78 (m, 4H), 1.36 (s, 18H). ESI/MS (m/z): 927.4 $[M+Na]^+$.

5. Mucic acid di(Asp(OBzl)-amine)

6 ml (80.8 mmol) of trifluoroacetic acid was slowly added to 2 g (2.21 mmol) of mucic acid di(Asp(OBzl)-Boc) dissolved in 18 ml of dichloromethane on an ice bath. The reaction was allowed to proceed for 4 h in ice bath. Solvent was removed, precipitate recrystallized with tetrahydrofuran and dried on vacuum to yield 1.74 g (84%) of product. ^1H NMR ($(CD_3)_2SO$) δ 8.46 (t, 2H), 8.21 (s, 6H), 7.79 (t, 2H), 7.32-7.38 (m, 10H), 5.19 (t, 2H), 5.14 (s, 4H), 4.41 (s, 2H), 4.11-4.14 (d, 2H), 4.02-4.06 (d, 2H), 3.81 (s, 2H), 3.11-3.23 (m, 8H), 2.79-3.02 (m, 4H). ESI/MS (m/z): 705.4 $[M]^+$.

6. Mucic acid di(Asp-amine)

511 mg (13.5 mmol) of 20 wt% palladium hydroxide on carbon was transferred to 1.26 g (1.35 mmol) of mucic acid di(Asp(OBzl)-amine) dissolved in 50 ml of methanol. Reaction vessel was sealed and vented with argon. Hydrogen gas was added via double-layered balloon for 24 h. Catalyst was filtered away, solvent removed and precipitate dried on vacuum. This was then reconstituted in water, filtered with a 0.2 μm membrane filter (Acrodisc) and lyophilized to yield 711 mg (70%) of product. ^{1}H NMR ($(CD_3)_2SO$) δ 8.44 (t, 2H), 8.19 (broad, 6H), 7.80 (t, 2H), 5.22 (t, 2H), 4.48 (s, 2H), 4.12 (s, 2H), 3.94-3.99 (m, 2H), 3.80 (s, 2H), 3.11-3.23 (m, 8H), 2.70-2.85 (m, 4H). ESI/MS (m/z): 525.2 $[M]^+$.

7. MAP (Mucic Acid containing Polymer)

111 mg of mucic acid di(Asp-amine) (0.15 mM) and 500 mg of diSPA-PEG3.4kDa (0.15 mM) were dried under vacuum for 6 h. 3.5 ml of anhydrous dimethyl sulfoxide was added under argon to dissolve the reactants. 82 μl (0.47 mM) of anhydrous DIPEA was then added under argon and reaction was allowed to proceed for 40 h at room temperature under constant stirring. Reaction mixture was then dialyzed with 10 kDa MWCO membrane filter device (Amicon) 4 times, filtered through a 0.2 μm membrane filter (Acrodisc) and lyophilized to yield 466 mg (81%) MAP. GPC (for medium MAP): Mn = 55.5 kDa, Mw = 75.3 kDa, Mw/Mn = 1.36. ^{1}H NMR ($(CD_3)_2SO$, for medium MAP) δ 8.07 (d, 1H), 8.04 (d, 1H), 7.83 (t, 1H), 7.77 (t, 1H), 7.69 (t, 2H), 4.43 (td, 2H), 4.10 (d, 2H), 3.75 (ddt, 2H), 3.55 (t, 4.3H), 3.42-3.52 (PEG peak, 330H), 3.05-3.16 (m, 8H), 2.90 (broad, 0.6H), 2.39-2.53 (m, 4H), 2.34 (t, 4.3H), 1.12 (m, 6H). ^{13}C NMR (D_2O,

for medium MAP) δ 175.7, 174.9, 174.0, 172.9, 66.5, 69.6, 70.6, 54.3, 50.6, 42.5, 38.8, 38.3, 36.5, 35.7, 17.7, 16.2, 12.1.

8. Absolute molecular weight determination of MAP

The absolute determination of molecular weights does not require standards for calibration. This was determined on a GPC system equipped with an Agilent pump, degasser and autosampler, double gel permeation columns (PL aquagel-OH 40 8 μm 300 x 7.5 mm, Polymer Laboratory) in series connected to a multi-angle laser light scattering (MALS) detector (DAWN HELEOS, Wyatt) and a refractive index (RI) detector (Optilab rEX, Wyatt). PBS (1x, 0.02 w/w% sodium azide, pH 7.4) was used as the eluent at a flow rate of 0.7 ml/min. Specific refractive increment, dn/dc was measured by batch injection of various concentrations of MAP dissolved in PBS into Optilab rEX at 0.2 ml/min.

9. Molecular weight control of MAP

Molecular weight of MAP was controlled by the amount of tertiary base, N, N-diisopropylethylamine (DIPEA) added to the reaction. After dissolving equal molar ratios of mucic acid di(Asp-amine) and diSPA-PEG3.4kDa in anhydrous dimethyl sulfoxide, different equivalents (1.1, 1.6 and 2) of anhydrous DIPEA to amine groups on mucic acid di(Asp-amine) were added. The reactions were then carried out and the polymers processed as per the methods described in section 7 (vide supra). Three polymers of differing molecular weights were prepared and denoted as short, medium and long.

10. 20-O-glycinylcamptothecin trifluoroacetic acid salt (CPT-gly·TFA)

20-O-glycinylcamptothecin trifluoroacetic acid salt (CPT-gly·TFA) was synthesized as previously reported (*14*).

11. MAP-CPT conjugate

403 mg (0.22 mM on -CO_2H basis) of MAP was dissolved in 20 ml of anhydrous dimethyl sulfoxide. To this was added 167 mg (0.87 mM) of EDC and 75 mg (0.65 mM) of NHS dissolved in 6 ml of anhydrous dimethyl sulfoxide, 340 mg (0.65 mM) of 20-O-glycinylcamptothecin trifluoroacetic acid salt (CPT-gly.TFA) dissolved in 6 ml of anhydrous dimethyl sulfoxide and 114 µl (0.65 mM) of anhydrous DIPEA under argon. After overnight reaction under constant stirring, the reaction mixture was dialyzed against dimethyl sulfoxide 3 times and water 2 times using 10 kDa MWCO membrane (Spectra/Por 7). Any insoluble material was removed by centrifugation and supernatant was filtered with a 0.2 µm filter (Acrodisc). A portion of this clear yellow solution was lyophilized for yield determination and percent CPT conjugation analysis. The remaining was formulated into 0.9 w/v% saline and stored at -20 ^{o}C.

12. CPT content in MAP-CPT

Weight percent of CPT in MAP-CPT was determined by the intrinsic fluorescence of CPT. MAP-CPT was dissolved in dimethyl sulfoxide at 10 mg/ml. This was diluted into 0.1 mg/ml with 1 N NaOH and incubated overnight. Fluorescence was measured at excitation 370 nm, emission 440 nm, and compared to that of known concentrations of CPT.

13. Nanoparticle composition

Nanoparticle compositions were analyzed as per the methods described in section 8 (vide supra) except gel permeation columns were bypassed. Dn/dc value of MAP-CPT nanoparticles was measured by batch injection of various concentrations of MAP-CPT nanoparticles dissolved in PBS into Optilab rEX at 0.2 ml/min. This allowed for the molecular weight determination of MAP-CPT nanoparticles. The number of MAP-CPT conjugates per nanoparticle was then calculated from this data.

14. Nanoparticle size and surface charge

Particle size and zeta potential measurements were determined by dynamic light scattering (DLS) using a ZetaPALS instrument (Brookhaven Instruments, Holtsville, NY). Effective hydrodynamic diameter was recorded and averaged from 10 runs at 1 min each. Zeta potential measurements were collected for three sets of 10 runs at a target residual of 0.012, and the results were averaged.

15. Nanoparticle morphology

Nanoparticle morphology was visualized by cryo-electron microscopy (cryo-EM). Glow discharged Quantifoil holey carbon grid (SPI Supplies) was loaded into an automated climate-controlled plunge-freezer (Vitrobot, FEI) and 3 μl of sample was applied. Grid was blotted, drained, plunged into liquid ethane, transferred and stored in liquid nitrogen. Samples were visualized under cryogenic temperatures with transmission electron microscope (Tecnai T12, FEI) equipped with a cryo-specimen holder. Acceleration voltage was set at 120 kV.

2.3.3 Preparation and Characterization of Targeted MAP-CPT Nanoparticles

1. PBA-PEG-CO_2H (3-amide-PEG5kDa-carboxylic acid phenylboronic acid)

To 200 mg (1.21 mM) of 3-carboxyphenylboronic acid dissolved in 5 ml of anhydrous tetrahydrofuran was added 18.7 µl (0.24 mM) of anhydrous dimethylformamide under argon. This reaction vessel was transferred into an ice bath and 195 µl (2.89 mM) of oxalyl chloride was slowly added under argon. Reaction was allowed to proceed under vent and constant stirring for 2 h at room temperature. Solvent and excess reagent were removed under vacuum. 37 mg (0.2 mM) of this dried acyl chloride compound was dissolved in 15 ml of anhydrous dichloromethane under argon. To this was added 500 mg (0.1 mM) of NH_2-PEG5kDa-CO_2H and 52 µl (0.3 mM) of dry DIPEA under argon. After overnight reaction under constant stirring, solvent was removed under vacuum and the dried product was reconstituted in 0.5 N HCl. This solution was passed through a 0.2 µm filter (Acrodisc) and dialyzed against water with a 3 kDa MWCO membrane filter device (Amicon) until constant pH was attained. The supernatant was then filtered with a 0.2 µm filter (Acrodisc) and lyophilized to yield 377 mg (73%) of PBA-PEG-CO_2H. ^1H NMR ($(CD_3)_2SO$) δ 12.52 (s, 1H), 8.39 (t, 1H), 8.22 (s, 1H), 8.14 (s, 2H), 7.88 (d, 1H), 7.82 (d, 1H), 7.39 (t, 1H), 3.99 (s, 2H), 3.35-3.62 (PEG peak). MALDI-TOF (m/z): 5600 g/mol (NH_2-PEG5kDa-CO_2H, 5400 g/mol).

2. nitroPBA-PEG-CO_2H (3-amide-PEG5kDa-carboxylic acid, 5-nitrophenylboronic acid)

Synthesis of nitroPBA-PEG-CO_2H was performed in the same way as for PBA-PEG-CO_2H except the starting material was 3-carboxy 5-nitrophenylboronic acid. The

reaction yielded 393 mg (76%) of nitroPBA-PEG-CO_2H. ^1H NMR ($(CD_3)_2SO$) δ 12.52 (s, 1H), 8.89 (t, 1H), 8.72 (s, 1H), 8.68 (s, 1H), 8.64 (s, 1H), 8.61 (s, 2H), 3.99 (s, 2H), 3.35-3.62 (PEG peak). MALDI-TOF (m/z): 5600 g/mol (NH_2-PEG5kDa-CO_2H, 5400 g/mol).

3. *pKa determination for PBA*

pKa of PBA was found by measuring the change in absorbance of PBA as it converted from trigonal (in low pH) to tetrahedral (in high pH) conformation. To a solution of 10^{-3} M PBA in 0.1 M PBS, pH 7.4 was titrated 1 N NaOH. pH was recorded and corresponding samples were removed for absorbance measurements at 268 nm.

4. Binding constant determination between PBA and MAP

A three component competitive assay involving fluorescent dye Alizarin Red S, PBA and MAP (diol-containing) was used to determine the binding constant between PBA and MAP. This technique was developed by Springsteen and Wang (*15*). Briefly, the association constant K_{eq1} for Alizarin Red S-PBA complex was determined by changes in fluorescence as PBA was titrated into Alizarin Red S. MAP was then titrated into a solution containing Alizarin Red S and PBA. The addition of the MAP perturbed the first equilibrium due to MAP competing with Alizarin Red S for binding to PBA. Changes in fluorescence were measured and the association constant K_{eq} between PBA and MAP was then determined. Measurements were performed in 0.1 M PBS at pH 7.4.

5. Herceptin-PEG-nitroPBA (Herceptin-PEG5kDa-5-nitrophenylboronic acid)

36 mg (6.4 μM) of nitroPBA-PEG-CO_2H, 12.3 mg (64 μM) of EDC and 11.1 mg (96 μM) of NHS were dissolved in 2.4 ml of 0.1 M MES buffer, pH 6.0. This mixture

was reacted for 15 min on a rotating shaker at room temperature. Excess reactants were dialyzed away with 3 kDa MWCO membrane filter device (Amicon). This activated carboxylic acid PEG compound was added to 20 mg (0.14 mM) of Herceptin in 0.1 M PBS, pH 7.2. Reaction was carried out on a rotating shaker at room temperature for 2 h and then dialyzed 4 times with 50 kDa MWCO membrane filter device (Amicon) against 1x PBS at pH 7.4. MALDI-TOF: average conjugation of 1 to 2 nitroPBA-PEG per antibody.

6. Formulation of targeted MAP-CPT nanoparticles

Herceptin-PEG-nitroPBA was added to the medium MAP-CPT nanoparticles to form targeted MAP-CPT nanoparticles at a ratio of one Herceptin per nanoparticle in 1x PBS, pH 7.4.

7. Particle size, surface charge and morphology

The methods used for the targeted nanoparticle were the same as for the non-targeted nanoparticles as described in Preparation and Characterization of MAP-CPT Nanoparticles sections 14 and 15 (vide supra).

2.4 Results and Discussion

2.4.1 Preparation and Characterization of MAP-CPT Nanoparticles

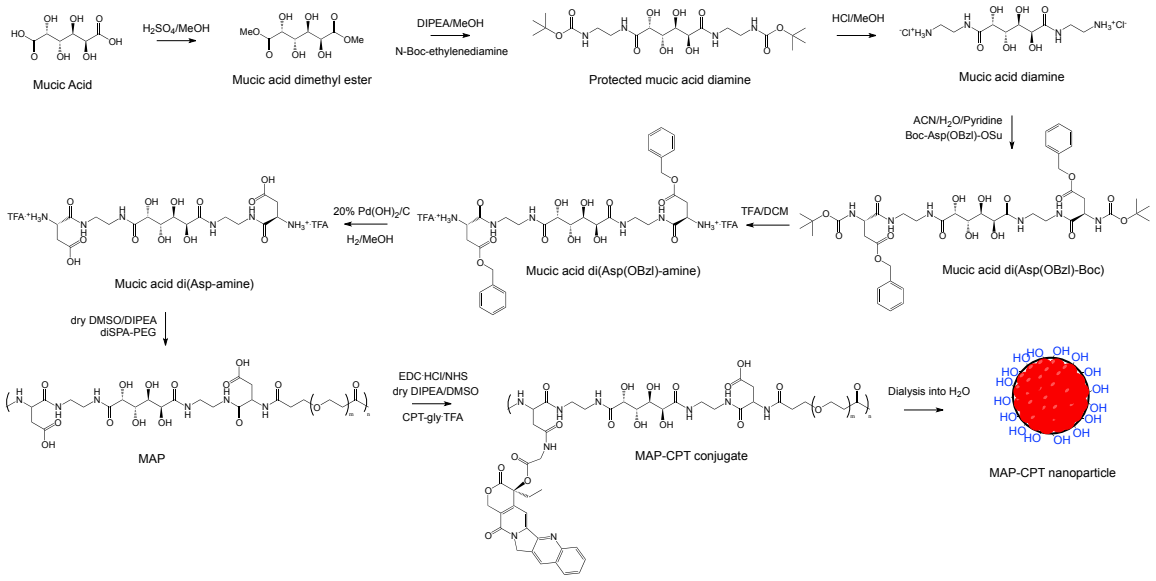

Scheme 2.2 Synthesis of MAP-CPT nanoparticles.

The synthesis methodology of the MAP-CPT conjugate and its assembly into MAP-CPT nanoparticles is outlined in Scheme 2.2. Mucic acid was modified to contain both amino and carboxyl groups to allow for polymerization with PEG (amine group) and for conjugation of CPT (carboxyl group), respectively. It was observed via ^{19}F NMR that the mucic acid di(Asp-amine) formed was the trifluoroacetic acid salt by comparing against standard (2-(trifluoromethyl)acetophenone). Therefore, for the polymerization reaction between mucic acid di(Asp-amine) and diSPA-PEG to proceed, a base was required for the deprotonation of $-NH_3^+$ group into the reactive $-NH_2$ form. Here, tertiary

base N, N-diisopropylethylamine (DIPEA) was used. Figure 2.1 shows representative NMR data for the MAP polymers. The polymer end groups were determined to be -PEG-CO_2H by ^1H NMR comparison of PEG and mucic acid di(Asp-amine) peak integrals. The molecular weight of MAP can be controlled by the amount of DIPEA added per NH_3^+ group on mucic acid di(Asp-amine) (Table 2.1). As the amount of DIPEA was increased, an increase in viscosity of the reaction mixture was observed. Three polymers were prepared and their properties are listed in Table 2.1.

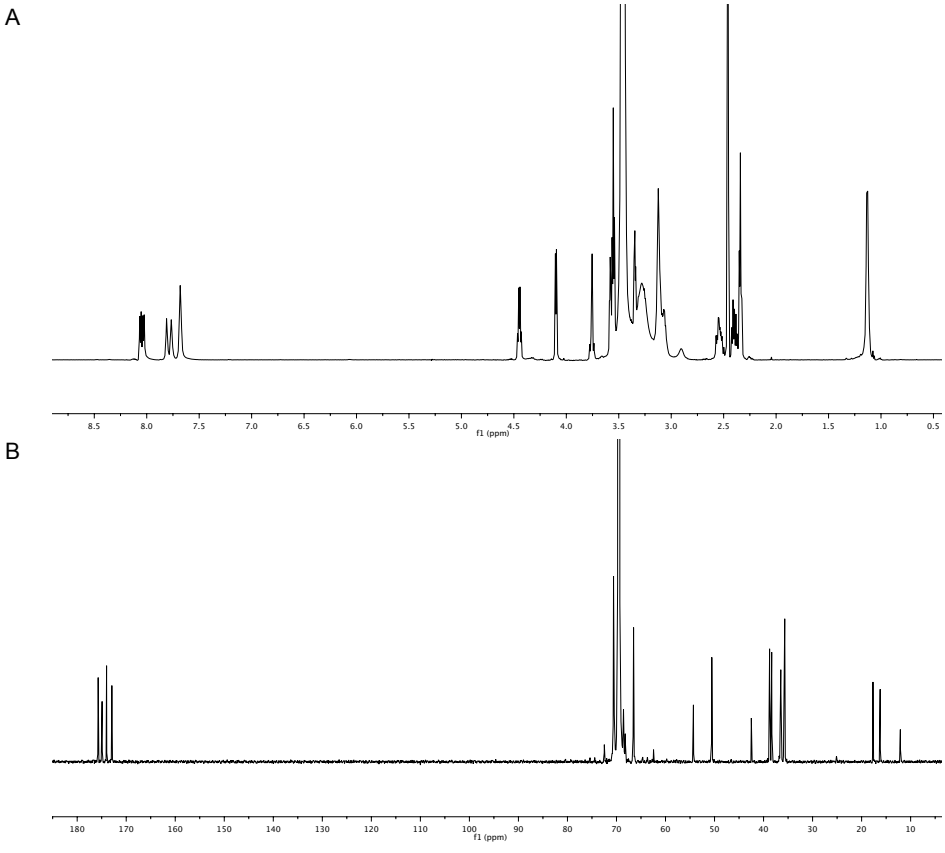

Figure 2.1 ^1H and ^{13}C NMR spectra of medium MAP (A) ^1H NMR in DMSO-*d6*. (B) ^{13}C NMR in D_2O.

		Short	Medium	Long
MAP	Base added (equivalent)[a]	1.1	1.6	2
	MW[b] (kDa)	20	65	102
	Polydispersity[c]	1.22	1.36	1.13
	# repeat units (n)	5-7	15-21	25-30
MAP-CPT conjugate	MW[b] (kDa)	22	75	114
	wt % CPT conjugated	9.8	12.7	10.1
MAP-CPT nanoparticle	# conjugates/particle	2-3	2-3	2-3
	# CPT/particle	~14	~60	~72
	particle size (nm)	~30	~30	~30
	zeta potential (mV)	-1.3+/-0.6	-0.5+/-0.5	-0.8+/-0.5

Table 2.1 Characterization of MAP, MAP-CPT conjugate and MAP-CPT nanoparticles. [a]Equivalent amount of N, N-diisopropylethylamine (DIPEA) added per amine group in mucic acid di(Asp-amine). [b]MW, molecular weight determined as (Mw+Mn)/2; Mw, weight average molecular weight; Mn, number average molecular weight. [c]Polydispersity determined as Mw/Mn.

It is noted that extra peaks were observed in ^{1}H and ^{13}C NMR spectra for MAP. This was identified as N-diisopropylethylamine (DIPEA) (Figure 2.2) and had a weight contribution of 1%. DIPEA was used in the synthesis of MAP and some residue likely remained after the dialysis process. This is largely due to DIPEA having a low solubility in water. Thus, in future synthesis, to remove the residue DIPEA, additional dialysis in DMSO is recommended.

The absolute molecular weights of different lengths MAP were measured using multi-angle laser light scattering (MALS) and refractive index (RI) detections. A refractive index increment (dn/dc) value of 0.134 ml/g was found for the medium MAP. This dn/dc value along with MALS and RI data were used to determine the number

average molecular weight (Mn), weight average molecular weight (Mw) and polydispersity (Mw/Mn) of MAP (Table 2.1).

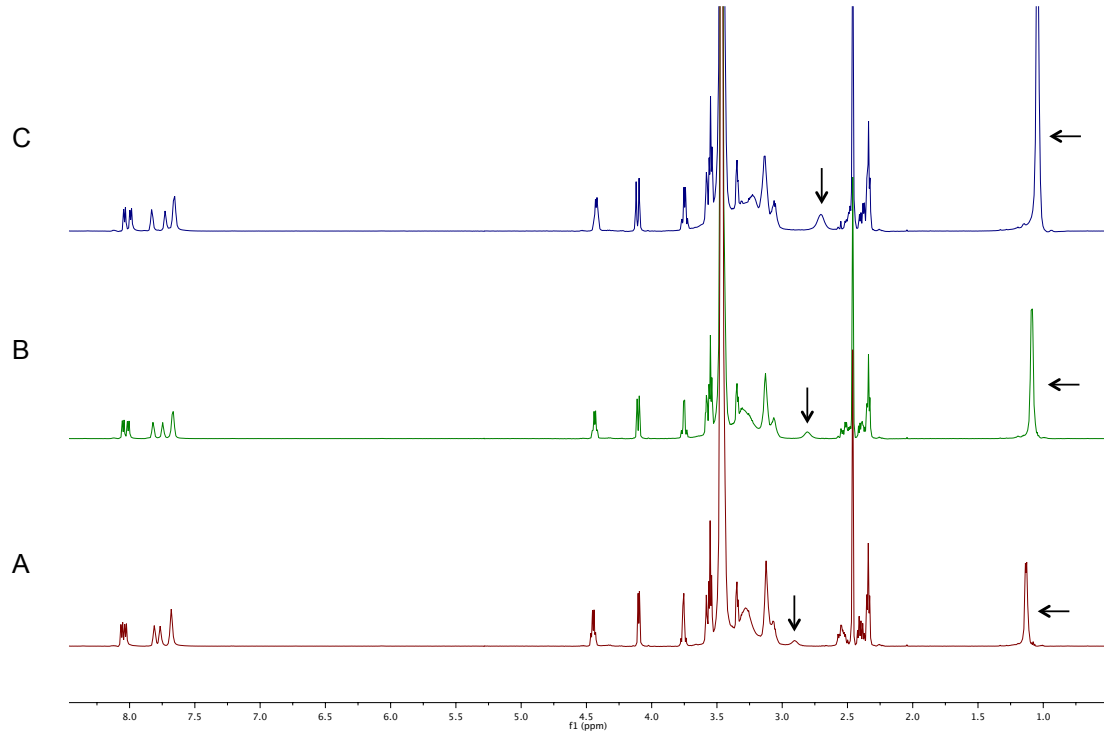

Figure 2.2 Identification of extra peaks in NMR spectra of medium MAP (A) ^{1}H NMR in DMSO-*d6*. (B) Addition of N-diisopropylethylamine (DIPEA). (C) Addition of more DIPEA. Arrows indicate the contaminate DIPEA peaks.

CPT modified at 20-OH position has been reported to show significant reduction in deactivation caused by ring opening of the lactone (*16*). We therefore used CPT modified at this site with a glycine linker, CPT-gly, as was done previously with IT-101

(*14*). The CPT-gly was conjugated onto MAP to form MAP-CPT conjugate by standard EDC coupling technique (Scheme 2.1). The amount of CPT conjugated onto the three MAP polymers is reported in Table 2.1.

Upon addition of water, the MAP-CPT conjugates self-assemble into nanoparticles since CPT is very soluble in dimethyl sulfoxide but not soluble to any significant amount in water. To determine the number of MAP-CPT conjugates per MAP-CPT nanoparticle. Dn/dc values of the MAP-CPT nanoparticles were found and the nanoparticles were characterized by MALS and RI detection. From these data, the molecular weight of each MAP-CPT nanoparticle was determined. Since the molecular weights of the MAP-CPT conjugates were known, the MAP-CPT nanoparticles were found to be composed of 2 to 3 MAP-CPT conjugates.

MAP-CPT nanoparticles have an average particle size of ca. 30 nm (by DLS measurements) and a slightly negative surface charge (by Zeta Potential measurements). The negative surface charge is presumably due to the presence of unconjugated carboxylic acid groups on the MAP backbone. Cryo-EM was used to visualize the medium MAP-CPT nanoparticles in their native environment. Spherical nanoparticles with a narrow size range of 20-40 nm are observed (Figure 2.3).

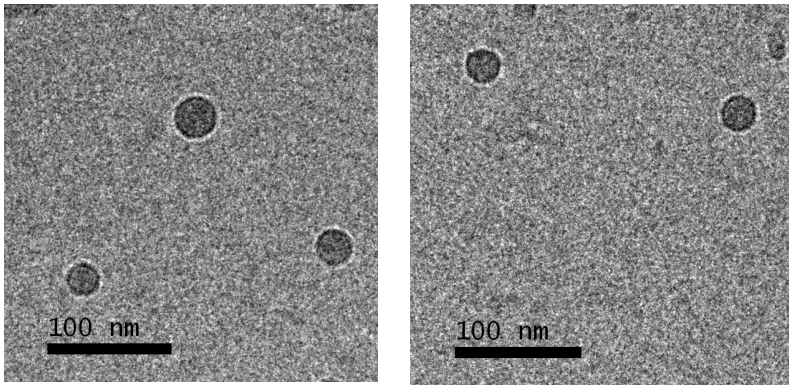

Figure 2.3 Cryo-EM images of medium MAP-CPT nanoparticles.

2.4.2 Preparation and Characterization of Targeted MAP-CPT Nanoparticles

To prepare a targeted nanoparticle, the covalent, reversible binding property between boronic acids and MAP (diol-containing) was used. The binding constant between phenylboronic acid (PBA) and MAP is low at ca. 20 M^{-1}. To increase the binding constant, PBAs with electron withdrawing groups on the phenyl ring were employed to increase the acidity of the boron atom and thus elevate the binding constant with MAP. Commercially available 3-carboxyPBA and 3-carboxy 5-nitroPBA were converted into acyl chlorides using oxalyl chloride (Scheme 2.3). These acyl chloride species were then reacted with NH_2-PEG-CO_2H to form PBA-PEG-CO_2H and nitroPBA-PEG-CO_2H respectively (Scheme 2.3). The addition of bases DMF and DIPEA were required for the synthesis reactions to proceed. However, the presence of these bases resulted in tetrahedral adduct formations with acidic PBA. To remove these adducts, work up in 0.5 N HCl with subsequent equilibration to neutral pH by dialysis against water was carried out.

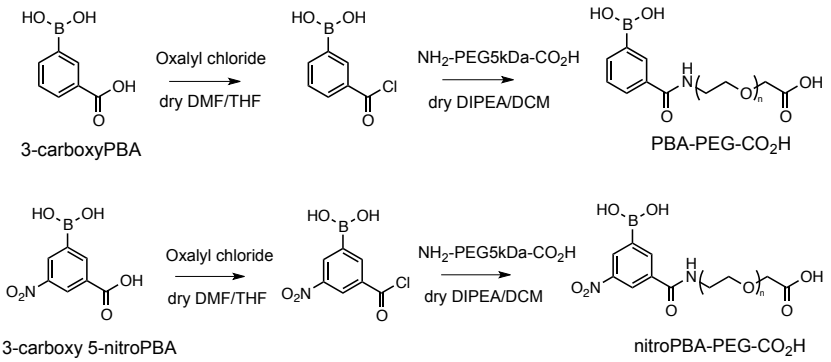

Scheme 2.3 Synthesis of PBA-PEG-CO_2H and nitroPBA-PEG-CO_2H.

pKa values of the modified PBAs were determined by absorbance changes due to conformational change of PBA from trigonal to tetrahedral form as pH increased (Table 2.3). PBA with electron withdrawing groups resulted in lower pKa's, with nitroPBA-PEG-CO_2H having the lowest pKa of 6.8. Thus, at physiological pH, most of the PBA was present in the reactive anionic tetrahedral form. Binding constants between PBA and MAP were found by competitive binding with Alizarin Red S in 0.1 M PBS, pH 7.4. Because of the low pKa value and high binding constant with MAP observed for nitroPBA-PEG-CO_2H, it was chosen as the linker between Herceptin and MAP-CPT nanoparticles.

	pKa	Binding Constant with MAP (M^{-1})
PBA	8.8	20
PBA-PEG-CO_2H	8.3	520
nitroPBA-PEG-CO_2H	6.8	1420

Table 2.2 pKa values and binding constants of different PBAs (phenylboronic acids) with MAP.

The conjugation reaction between Herceptin and nitroPBA-PEG-CO_2H proceeded via EDC coupling (Scheme 2.4). An average of 1 to 2 PEGs were attached per Herceptin antibody.

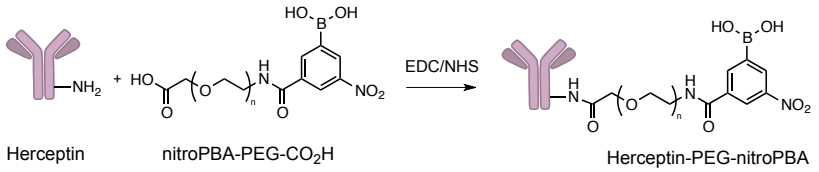

Scheme 2.4 Synthesis of Herceptin-PEG-nitroPBA.

An average size of ca. 40 nm was observed for targeted MAP-CPT nanoparticles by DLS and cryo-EM (Table 2.2 and Figure 2.4). This increase in ca. 10 nm from the non-targeted nanoparticle suggests the attachment of ca. one Herceptin per nanoparticle. Indeed, from cryo-EM images, the targeted nanoparticles were not spherical but appeared to have protrusions indicating the attachment of antibodies. The surface charge of targeted MAP-CPT nanoparticles was slightly higher than MAP-CPT nanoparticles due to the presence of a positively charged Herceptin at pH 7.4 (pI of Herceptin, 9.2 (*17*)).

Targeted MAP-CPT nanoparticle	MAP	medium
	# CPT/particle	~60
	# Herceptin/particle	1
	particle size (nm)	~40
	zeta potential (mV)	-0.4+/-0.6

Table 2.3 Characterization of targeted MAP-CPT nanoparticles.

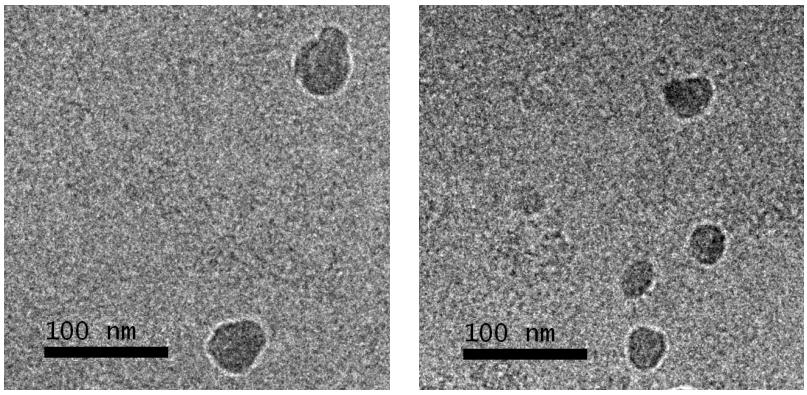

Figure 2.4 Cryo-EM images of targeted MAP-CPT nanoparticles.

2.5 Conclusions

An example for the use of boronic acid-diol complexation in the targeted delivery of anticancer drugs via nanoscaled vehicles was presented. Targeted MAP-CPT nanoparticle delivery system for the small hydrophobic drug, CPT, was synthesized and characterized. It was composed of a biocompatible copolymer of mucic acid and PEG (MAP) enveloping the cytotoxic drug CPT. Targeting was achieved by attaching boronic acid to the targeting moiety of choice, in this case Herceptin antibody, and the subsequent complexation via boronic acid-diol formation with the mucic acid repeats in the MAP polymer.

2.6 References

(1) Davis, M. E., Chen, Z., and Shin, D. M. (2008) Nanoparticle therapeutics: an emerging treatment modality for cancer. *Nature Reviews Drug Discovery 7*, 771-782.

(2) Kamaly, N., Xiao, Z. Y., Valencia, P. M., Radovic-Moreno, A. F., and Farokhzad, O. C. (2012) Targeted polymeric therapeutic nanoparticles: design, development and clinical translation. *Chemical Society Reviews 41*, 2971-3010.

(3) Maeda, H., Wu, J., Sawa, T., Matsumura, Y., and Hori, K. (2000) Tumor vascular permeability and the EPR effect in macromolecular therapeutics: a review. *Journal of Controlled Release 65*, 271-284.

(4) Kirpotin, D. B., Drummond, D. C., Shao, Y., Shalaby, M. R., Hong, K. L., Nielsen, U. B., Marks, J. D., Benz, C. C., and Park, J. W. (2006) Antibody targeting of long-circulating lipidic nanoparticles does not increase tumor localization but does increase internalization in animal models. *Cancer Research 66*, 6732-6740.

(5) Bartlett, D. W., Su, H., Hildebrandt, I. J., Weber, W. A., and Davis, M. E. (2007) Impact of tumor-specific targeting on the biodistribution and efficacy of siRNA nanoparticles measured by multimodality in vivo imaging. *Proceedings of the National Academy of Sciences of the United States of America 104*, 15549-15554.

(6) Choi, C. H. J., Alabi, C. A., Webster, P., and Davis, M. E. (2010) Mechanism of active targeting in solid tumors with transferrin-containing gold nanoparticles. *Proceedings of the National Academy of Sciences of the United States of America 107*, 1235-1240.

(7) Davis, M. E. (2009) Design and development of IT-101, a cyclodextrin-containing polymer conjugate of camptothecin. *Advanced Drug Delivery Reviews 61*, 1189-1192.

(8) Davis, M. E. (2009) The First Targeted Delivery of siRNA in Humans via a Self-Assembling, Cyclodextrin Polymer-Based Nanoparticle: From Concept to Clinic. *Molecular Pharmaceutics 6*, 659-668.

(9) Davis, M. E., Zuckerman, J. E., Choi, C. H. J., Seligson, D., Tolcher, A., Alabi, C. A., Yen, Y., Heidel, J. D., and Ribas, A. (2010) Evidence of RNAi in humans from systemically administered siRNA via targeted nanoparticles. *Nature 464*, 1067-1071.

(10) Yang, W. Q., Gao, X. M., and Wang, B. H. (2003) Boronic acid compounds as potential pharmaceutical agents. *Medicinal Research Reviews 23*, 346-368.

(11) Chen, W. X., Cheng, Y. F., and Wang, B. H. (2012) Dual-Responsive Boronate Crosslinked Micelles for Targeted Drug Delivery. *Angew Chem Int Edit 51*, 5293-5295.

(12) Li, Y. P., Xiao, W. W., Xiao, K., Berti, L., Luo, J. T., Tseng, H. P., Fung, G., and Lam, K. S. (2012) Well-Defined, Reversible Boronate Crosslinked Nanocarriers for

Targeted Drug Delivery in Response to Acidic pH Values and cis-Diols. *Angew Chem Int Edit 51*, 2864-2869.

(13) Gottesman, M. M., Fojo, T., and Bates, S. E. (2002) Multidrug resistance in cancer: Role of ATP-dependent transporters. *Nat Rev Cancer 2*, 48-58.

(14) Cheng, J. J., Khin, K. T., Jensen, G. S., Liu, A. J., and Davis, M. E. (2003) Synthesis of linear, beta-cyclodextrin-based polymers and their camptothecin conjugates. *Bioconjugate Chemistry 14*, 1007-1017.

(15) Springsteen, G., and Wang, B. H. (2002) A detailed examination of boronic acid-diol complexation. *Tetrahedron 58*, 5291-5300.

(16) Zhao, H., Lee, C., Sai, P. K., Choe, Y. H., Boro, M., Pendri, A., Guan, S. Y., and Greenwald, R. B. (2000) 20-O-acylcamptothecin derivatives: Evidence for lactone stabilization. *J Org Chem 65*, 4601-4606.

(17) Wiig, H., Gyenge, C. C., and Tenstad, O. (2005) The interstitial distribution of macromolecules in rat tumours is influenced by the negatively charged matrix components. *J Physiol-London 567*, 557-567.

Chapter III

In Vitro Characterization of Targeted MAP-CPT Delivery System

3.1 Abstract

The synthesis of targeted MAP-CPT delivery system was described in chapter II. In here, *in vitro* studies are conducted to understand the system and as a stepping-stone leading to *in vivo* studies. Cellular uptake of nanoparticles into BT-474, a HER2 (Herceptin is antibody to this receptor) overexpressing cell line is enhanced by 70% compared to non-targeted version by the incorporation of a single Herceptin antibody targeting agent per nanoparticle. The main mechanisms of CPT release from MAP-CPT nanoparticles are found by *in vitro* release studies to be hydrolysis and nanoparticle disruption by the presence of fat. Cytotoxicity studies conducted in HER2 overexpressing breast cancer cells lines indicate lower IC_{50} values when treated with the Herceptin targeted nanoparticles compared to that treated with the non-targeted version; while the IC_{50} values for the HER2 negative cells lines are unaffected by the addition of the Herceptin targeting agent.

3.2 Introduction

One main objective for the use of targeted delivery of therapeutics is to reduce the proportion of therapeutics reaching the healthy tissues compared to the diseased tissues, such as solid tumors. This can be achieved by passive targeting. Macromolecules such as nanoparticles have an intrinsic ability to passively target solid tumors by preferentially accumulating in this site. This is because solid tumors are characterized by irregular and leaky vasculature with 200 nm to 600 nm pore sizes (*1, 2*) compared to normal vasculature which has pore sizes of 1 to 2 nm. This combined with the impaired lymphatic drainage in the solid tumor vasculature result in the enhanced accumulation of macromolecules in the tumor site. This process is known as the enhanced permeability and retention (EPR) effect (*3*).

Another objective for the use of targeted delivery of therapeutics is to increase the amount of cellular uptake of the therapeutics into the desired cells, in this case, solid tumor cells. This is often achieved by active targeting whereby targeting agents such as antibodies, antibody fragments and peptides are used to engage over-expressed or specific receptors on the cell surfaces for receptor mediated endocytosis. Recent studies show that nanoparticles with and without targeting demonstrate similar biodistribution and amount reaching the tumor site (*4-6*). Yet the targeted nanoparticles show greater tumor reduction efficacy compared to the non-targeted versions. This led to the deduction that active targeting via targeting agents on the surface of nanoparticles enhances cellular uptake of nanoparticles by receptor mediated endocytosis.

The effect of using targeting in the delivery of therapeutics via nanoparticles can

be examined by *in vitro* studies by comparing the cellular uptake of targeted versus non-targeted nanoparticles (*7, 8*). In here, the HER2 overexpressing breast cancer cell line, BT-474 is used to see the effect of targeting on MAP-CPT nanoparticles as well as to determine the optimal amount of the targeting agent, Herceptin, that is required to achieve a higher uptake of nanoparticles compared to the non-targeted version. Competing free Herceptin, and a HER2 negative cell line (MCF-7), are used to determine the specificity of Herceptin targeting.

Cytotoxicity studies of targeted versus non-targeted nanoparticles in cell lines with different expressions of the targeted receptor can also be used to examine the effect of targeting. As well, it is used to determine the toxicity of the components in the delivery system on cells. It is expected that the carrier polymer, MAP and the boronic acid PEG linker between the MAP-CPT nanoparticles and the targeting agent, Herceptin, to show negative or minimal cellular toxicity. In here, four breast cancer cell lines, BT-474, SKBR-3, MCF-7 and MDA-MB-231 with different expressions of HER2 receptors are used.

In vitro release studies are employed to understand the mechanisms of release of therapeutics from its carrier and can be used as a predictor for its *in vivo* behavior. For IT-101, a nanoparticle composed of cyclodextrin-containing polymer conjugate of CPT, it was found that the mechanisms of release of CPT are hydrolysis and enzyme induced release (*9*). In here, a comprehensive examination of the release of CPT from the MAP-CPT nanoparticles in various media and conditions are taken in an attempt to thoroughly understand its release mechanisms.

3.3 Experimental

3.3.1 General

All commercially purchased reagents and solvents including anhydrous and HPLC grade were used without further purification. BT-474, MCF-7, SKBR-3 and MDA-MB-231 breast cancer cell lines were purchased from American Type Culture Collection (Manassas, VA). Female BALB/c mice were purchased from Jackson Laboratory (Bar Harbor, ME). Mice plasma was processed from fresh blood collected from female BALB/c mice. All other reagents were purchased from Sigma (St Louis, MO).

Concentrations of unconjugated CPT and polymer-bound CPT were analyzed on a HPLC system (Agilent) equipped with a fluorescence detector (excitation 370 nm, emission 440 nm) and a reverse phase column (Synergi 4 μm Hydro-RP 80 Å, Phenomenex) complete with guard column. 50% acetonitrile, 50% potassium phosphate buffer (10 mM, pH 4) was used as the eluent at a flow rate of 0.5 ml/min.

Absorbance and other fluorescence measurements were taken on a microplate reader (Infinite 200, Tecan).

3.3.2 Cellular Uptake Studies

24 well plates were seeded with either BT-474 (in RPMI-1640 medium supplemented with 10% fetal calf serum) or MCF-7 (in Dulbecco's Modified Eagle medium supplemented with 10% fetal calf serum) (Cellgro, Manassas, VA) at 20,000

cells per well and kept at 37 ^{o}C in a humidified oven with 5% CO_2. After 40 h, media were replaced with 0.3 ml of fresh media containing either medium MAP-CPT nanoparticles (40 μg CPT/ml), medium MAP-CPT nanoparticles with free Herceptin at 10 mg/ml, targeted MAP-CPT nanoparticles (40 μg CPT/ml) at varying targeting densities or targeted MAP-CPT nanoparticles with free Herceptin at 10 mg/ml. Transfection was conducted for 30 min at 37 ^{o}C. Formulations were then removed and cells washed twice with cold PBS. 200 μl of RIPA buffer was added per well for cell detachment and lysis. Lysed cells were incubated at 4 ^{o}C for 15 min and centrifuged at 14,000 g for 10 min at 4 ^{o}C. A portion of the supernatant was used for protein quantification via BCA assay. To another portion was added an equal amount of 0.1 N NaOH, this was incubated at room temperature overnight and fluorescence was measured at 370/440 nm using known concentrations of medium MAP-CPT nanoparticles as standard.

3.3.3 *In Vitro* Release Studies

Release of CPT from short, medium, long MAP-CPT nanoparticles and targeted MAP-CPT nanoparticles were conducted at 0.32 mg CPT/ml in 1x PBS at pH 6.5, 7 or 7.4; BALB/c mice plasma, human plasma, and 1x PBS at pH 7.4 containing 3 mg/ml of low density lipoprotein (LDL), or 100 units/ml of Butyrylcholinesterase (BCHE) or a combination of LDL and BCHE.

Media pipetted into 96 well plates were incubated at 37 ^{o}C in a humidified oven for 2 h for equilibration. Formulations were mixed into the relevant media and placed

back into the oven. Samples were taken at predetermined time points and immediately frozen at -80 ^{o}C until time for analysis. For release in BALB/c mice plasma and in human plasma, incubation was carried out in a humidified oven at 37 ^{o}C with 5% CO_2 to maintain the carbonic acid/bicarbonate buffer system, the major pH buffer system in plasma at physiological pH levels.

The amount of unconjugated CPT was determined by first mixing 10 µl of sample with 10 µl of 0.1 N HCl and incubating at room temperature for 30 min. 80 µl of methanol was then added and the mixture incubated at room temperature for 3 h for protein precipitation. This mixture was centrifuged at 14,000 g for 10 min at 4 ^{o}C, supernatant was filtered with a 0.45 µm filter (Millex-LH), diluted 20 fold with methanol and 10 µl of the resulting solution injected into HPLC. The peak area of the eluted CPT (at 7.8 min) was compared to that of control. To measure the total amount of CPT, 10 µl of sample was mixed with 6.5 µl of 0.1 N NaOH. This solution was incubated at room temperature for 1 h for CPT to be released from parent polymer. 10 µl of 0.1 N HCl was then added to convert the carboxylate CPT form to the lactone form. 73.5 µl of methanol was subsequently added and mixture incubated for 3 h at room temperature. The sample was then centrifuged and processed as above. Polymer-bound CPT concentration was determined from the difference between total CPT and unconjugated CPT concentrations.

3.3.4 Cytotoxicity Assays

Cells were kept at 37 ^{o}C in a humidified oven with 5% CO_2. BT-474, MCF-7, SKBR-3 and MDA-MB-231 cell lines were incubated in RPMI-1640 medium,

Dulbecco's Modified Eagle medium, McCoy's 5A Modified medium and Dulbecco's Modified Eagle medium respectively (all supplemented with 10% fetal calf serum). 3,000 cells per well were plated into 96 well plates. After 24 h, media was removed and replaced with fresh media containing different concentrations of either medium MAP, nitroPBA-PEG, CPT, medium MAP-CPT nanoparticles, targeted MAP-CPT nanoparticles or Herceptin. After 72 h of incubation, formulations were replaced with fresh media, and 20 μl of CellTiter 96® AQueous One Solution cell proliferation assay (Promega) was added per well. This was incubated for 2 h in a humidified oven at 37 ^{o}C with 5% CO_2 before absorbance measurements at 490 nm. Wells containing untreated cells were used as controls.

3.4 Results and Discussion

3.4.1 Cellular Uptake Studies

BT-474, a HER2 overexpressing human breast cancer cell line, was used to examine the cellular uptake of the Herceptin targeted MAP-CPT nanoparticles versus the non-targeted nanoparticles. MCF-7, a HER2 negative breast cancer cell line, was used as a negative control. It was observed that one Herceptin-PEG-nitroPBA per nanoparticle was sufficient to achieve ca. 70% greater uptake in BT-474 cell line compared to the non-targeted nanoparticle (Figure 3.1A).

Uptake of the targeted MAP-CPT nanoparticles in BT-474 cells showed inhibition in the presence of free Herceptin (Figure 3.1B). In contrast, uptake of the non-targeted MAP-CPT nanoparticles in MCF-7 exhibited no dependence on targeting or on presence of free Herceptin (Figure 3.1B). These data indicate that there is receptor mediated uptake in the BT-474 cells by the targeted MAP-CPT nanoparticles via engagement of the HER2 receptor. Cellular uptake of both the targeted and non-targeted MAP-CPT nanoparticles also occurred via nonspecific fluid phase endocytosis.

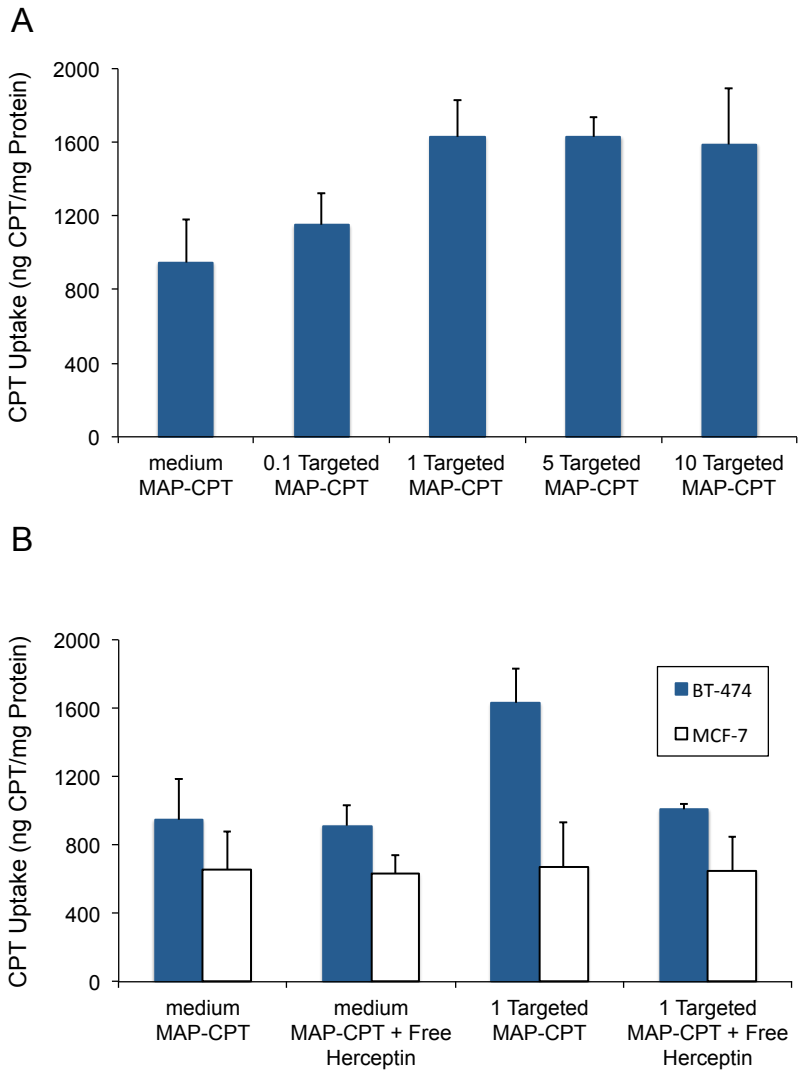

Figure 3.1 Cellular uptake studies. (A) Targeted MAP-CPT nanoparticles at increasing ratio of Herceptin-PEG-nitroPBA to nanoparticle in BT-474. (B) Medium MAP-CPT nanoparticles or targeted MAP-CPT nanoparticles with or without free Herceptin (10 mg/ml) in BT-474 and MCF-7 cell lines.

3.4.3 *In Vitro* Release Studies

Release of CPT from the short, medium, long MAP-CPT nanoparticles and from the targeted MAP-CPT nanoparticles all exhibited first-order kinetics. Release half-lives of CPT from the short, medium and long MAP-CPT nanoparticles were very similar in all conditions tested, while longer half-lives for the targeted MAP-CPT nanoparticles were observed (Table 3.1).

A strong dependence of release rate with pH was observed (Table 3.1). As the pH increased from 6.5 to 7.4, the release half-lives reduced from 338 h to 58 h for the short, medium and long MAP-CPT nanoparticles. These data indicate that hydrolysis plays an important role in the release of CPT.

PBS	$t_{1/2}$ (h)	pH 6.5	pH 7	pH 7.4
	Short, medium, long MAP-CPT	338	178	58
	Targeted MAP-CPT	396	204	78
Plasma	$t_{1/2}$ (h)	Mice	Human	
	Short, medium, long MAP-CPT	59	38	
	Targeted MAP-CPT	63	46	
PBS pH 7.4	$t_{1/2}$ (h)	LDL[a]	BCHE[b]	LDL + BCHE[c]
	Short, medium, long MAP-CPT	45	61	44
	Targeted MAP-CPT	62	76	62

Table 3.1 *In vitro* release half-lives ($t_{1/2}$) of CPT from short, medium and long MAP-CPT nanoparticles, and from targeted MAP-CPT nanoparticles in various media. Abbreviations: PBS, phosphate buffered saline; LDL, low density lipoprotein; BCHE,

Butyrylcholinesterase. [a]PBS, pH 7.4, containing 3 mg/ml LDL. [b]PBS, pH 7.4, containing 100 units/ml BCHE. [c]PBS, pH 7.4, containing 3 mg/ml LDL and 100 units/ml BCHE.

A release half-life of 59 h was observed in BALB/c mice plasma, while a significantly lower half-life of 38 h was obtained in human plasma for the short, medium and long MAP-CPT nanoparticles (Table 3.1). It is known that mice plasma contains more esterase activity than human plasma, while human plasma contains more fat than mice plasma. Therefore, to understand the differences in release rates between human and mice plasma, the contributions of esterase and fat to CPT release rates were individually tested. Butyrylcholinesterase (BCHE) is present in both mice and human plasma and was used to test esterase contribution to the release rate. Low density lipoprotein (LDL) was chosen to test the contribution of fat to the release rate. These components were constituted in PBS (pH 7.4). It was found that the presence of BCHE did not affect release rate (half-life of 61 h compared to 58 h in PBS, pH 7.4, for the short, medium and long MAP-CPT nanoparticles). However, the addition of LDL dramatically increased the release rates (Table 3.1). This effect is likely due to nanoparticle disruption by competing hydrophobic interactions. Therefore, nanoparticle disruption by the presence of fat, and the subsequent CPT cleavage by hydrolysis appears to be another main mechanism of CPT release from MAP-CPT nanoparticles.

In vitro release from the Herceptin targeted MAP-CPT nanoparticles shows longer half-lives than the non-targeted versions (Table 3.1). It is possible that the presence of Herceptin with a pI of 9.2 [17] increased the stability of the negatively

charged nanoparticles by electrostatic interactions, and thus shielded the nanoparticles from some of the hydrolysis and/or competing hydrophobic interactions.

3.4.3 Cytotoxicity Assays

In vitro cytotoxicities of medium MAP, nitroPBA-PEG, CPT, medium MAP-CPT nanoparticles, targeted MAP-CPT nanoparticles and Herceptin were evaluated in two HER2+ breast cancer cell lines (BT-474, SKBR-3) and two HER2- breast cancer cell lines (MCF-7, MDA-MB-231) (Table 3.2).

		MCF-7	MDA-MB-231	SKBR-3	BT-474
HER2 expression		-	-	+	+
IC_{50} (μM)	Medium MAP	>500	>500	>500	>500
	nitroPBA-PEG	>1000	>1000	>1000	>1000
	CPT	0.3	0.1	0.03	4
	Medium MAP-CPT	0.5	0.6	0.2	40
	Targeted MAP-CPT	0.5	0.6	0.1	6
	Herceptin	no effect	no effect	cytostatic	cytostatic

Table 3.2 IC_{50} values of medium MAP, nitroPBA-PEG, CPT, medium MAP-CPT nanoparticles, targeted MAP-CPT nanoparticles and Herceptin in a range of breast cancer cell lines.

Medium MAP and nitroPBA-PEG gave IC_{50} values of above 500 μM and 1000 μM (highest concentrations tested), respectively (Table 3.2), indicating minimal toxicity. IC_{50} concentrations of CPT, medium MAP-CPT nanoparticles and targeted MAP-CPT

nanoparticles were based on the content of the CPT. It is noted that CPT was released gradually from medium MAP-CPT nanoparticles and targeted MAP-CPT nanoparticles (see *In Vitro* Release Studies). Additionally, nanoparticle uptake by cells results in long release times due to the acidic nature of the endosomes. These factors contribute to the observed higher IC_{50} values for the medium MAP-CPT nanoparticles and targeted MAP-CPT nanoparticles compared to CPT (Table 3.2). In HER2+ cell lines, the targeted MAP-CPT nanoparticles gave lower IC_{50} values compared to MAP-CPT alone, while in HER2- cell lines, targeting did not affect the IC_{50}. BT-474 was the most resistant cell line to CPT, and consequently to medium MAP-CPT nanoparticles. The cytostatic nature of Herceptin was observed at the lowest Herceptin concentration tested at 0.001 μM in HER2+ cell lines, while no effect was observed in HER2- cell lines at Herceptin concentrations of up to 0.5 μM.

3.5 Conclusions

Targeted MAP-CPT delivery system was characterized by *in vitro* studies. It was found that a single Herceptin targeting agent is sufficient to achieve greater than 70% cellular uptake of nanoparticles compared to control in BT-474, a HER2 overexpressing cell line, by cellular uptake studies. The main mechanisms of CPT release from MAP-CPT nanoparticles were found to be hydrolysis and particle disruption by the presence of fat by *in vitro* release studies. Cytotoxicity studies conducted in HER2 overexpressing breast cancer cells lines indicate lower IC_{50} values when treated with Herceptin targeted nanoparticles compared to that treated with the non-targeted version; while the IC_{50} values for HER2 negative cells lines are unaffected by the addition of the Herceptin targeting agent.

3.6 References

(1) Yuan, F., Dellian, M., Fukumura, D., Leunig, M., Berk, D. A., Torchilin, V. P., and Jain, R. K. (1995) Vascular-Permeability in a Human Tumor Xenograft - Molecular-Size Dependence and Cutoff Size. *Cancer Research 55*, 3752-3756.

(2) Hobbs, S. K., Monsky, W. L., Yuan, F., Roberts, W. G., Griffith, L., Torchilin, V. P., and Jain, R. K. (1998) Regulation of transport pathways in tumor vessels: Role of tumor type and microenvironment. *Proceedings of the National Academy of Sciences of the United States of America 95*, 4607-4612.

(3) Maeda, H., Wu, J., Sawa, T., Matsumura, Y., and Hori, K. (2000) Tumor vascular permeability and the EPR effect in macromolecular therapeutics: a review. *Journal of Controlled Release 65*, 271-84.

(4) Kirpotin, D. B., Drummond, D. C., Shao, Y., Shalaby, M. R., Hong, K. L., Nielsen, U. B., Marks, J. D., Benz, C. C., and Park, J. W. (2006) Antibody targeting of long-circulating lipidic nanoparticles does not increase tumor localization but does increase internalization in animal models. *Cancer Research 66*, 6732-6740.

(5) Choi, C. H. J., Alabi, C. A., Webster, P., and Davis, M. E. (2010) Mechanism of active targeting in solid tumors with transferrin-containing gold nanoparticles. *Proceedings of the National Academy of Sciences of the United States of America 107*, 1235-1240.

(6) Bartlett, D. W., Su, H., Hildebrandt, I. J., Weber, W. A., and Davis, M. E. (2007) Impact of tumor-specific targeting on the biodistribution and efficacy of siRNA nanoparticles measured by multimodality in vivo imaging. *Proceedings of the National Academy of Sciences of the United States of America 104*, 15549-15554.

(7) Yang, T., Choi, M. K., Cui, F. D., Kim, J. S., Chung, S. J., Shim, C. K., and Kim, D. D. (2007) Preparation and evaluation of paclitaxel-loaded PEGylated immunoliposome. *Journal of Controlled Release 120*, 169-177.

(8) Hong, M. H., Zhu, S. J., Jiang, Y. Y., Tang, G. T., and Pei, Y. Y. (2009) Efficient tumor targeting of hydroxycamptothecin loaded PEGylated niosomes modified with transferrin. *Journal of Controlled Release 133*, 96-102.

(9) Cheng, J. J., Khin, K. T., Jensen, G. S., Liu, A. J., and Davis, M. E. (2003) Synthesis of linear, beta-cyclodextrin-based polymers and their camptothecin conjugates. *Bioconjugate Chemistry 14*, 1007-1017.

Chapter IV

In Vivo Characterization of Targeted MAP-CPT Delivery System

4.1 Abstract

We have developed a new method for assembling targeted nanoparticles that utilizes the complexation between targeting agents that contain boronic acids and polymer-drug conjugates that possess diols. In this chapter, we report the first *in vivo*, antitumor results of a targeted nanoparticle formed via this new assembly methodology. An antibody targeted nanoparticle consisting of a single Herceptin antibody targeting agent and a mucic acid containing polymer-conjugate of camptothecin (MAP-CPT) is evaluated in nude mice bearing HER2 overexpressing BT-474 human breast cancer tumors. Single antibody targeted and non-targeted MAP-CPT nanoparticles show similar biodistributions at 4 and 24 h after intravenous tail vein injection. However, confocal imaging of tumor sections shows faster cancer cellular accumulation of CPT when the targeting agent is present on the nanoparticle. This single Herceptin antibody targeted MAP-CPT nanoparticle system carries ca. 60 CPT molecules per nanoparticle and shows prolonged *in vivo* pharmacokinetics with an elimination half-life of 21.2 h and AUC value of 2766 μg*h/ml at a 10 mg CPT/kg tail vein injection in mice. The maximum tolerated dose (MTD) of the targeted MAP-CPT nanoparticle is found to be 8 mg CPT/kg. Animals treated with non-targeted MAP-CPT nanoparticles at 8 mg CPT/kg show tumor growth inhibition (mean tumor volume of 63 mm^3) when compared to Irinotecan at 80 mg/kg (mean tumor volume of 575 mm^3) and CPT at 8 mg/kg (mean tumor volume of 808 mm^3). Herceptin antibody treatment at 5.9 mg/kg results in 5 out of 8 mice having tumors being completely regressed, and a mean tumor volume of 60 mm^3 at the end of study. Non-targeted MAP-CPT nanoparticles at 1 mg CPT/kg did not show tumor inhibition. However, the single antibody Herceptin-MAP-CPT nanoparticles (5.9 mg

Herceptin/kg and 1 mg CPT/kg) resulted in all treated mice revealing complete tumor regression at the end of study. These results demonstrate that single antibody containing nanoparticles can be formulated, and that these targeted nanoparticles can show significant antitumor efficacy.

4.2 Introduction

Camptothecin is a highly potent, naturally occurring anticancer alkaloid that acts by inhibiting both DNA enzyme topoisomerase I and HIF-1α activities (*1, 2*). However, its systemic delivery is problematic due to its low aqueous solubility and nonspecific toxicity. In addition, its anticancer activity of CPT is derived only from its lactone form. The inactive ring-opened carboxylate form is favored at physiological pH. Furthermore, the carboxylate form binds to human serum albumin (HSA) leading to further CPT ring opening and deactivation (*3*). The FDA approved CPT derivatives Irinotecan and Topotecan are used to treat solid tumors in a variety of cancers, but numerous toxicities remain problematic and play a significant role in their clinical efficacy and safety (*4, 5*).

CPT conjugates to various polymers have been and are currently being evaluated in clinical trials for the treatment of solid tumors (*6-9*). All of these molecular conjugates and nanoparticles seek to exploit the enhanced permeability and retention (EPR) effect that causes the preferential accumulation of macromolecules/nanoparticles in solid tumors (*10*). Active targeting can be gained by functionalizing the surface of nanoparticles with ligands against over-expressed or specific receptors on tumor cell surfaces. Studies show that active targeting improves the efficacy of nanoparticle therapeutics by increasing the cellular uptake of the targeted nanoparticles compared with non-targeted nanoparticles with similar size and surface charge (*11-13*).

In the past years, antibody targeted therapy has received wide attention due to its improved clinical results. One example is the use Herceptin® (Trastuzumab) in combination with chemotherapy or as a single agent after adjuvant chemotherapy to treat

HER2 (human epidermal growth hormone receptor 2) overexpressing metastatic breast cancers (*14, 15*). Herceptin is an antibody against HER2 tyrosine kinase that is overexpressed in 20% to 30% of breast cancers and is associated with resistance to therapy and poor prognosis (*16, 17*). Herceptin containing treatments show better response compared to chemotherapy treatments alone, however a significant proportion of patients treated either do not respond initially or relapse after a period of clinical response (*14, 18, 19*). This resistance to HER2-based therapy has been attributed to signaling through alternate receptor pathways such as insulin-like growth factor-I receptor, or aberrant activation of downstream signaling pathways including phosphatidylinositol 3-kinase pathway, or expression of truncated form of HER2 receptor, p95HER2, or steric hindrance of Herceptin-HER2 receptor interaction (*20, 21*).

Recently, there is great interest in antibody-drug conjugates (*22, 23*) due to the combination of the therapeutic effects from an antibody and an anticancer drug. For instance, Trastuzumab (Herceptin®) Emtansine, composed of a Herceptin antibody conjugated to ca. 3 anticancer drug molecules, DM1 (derivative of maytanosoid), shows better clinical response compared to lapatinib and capecitabine in patients with HER2 overexpressing metastatic breast cancers (*24, 25*). Antibody targeted nanoparticles can be used to increase and protect the payload of anticancer drugs (*26-28*).

We have created a targeted nanoparticle delivery system for CPT through the use of boronic acid-diol complexation. Hydrophobic CPT conjugated onto a biocompatible hydrophilic copolymer of mucic acid and polyethylene glycol (MAP) self-assembled into MAP-CPT nanoparticles. The antibody Herceptin is attached to a boronic acid via a polyethylene glycol (PEG) spacer, and this boronic acid-containing targeting moiety is

complexed with the diol-containing MAP to form a targeted MAP-CPT nanoparticle (Scheme 4.1).

In chapter III, we found that targeting of MAP-CPT nanoparticles via a single Herceptin antibody is capable of achieving receptor mediated uptake in BT-474, a HER2 overexpressing human breast cancer cell line *in vitro*. To date, no single antibody targeted nanoparticle carrying anticancer drugs has been investigated. We therefore examine the biodistribution, pharmacokinetics and antitumor efficacy of targeted versus non-targeted MAP-CPT nanoparticles in a mouse xenograft model using BT-474, to determine whether a single antibody on a nanoparticle can provide targeting *in vivo*.

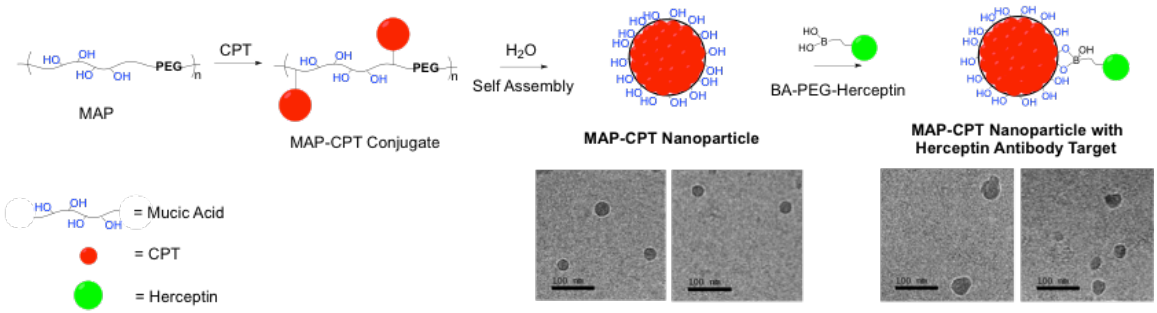

Scheme 4.1 Schematic of targeted MAP-CPT nanoparticle delivery system. MAP = mucic acid and polyethylene glycol copolymer, CPT = camptothecin, BA = boronic acid. Representative cryo-EM images are shown.

4.3 Experimental

4.3.1 General

Breast carcinoma cell line BT-474 was purchased from American Type Culture Collection (Manassas, VA). Cells were maintained in RPMI-1640 medium supplemented with 10% fetal calf serum (Cellgro, Manassas, VA). Female NCr nude mice were purchased from Taconic (Oxnard, CA). 17β-estradiol pellets (0.72 mg, 90 day release) were purchased from Innovative Research of America (Sarasota, FL). Herceptin® (Trastuzumab) was obtained from Dr. Y. Yen at the City of Hope (Duarte, CA). Camptothecin (CPT) was obtained from Boehringer Ingelheim (Ingelheim, Germany). Irinotecan hydrochloride was purchased from Sigma (St Louis, MO). Goat serum was obtained from Vector Laboratories (Burlingame, CA). Rat anti-PEG primary antibody was purchased from AbCam (Cambridge, MA). Alexa Fluor 488 goat anti-rat IgM secondary antibody, Alexa Fluor 633 goat anti-human IgG secondary antibody and Prolong Gold Antifade reagent were obtained from Invitrogen (Grand Island, NY). All other reagents were obtained from Sigma (St Louise, MO) unless otherwise stated.

Medium MAP and nitroPBA-PEG (3-amide-PEG5kDa, 5-nitrophenylboronic acid); short, medium and long MAP-CPT nanoparticles; and targeted MAP-CPT nanoparticles were synthesized as before (Chapter II).

Concentrations of unconjugated CPT and polymer-bound CPT were analyzed on a HPLC system (Agilent) equipped with a fluorescence detector (excitation 370 nm, emission 440 nm) and a reverse phase column (Synergi 4 μm Hydro-RP 80 Å,

Phenomenex) complete with guard column. 50% acetonitrile, 50% potassium phosphate buffer (10 mM, pH 4) was used as the eluent at a flow rate of 0.5 ml/min.

All animals were treated as per National Institute of Health Guidelines for Animal Care and approved by the California Institute of Technology Institutional Animal Care and Use Committee.

4.3.2 Pharmacokinetics in BALB/c Mice

The nanoparticles formulated in 0.9 wt% NaCl (non-targeted nanoparticles) or PBS (targeted MAP-CPT nanoparticles) were administered via bolus, tail vein injection into 12-16 weeks old female BALB/c mice. At predetermined time points, blood was collected via saphenous vein bleed with blood collection tubes (Microvette CB 300 EDTA, Sarstedt). Samples were immediately centrifuged at 10,000 g, 4 ^{o}C for 15 min and supernatant removed and stored at -80 ^{o}C until time for analysis.

The amount of unconjugated CPT was determined by first mixing 10 µl of sample with 10 µl of 0.1 N HCl and incubating at room temperature for 30 min. 80 µl of methanol was then added and the mixture incubated at room temperature for 3 h for protein precipitation. This mixture was centrifuged at 14,000 g for 10 min at 4 ^{o}C, supernatant was filtered with a 0.45 µm filter (Millex-LH), diluted 20 fold with methanol and 10 µl of the resulting solution injected into HPLC. The peak area of the eluted CPT (at 7.8 min) was compared to that of control. To measure the total amount of CPT, 10 µl of sample was mixed with 6.5 µl of 0.1 N NaOH. This solution was incubated at room temperature for 1 h for CPT to be released from parent polymer. 10 µl of 0.1 N HCl was

then added to convert the carboxylate CPT form to the lactone form. 73.5 µl of methanol was subsequently added and mixture incubated for 3 h at room temperature. The sample was then centrifuged and processed as above. Polymer-bound CPT concentration was determined from the difference between total CPT and unconjugated CPT concentrations.

Non-compartmental modeling software PK Solutions 2.0 by Summit Research Services (Montrose, CO) was used for pharmacokinetic data analysis.

4.3.3 Determination of Maximum Tolerable Dose (MTD) in Nude Mice

12 weeks old female NCr nude mice were randomly divided into thirteen groups containing five mice each. Formulations medium MAP or nitroPBA-PEG at 200 mg/kg, short MAP-CPT nanoparticles at 10, 15 or 20 mg/kg (CPT basis), medium MAP-CPT nanoparticles at 8, 10 or 15 mg/kg (CPT basis), long MAP-CPT nanoparticles at 5, 8 or 10 mg/kg (CPT basis) and targeted MAP-CPT nanoparticles at 8 or 10 mg/kg (CPT basis) were administered on day 0 and day 7 via intravenous tail vein injection. All injections were formulated in 0.9 w/v% saline except for targeted MAP-CPT which was formulated in PBS, pH 7.4. Weight and health of the mice were recorded and monitored daily for 2 weeks after the start of the treatment. MTD was defined as the highest dose resulting in less than 15% body weight loss and with no treatment related deaths. Animals were euthanized when criteria for MTD was exceeded or at the end of the study by CO_2 asphyxiation.

4.3.4 Biodistribution in Nude Mice

7 weeks old NCr nude mice were transplanted subcutaneously with 17β-estradiol pellets. After 2 days, BT-474 carcinoma cells suspended in RPMI-1640 medium were injected subcutaneously into the right front flank at 10 million cells/animal. Treatment began a day after the tumors reached an average size of 260 mm^3. Animals were randomized into two groups of six mice per group and treated via intravenous tail vein injections with either medium MAP-CPT nanoparticles at 5 mg CPT/kg (in PBS, pH 7.4) or targeted MAP-CPT nanoparticles at 5 mg CPT/kg and 29 mg Herceptin/kg (in PBS, pH 7.4). After 4 h and 24 h, blood was collected from three animals from each group via saphenous vein bleed. Animals were then euthanized by CO_2 asphyxiation and perfused with PBS. Tumor, lung, heart, spleen, kidney and liver were harvested and sectioned into two equal sized pieces. One piece was embedded in Tissue-Tek® OCT (Sakura) and the other collected in Eppendorf tubes, both were frozen immediately at -80 ^oC until time for processing.

Organs were weighed and 100 mg of each were placed in Lysing Matrix A homogenizer tubes containing an added ¼ inch ceramic sphere (MP Biomedicals, Solon, Ohio). 1 ml of RIPA lysis buffer (Thermo Scientific) was added and tissues were homogenized using a FastPrep®-24 homogenizer (MP Biomedicals, Solon, Ohio) at 6 m/s for 30 s. This was repeated for 3 times with 1 min of cooling on ice in between each round. Samples were then centrifuged at 14,000 g for 15 min at 4 ^oC. The amount of unconjugated CPT was determined by first mixing 10 µl of the supernatant with 10 µl of 0.1 N HCl and incubating at room temperature for 30 min. 80 µl of methanol was then added and the mixture incubated at room temperature for 3 h for protein precipitation.

This mixture was centrifuged at 14,000 g for 10 min at 4 ^{o}C, supernatant was filtered with a 0.45 μm filter (Millex-LH) and 10 μl of the resulting mixture injected into HPLC. The peak area of the eluted CPT (at 7.8 min) was compared to that of control. To measure the total amount of CPT, 10 μl of sample was mixed with 6.5 μl of 0.1 N NaOH. This solution was incubated at room temperature for 1 h for CPT to be released from parent polymer. 10 μl of 0.1 N HCl was then added to convert carboxylate CPT form to lactone form. 73.5 μl of methanol was subsequently added and mixture incubated for 3 h at room temperature. The sample was then centrifuged and processed as above.

4.3.5 Tumor Processing and Confocal Imaging

Tumors were sectioned using a cryostat to a thickness of 20-30 μm. The tumor sections were placed on Superfrost Plus slides (Fisher Scientific, Hampton, NH) and stored at -80 ^{o}C until time for processing. Slides were defrosted and tissue sections were fixed directly onto the slide for 15 min with a 10% formalin solution. The slides were then washed three times with PBS for 5 min each, and blocked for 1 h in a 5% goat serum blocking buffer. A rat anti-PEG primary antibody that recognizes internal PEG units at 14 μg/ml was placed on the section and incubated at 4 ^{o}C overnight. This was followed by three PBS washes and 1 h incubation with 2 μg/ml of Alexa Fluor 488 goat anti-rat IgM secondary antibody. The slides were then washed three times with PBS, and incubated for 1 h with 2 μg/ml of Alexa Fluor 633 goat anti-human IgG secondary antibody to visualize Herceptin. The slides were washed three more times with PBS, mounted with a

Prolong Gold Antifade reagent and stored at 4 ^{o}C until time for imaging. (This was performed by Aaron Gale from the Davis lab).

Images were acquired with a Zeiss LSM 510 Meta Confocal Microscope (Carl Zeiss, Germany) using a 63x Plan-Neofluor oil objective. 2-Photon excitation at 720 nm (emission filter BP 390-465 nm) was used to detect CPT. Excitation at 488 nm (emission filter LP 530) and at 633 nm (emission filter BP 645-700 nm) were used to detect PEG and Herceptin respectively. All laser and gain settings were set at the beginning of imaging and were unchanged. Image analysis was performed on Zeiss lsm image browser. (This was performed by Devin Wiley from the Davis lab).

4.3.6 Antitumor Efficacy Study in Nude Mice

17β-estradiol pellets were transplanted subcutaneously into 7 weeks old NCr nude mice. After 2 days, BT-474 human breast cancer cells suspended in RPMI-1640 medium were injected subcutaneously into the right front flank at 10 million cells/animal. Treatment began a day after tumors reached an average size of 250 mm^3. Animals were randomly divided into nine groups with six to eight mice per group and treated with either, MAP-CPT nanoparticles at 1 mg or 8 mg/kg (CPT basis, in PBS, pH 7.4), CPT at 8 mg/kg (dissolved in 20% DMSO, 20% PEG 400, 30% ethanol and 30% 10 mM pH 3.5 phosphoric acid), Irinotecan at 80 mg/kg (in 5 w/v% dextrose solution, D5W), Herceptin at 2.9 or 5.9 mg/kg (in PBS, pH 7.4), targeted MAP-CPT nanoparticles at 0.5 mg CPT/kg and 2.9 mg Herceptin/kg or 1 mg CPT/kg and 5.9 mg Herceptin/kg (in PBS, pH 7.4), or saline. All treatments were freshly prepared and given via intravenous tail vein injection.

Injections were standardized at 150 µl per 20 g body weight of mice. Treatments containing Herceptin were given once per week for 2 weeks, all other groups were given once per week for 3 weeks. Tumor sizes were recorded thrice a week using caliper measurements (length x $width^2/2$) and health of the animals was continuously monitored. Animals were euthanized when tumor volumes exceeded 1000 mm^3. 6 weeks after beginning of the treatment, animals were euthanized by CO_2 asphyxiation.

When animals exited the study due to tumor size exceeding limit, treatment related or non-treatment related deaths, the last tumor volume value recorded was included in the subsequent time points. Two-tailed statistical analyses were conducted at $P = 0.05$. Results were considered significant at $0.01 \leq P \leq 0.05$ and highly significant at $P < 0.01$.

4.4 Results and Discussion

4.4.1 Pharmacokinetics in BALB/c Mice

Plasma pharmacokinetic studies of short, medium, long MAP-CPT nanoparticles and targeted MAP-CPT nanoparticles at 10 mg/kg (CPT basis) injections were conducted in female BALB/c mice (Figure 4.1). Non-compartmental modeling was used for data analysis (Table 4.1).

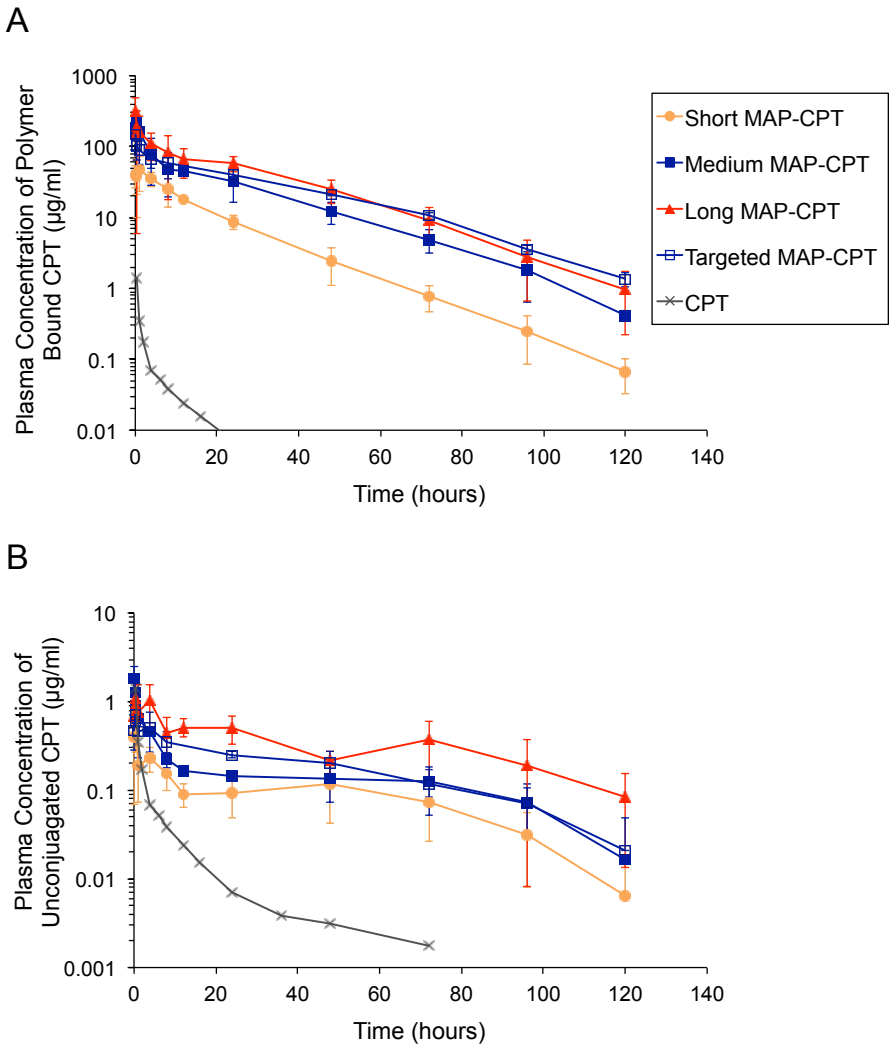

Figure 4.1 Plasma pharmacokinetics of short, medium and long MAP-CPT nanoparticles and targeted MAP-CPT nanoparticles in BALB/c mice at 10 mg CPT/kg injections. Free CPT injected at 10 mg/kg into CD2F1 mice is shown as comparison (*30*). (A) Plasma concentration of polymer-bound CPT as a function of time. (B) Plasma concentration of unconjugated CPT as a function of time.

Polymer-bound CPT for all nanoparticles displayed a biphasic profile with a fast redistribution phase (α) and a long elimination phase (β) (Figure 4.1A). The elimination phase for medium and long MAP-CPT nanoparticles were particularly prolonged with half-lives of 16.6 and 17.6 h respectively and high AUC values of 2298 and 3636 μg*h/ml, respectively. Additionally, they show low volume of distributions and clearance rates. 24 h after injection, 11.3% of injected dose of medium MAP-CPT nanoparticles and 20.5% of injected dose of long MAP-CPT nanoparticles were still circulating in plasma as polymer-bound CPT. In contrast, mice injected with CPT alone at 10 mg/kg showed fast clearance, with an AUC of only 1.6 μg*h/ml and 0.01% of injected dose remaining in circulation after 8 h (modified from reference *30*). Targeting of medium MAP-CPT nanoparticles affected the pharmacokinetic profile by increasing the redistribution phase and prolonging the elimination phase to 21.2 h with a high AUC value of 2766 μg*h/ml. The amounts of unbound CPT in plasma for all nanoparticles were low at all time points (Figure 4.1B).

	$t_{1/2}$ α (h)	$t_{1/2}$ β (h)	AUC (μg h/ml)	Vd (ml)	Cl (ml/h)
Short MAP-CPT	0.6	13.2	728	6.5	0.34
Medium MAP-CPT	1.0	16.6	2298	2.6	0.11
Long MAP-CPT	0.4	17.6	3636	1.7	0.07
Targeted MAP-CPT	0.2	21.2	2766	2.8	0.09
CPT	-	-	1.6	5538	156

Table 4.1 Plasma pharmacokinetic parameters of polymer-bound CPT for short, medium and long MAP-CPT nanoparticles, and targeted MAP-CPT nanoparticles compared to CPT alone. Abbreviations: $t_{1/2}$ α, redistribution half-life; $t_{1/2}$ β, elimination half-life; AUC, area under curve; Vd, volume of distribution and Cl, systemic clearance.

4.4.2 Determination of Maximum Tolerable Dose (MTD) in Nude Mice

MTD values were determined in female NCr nude mice and defined as the highest dose resulting in less than 15% body weight loss and with no treatment related deaths. Mice treated with medium MAP, nitroPBA-PEG, short, medium and long MAP-CPT and targeted MAP-CPT were tracked for weight and monitored for health after two weekly doses on day 0 and day 7 (Figure 4.2).

The weight and health of the mice were unaffected by treatment at high doses of medium MAP or nitroPBA-PEG indicating minimal toxicity of these polymeric components. For groups containing CPT, maximum weight loss appeared 3 to 5 days after each treatment. Most of the groups gained back the lost weight. If body weight loss continued and exceeded an average of 15%, then the study was concluded. Some mice in groups treated with medium MAP-CPT at 15 mg/kg and long MAP-CPT at 10 mg/kg showed diarrhea and appeared weak. All other mice appeared healthy. MTD values were

found to be 20, 10, 8 and 8 mg/kg (on CPT basis) for short, medium, long MAP-CPT and targeted MAP-CPT respectively (Table 4.2).

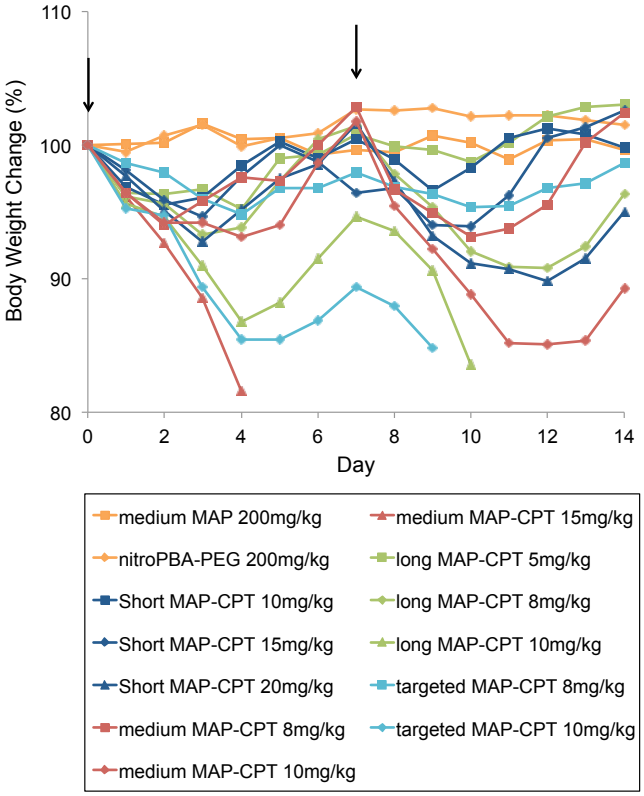

Figure 4.2 Determination of maximum tolerable dose (MTD) in female NCr nude mice. Arrows indicate treatments; all groups containing CPT are based on mg CPT/kg.

	Dose (mg/kg)[a]	Max % weight loss (day)[b]	Death
medium MAP	200	-1.1 (11)	0
nitroPBA-PEG	200	-0.5 (2)	0
short MAP-CPT	10	-4.5 (2)	0
short MAP-CPT	15	-6.1 (10)	0
short MAP-CPT	20	-10.2 (12)	0
medium MAP-CPT	8	-6.8 (10)	0
medium MAP-CPT	10	-14.9 (12)	0
medium MAP-CPT	15	-18.4 (4)	culled[c]
long MAP-CPT	5	-4.8 (4)	0
long MAP-CPT	8	-9.2 (12)	0
long MAP-CPT	10	-16.5 (10)	culled[c]
targeted MAP-CPT	8	-5.2 (4)	0
targeted MAP-CPT	10	-15.2 (9)	culled[c]

Table 4.2 Treatment response for maximum tolerable dose (MTD) study. [a]All groups containing MAP-CPT are based on mg CPT/kg. [b]Maximum percent body weight loss. [c]Animals culled due to exceeding 15% body weight loss.

4.4.3 Biodistribution in Nude Mice

The average percentage injected dose (ID) of total CPT per gram of tumor, heart, liver, spleen, kidney and lung is shown in Figure 4.3. After 4 h, 5.3 and 5.2% ID of total CPT were present in tumors for mice treated with MAP-CPT nanoparticles and targeted MAP-CPT nanoparticles respectively. 24 h after treatment, 2.6% ID of total CPT remained in tumors for MAP-CPT nanoparticles, while 3.2% ID of total CPT were found in tumors for targeted MAP-CPT nanoparticles. This indicates that targeting on nanoparticles does not increase tumor localization compared with non-targeted version and is consistent with literature observations (*11-13*). Animals treated with MAP-CPT nanoparticles and targeted MAP-CPT nanoparticles show similar distribution of CPT in

heart, liver, kidney and lung. There was, however, a comparatively significant amount of total CPT accumulation in the spleen for targeted MAP-CPT versus non-targeted at 24 h. This effect has been observed previously for humanized antibodies in mice (*29*).

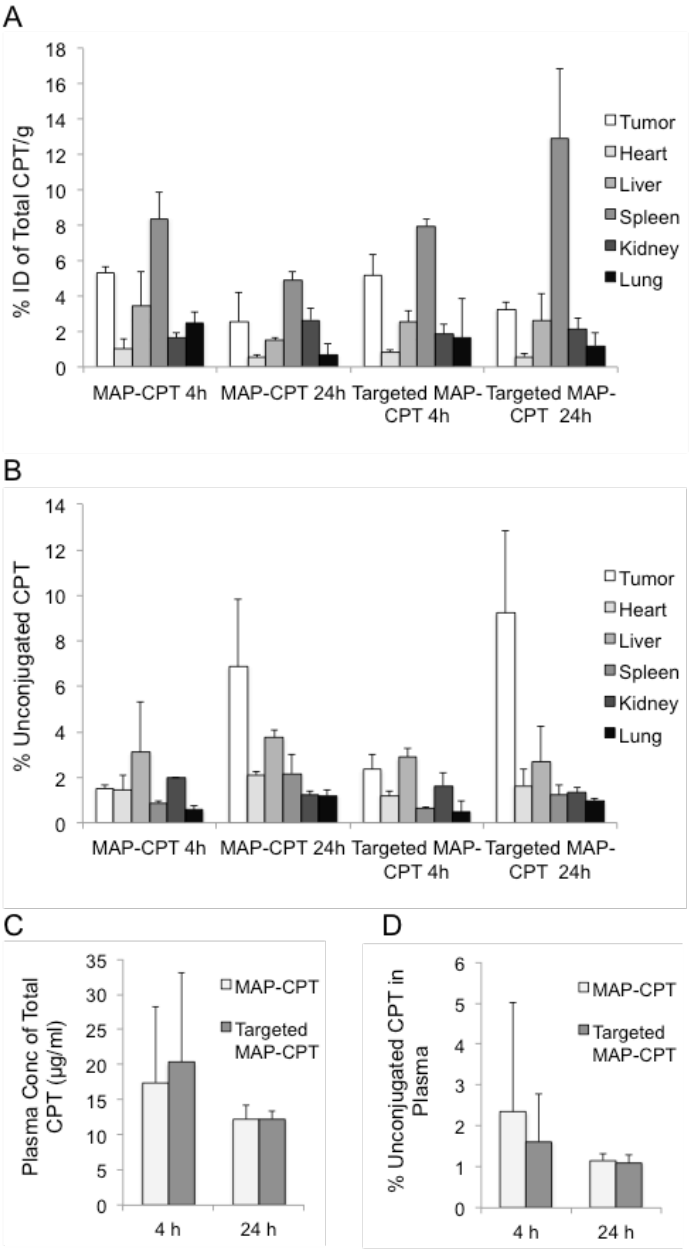

Figure 4.3 Biodistribution of MAP-CPT nanoparticles (5 mg CPT/kg) and targeted MAP-CPT nanoparticles (5 mg CPT/kg, 29 mg Herceptin/kg) after 4 and 24 h of

treatment. (A) Percent injected dose (ID) of total CPT per gram of tumor, heart, liver, spleen, kidney or lung. (B) Percentage of total CPT in each organ that is unconjugated in tumor, heart, liver, spleen, kidney and lung. (C) Plasma concentration of total CPT. (D) Percentage of total CPT that is unconjugated in plasma.

Figure 4.3B shows the average percentage of total CPT that was unconjugated in tumor, heart, liver, spleen, kidney and lung. The percentage unconjugated in heart, liver, spleen, kidney and lung were low at both 4 h and 24 h indicating fast clearance of free CPT from these organs. In tumor at 24 h, there were significantly higher percentages of unconjugated CPT for both MAP-CPT and targeted MAP-CPT nanoparticles compared to that at 4 h. The retention of free CPT within the tumor suggests cellular accumulation of CPT. The targeted nanoparticles show slightly higher percentage of unconjugated CPT in tumors for mice compared to the non-targeted nanoparticles at both 4 and 24 h.

The total plasma CPT concentration and percentage of total plasma CPT that was unconjugated were similar for both MAP-CPT and targeted MAP-CPT nanoparticles (Figure 4.3C). After 4 h, 17 and 20 μg/ml of total CPT remained in plasma for MAP-CPT and targeted MAP-CPT nanoparticles respectively. After 24 h, the amounts of total CPT remaining in plasma were the same for both MAP-CPT and targeted MAP-CPT nanoparticles at 12 μg/ml. The percentage of total CPT that is unconjugated in plasma was below 3% for all conditions indicating small release and fast clearance of unconjugated CPT from plasma (Figure 4.3D).

4.4.4 Confocal Imaging

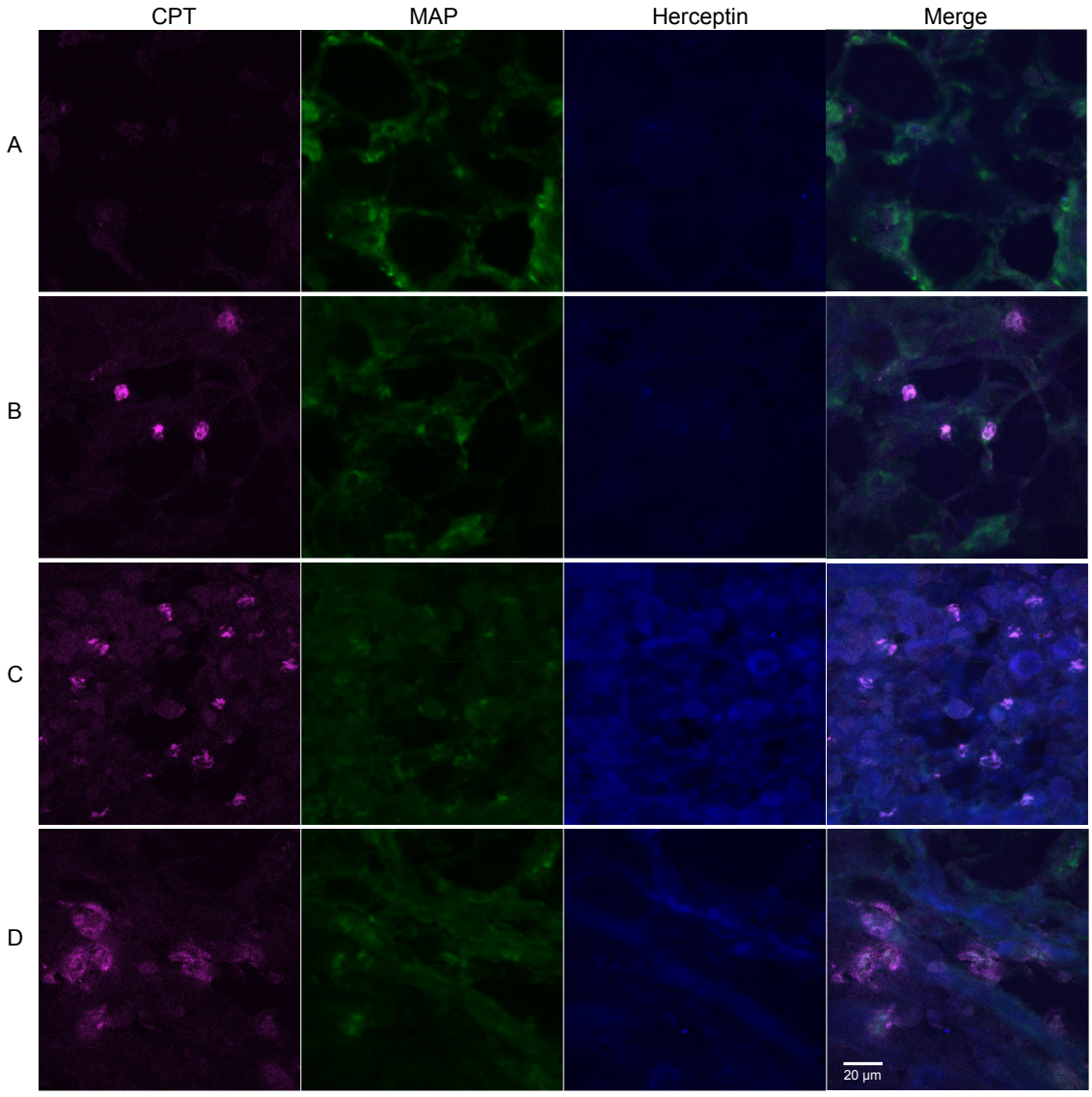

Figure 4.4 Confocal immunofluorescence microscopy of BT-474 tumor sections taken from NCr nude mice treated with (A) MAP-CPT (5 mg CPT/kg) at 4 h (B) MAP-CPT (5 mg CPT/kg) at 24 h. (C) Targeted MAP-CPT (5 mg CPT/kg, 29 mg Herceptin/kg) at 4 h. (D) Targeted MAP-CPT (5 mg CPT/kg, 29 mg Herceptin/kg) at 24 h. Left panel emission 440 nm (CPT, pink), center left panel emission 519 nm (MAP, green), center right panel emission 647 nm (Herceptin, blue), right panel overlay of images.

BT-474 tumor bearing NCr nude mice were treated with either MAP-CPT (5 mg CPT/kg) or targeted MAP-CPT (5 mg CPT/kg, 29 mg Herceptin/kg). After 4 and 24 h, mice were euthanized, tumors were removed and processed for confocal immunofluorescence imaging. CPT is naturally fluorescent with emission at 440 nm. To identify the location of MAP, the PEG within MAP was stained with anti-PEG antibody, then stained with secondary antibody containing Alexa Fluor 488 (emission 519 nm). All tumor sections were stained for Herceptin with an anti-human IgG labeled with Alexa Fluor 633 (emission 647 nm). Tumor section images were all taken at the same laser power and gain settings. Representative images are shown for each group in Figure 4.4.

Figure 4.4A shows tumor section of mice treated with MAP-CPT nanoparticles after 4 h. CPT signal was disperse. Signals for CPT and MAP appeared to colocalize in the merged image. 24 h after injection, there was accumulation of CPT signal in the form of punctate spots (Figure 4.4B). The merged image suggests colocalization of CPT and MAP. For mice treated with targeted MAP-CPT nanoparticles, spots indicating CPT accumulation were observed after both 4 and 24 h of treatment (Figure 4.4C and 4.4D). In the merged images, there was colocalization of CPT and MAP signals. The presence of Herceptin in targeted MAP-CPT nanoparticles is indicated by the strong blue signals in the Herceptin channel compared with weak background signals in the non-targeted version. In addition, the observation of CPT accumulation at both 4 and 24 h time points for mice treated with targeted MAP-CPT nanoparticles, while for mice treated with non-targeted MAP-CPT nanoparticles, accumulation of CPT was only appeared at 24 h suggests that the presence of Herceptin targeting may speed up the cellular accumulation

of CPT. This is likely through the cellular uptake of nanoparticles via receptor mediated endocytosis.

4.4.5 Antitumor Efficacy Study in Nude Mice

To promote tumor growth in nude mice, 17β-estradiol pellets were implanted two days prior to BT-474 tumor cell implantation. Tumors grew rapidly. On day 0 (five days after implantation), tumor sizes of each group averaged 250 mm^3. Treatments began on day 1. Irinotecan was administered at a dose of 80 mg/kg in D5W. CPT is highly insoluble in aqueous solutions, therefore it was dissolved in a solution containing 20% DMSO, 20% PEG 400, 30% ethanol and 30% 10 mM pH 3.5 phosphoric acid. Irinotecan and CPT were both administered via intravenous tail vein injection to be consistent with the rest of the treatment groups. A saline treatment group was used as the control. All other treatments were administered in PBS, at pH 7.4. Changes in tumor sizes were recorded by caliper measurement three times a week and health of the animals were continuously monitored (Figure 4.5 and Table 4.3).

Tumors in control group administered with saline grew rapidly. After 28 days, five out of eight mice had tumors exceeding size limit of 1000 mm^3. All animals in this group were euthanized at this time.

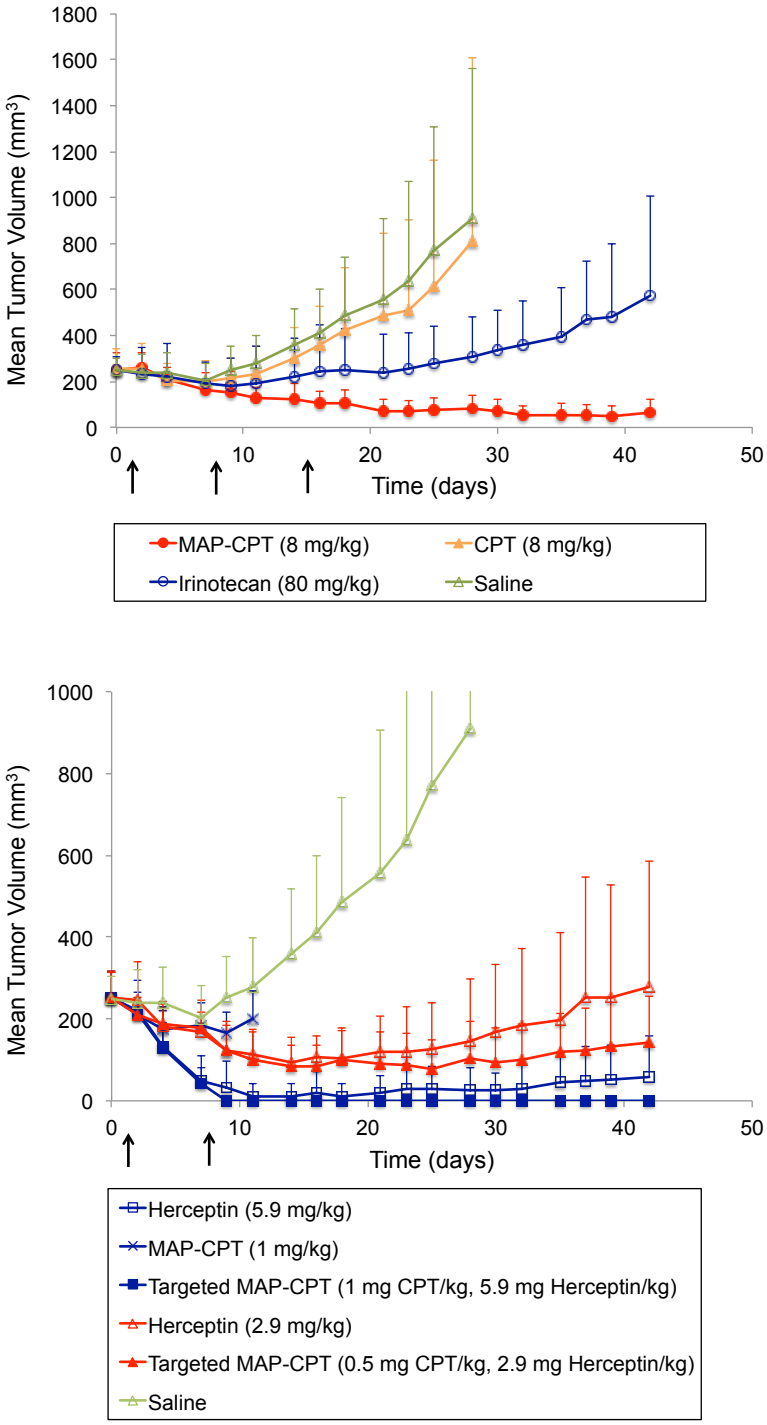

Figure 4.5 Antitumor efficacy study in NCr nude mice bearing BT-474 xenograft tumors. Mean tumor volume as a function time; groups containing Herceptin received 2 weekly doses; all other groups received 3 weekly doses.

Group treated with CPT (8 mg/kg) resulted in no tumor inhibition compared to that of the control group ($P > 0.05$). One and three treatment related deaths were recorded on day 9 and 16 respectively, as well as four euthanizations due to exceeding tumor size limit on day 28. None of the animals survived to the end of the study.

Irinotecan treated mice at 80 mg/kg showed non-significant tumor inhibition compared to control group ($P > 0.05$). One treatment related death occurred on day 11. Tumor sizes reached an average of 575 mm^3 by the end of the study.

Animals receiving MAP-CPT nanoparticles at 8 mg CPT/kg showed highly significant tumor inhibition compared to that of control group ($P < 0.01$). By the end of the study the mean tumor size reduced to 63 mm^3 and three out of the eight mice treated had tumor sizes regressed to zero. Although no death occurred in MTD study using non-tumor bearing NCr nude mice treated with MAP-CPT nanoparticles at 8 mg CPT/kg, one death occurred due to weight loss in this study on day 21. This maybe because of the added tumor burden in this study and/or because mice used in this study were 7 weeks old, while in MTD studies, 12 weeks old mice were used.

	N_{begin}/N_{end}[a]	$N_{TRD}/N_{NTRD}/N_{euthan}$[b]	Mean tumor volume (mm^3)	Median tumor volume (mm^3)	$N_{reg\ to\ zero}$[c]	P vs saline[d]
MAP-CPT (8 mg/kg)	8/7	1/0/0	63	68	3	0.002
Irinotecan (80 mg/kg)	8/7	1/0/0	575	479	0	0.242
CPT (8 mg/kg)	8/0	4/0/4	808	417	0	0.781
Herceptin (5.9 mg/kg)	8/8	0/0/0	60	0	5	0.003
Targeted MAP-CPT (1 mg CPT/kg, 5.9 mg Herceptin/kg)	8/7	0/1/0	0	0	7	0.001
Herceptin (2.9 mg/kg)	6/6	0/0/0	278	245	2	0.026
Targeted MAP-CPT (0.5 mg CPT/kg, 2.9 mg Herceptin/kg)	6/6	0/0/0	141	187	2	0.005
Saline	8/0	0/0/8	911	1087	0	-

Table 4.3 Antitumor efficacy study in NCr nude mice bearing BT-474 xenograft tumors. [a]N_{begin} is number of animals at beginning of study, N_{end} is number of animals surviving to

end of study. [b]N_{TRD} is number of treatment related death, N_{NTRD} is number of non-treatment related death, N_{euthan} is number of animals euthanized due to exceeding tumor size limit of 1000 mm3. [c]$N_{reg\ to\ zero}$ is number of animals with tumors regressed to zero at the end of study.

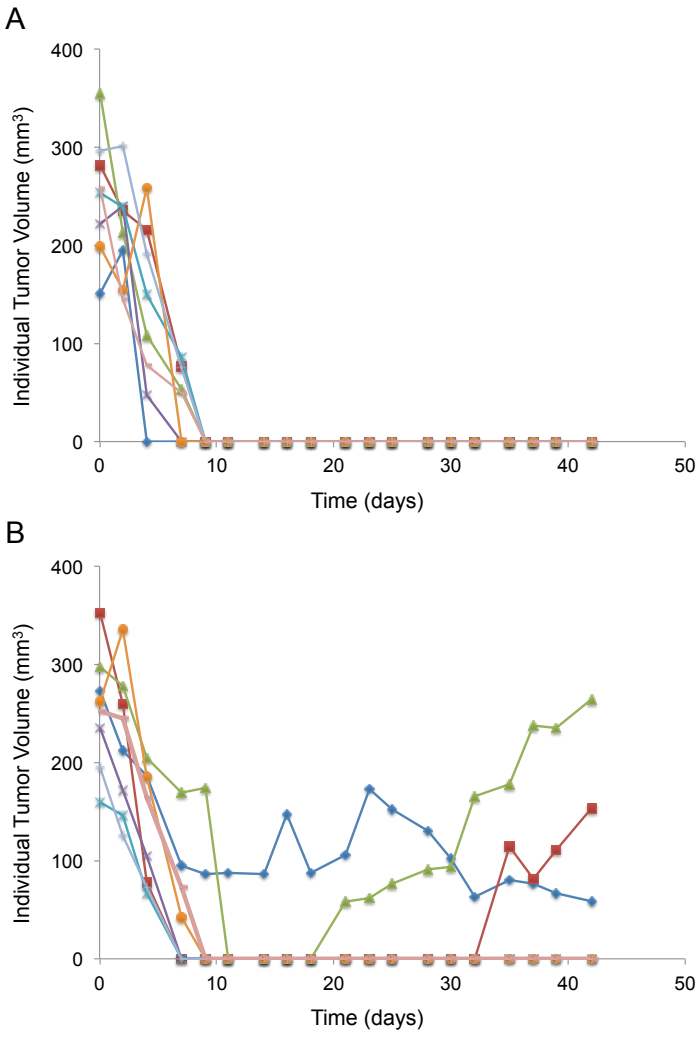

Figure 4.6 Individual tumor volumes for NCr nude mice bearing BT-474 xenograft tumors treated with (A) Targeted MAP-CPT nanoparticles (1 mg CPT/kg and 5.9 mg Herceptin/kg) and with (B) Herceptin at 5.9 mg/kg.

Animals treated with Herceptin at 5.9 mg/kg showed highly significant tumor inhibition compared to control group ($P < 0.01$). On day 11 of treatment, seven out of the eight animals treated had tumors regressed to zero. However, by the end of the study, two of the regressed tumors relapsed resulting in a total of five animals with tumors at zero volume and a group mean tumor volume of 60 mm^3 (Figure 4.6). MAP-CPT nanoparticles at 1 mg CPT/kg group was terminated early due to no observed antitumor effects. Nevertheless, when Herceptin at 5.9 mg/kg was added as a targeting agent via a nitroPBA-BA linker onto the MAP-CPT nanoparticles at a low CPT dosage of 1 mg/kg (targeted MAP-CPT at 1 mg CPT/kg and 5.9 mg Herceptin/kg group), all tumors regressed to zero on day 9 of treatment and remained at zero by the end of the study (Figure 4.6). One non-treatment related death occurred on day 37. This result is highly significant compared to control group ($P < 0.01$). The combination of results observed for these three groups indicates that there is improved efficacy of the MAP-CPT nanoparticles by the addition of the Herceptin targeting agent in addition to the intrinsic activity of the Herceptin.

Animals treated with Herceptin at 2.9 mg/kg resulted in two animals having tumors regressed to zero by the end of study. However, the average tumor size increased from the beginning of the study to 278 mm^3. This result is significant compared to control group ($0.01 \leq P \leq 0.05$). When animals were treated with targeted MAP-CPT nanoparticles containing 0.5 mg CPT/kg and 2.9 mg Herceptin/kg, two tumors regressed to zero. The average tumor size reduced to 141 mm^3 by the end of the study. This result is highly significant compared to control group ($P < 0.01$). These results further suggest the benefits of targeting in tumor inhibition.

5 weeks after 17β-estradiol pellets implantation, several mice irrespective of treatment groups were observed to have distended bladder and abdominal bloating. This was likely due to the use of 17β-estradiol pellets, which causes hydronephrosis and urine retention in athymic nude mice (*31*). 6 weeks after treatment, conditions became worse and more mice were observed to develop distended bladders and abdominal bloating, thus animals were euthanized and experiment was terminated.

4.5 Conclusions

Targeted MAP-CPT delivery system was characterized by *in vivo* studies. Single Herceptin antibody targeted and non-targeted MAP-CPT nanoparticles showed similar biodistributions at 4 and 24 h after intravenous tail vein injection. However, confocal imaging of tumor sections suggested faster tumor cellular accumulation of CPT when the targeting agent is present on the nanoparticle. This Herceptin antibody targeted MAP-CPT nanoparticle system demonstrated prolonged *in vivo* pharmacokinetics with an elimination half-life of 21.2 h and AUC value of 2766 μg*h/ml at a 10 mg CPT/kg tail vein injection in mice. Animals treated with non-targeted MAP-CPT nanoparticles at 8 mg CPT/kg showed significant tumor growth inhibition when compared to Irinotecan at 80 mg/kg and CPT at 8 mg/kg. Herceptin antibody treatment at 5.9 mg/kg resulted in 5 out of 8 mice having tumors being completely regressed, and a mean tumor volume of 60 mm^3 at the end of study. Non-targeted MAP-CPT nanoparticles at 1 mg CPT/kg did not show tumor inhibition. However, the single antibody Herceptin-MAP-CPT nanoparticles (5.9 mg Herceptin/kg and 1 mg CPT/kg) resulted in all treated mice showing complete tumor regression at the end of study.

4.6 References

(1) Hsiang, Y. H., Hertzberg, R., Hecht, S., and Liu, L. F. (1985) Camptothecin Induces Protein-Linked DNA Breaks Via Mammalian DNA Topoisomerase-I. *J Biol Chem 260*, 4873-4878.

(2) Rapisarda, A., Uranchimeg, B., Scudiero, D. A., Selby, M., Sausville, E. A., Shoemaker, R. H., and Melillo, G. (2002) Identification of small molecule inhibitors of hypoxia-inducible factor 1 transcriptional activation pathway. *Cancer Research 62*, 4316-4324.

(3) Mi, Z. H., and Burke, T. G. (1994) Marked Interspecies Variations Concerning the Interactions of Camptothecin with Serum Albumins - a Frequency-Domain Fluorescence Spectroscopic Study. *Biochemistry 33*, 12540-12545.

(4) Xu, Y., and Villalona-Calero, M. A. (2002) Irinotecan: mechanisms of tumor resistance and novel strategies for modulating its activity. *Annals of Oncology 13*, 1841-1851.

(5) Tian, Q., Zhang, J., Chan, S. Y., Tan, T. M. C., Duan, W., Huang, M., Zhu, Y. Z., Chan, E., Yu, Q., Nie, Y. Q., Ho, P. C. L., Li, Q., Ng, K. Y., Yang, H. Y., Wei, H., Bian, J. S., and Zhou, S. F. (2006) Topotecan is a substrate for multidrug resistance associated protein 4. *Curr Drug Metab 7*, 105-116.

(6) Svenson, S., Wolfgang, M., Hwang, J., Ryan, J., and Eliasof, S. (2011) Preclinical to clinical development of the novel camptothecin nanopharmaceutical CRLX101. *Journal of Controlled Release 153*, 49-55.

(7) Homsi, J., Simon, G. R., Garrett, C. R., Springett, G., De Conti, R., Chiappori, A., Munster, P. N., Burton, M. K., Stromatt, S., Allievi, C., Angiulli, P., Eisenfeld, A., Sullivan, D. M., and Daud, A. I. (2007) Phase I trial of poly-L-glutamate camptothecin (CT-2106) administered weekly in patients with advanced solid malignancies. *Clinical Cancer Research 13*, 5855-5861.

(8) Yurkovetskiy, A. V., and Fram, R. J. (2009) XMT-1001, a novel polymeric camptothecin pro-drug in clinical development for patients with advanced cancer. *Advanced Drug Delivery Reviews 61*, 1193-1202.

(9) Scott, L., Yao, J., Benson, A. B., Thomas, A., Falk, S., Mena, R., Picus, J., Wright, J., Mulcahy, M., Ajani, J., and Evans, T. (2009) A phase II study of pegylated-camptothecin (pegamotecan) in the treatment of locally advanced and metastatic gastric and gastro-oesophageal junction adenocarcinoma. *Cancer Chemotherapy and Pharmacology 63*, 363-370.

(10) Maeda, H., Wu, J., Sawa, T., Matsumura, Y., and Hori, K. (2000) Tumor vascular permeability and the EPR effect in macromolecular therapeutics: a review. *Journal of Controlled Release 65*, 271-284.

(11) Kirpotin, D. B., Drummond, D. C., Shao, Y., Shalaby, M. R., Hong, K. L., Nielsen, U. B., Marks, J. D., Benz, C. C., and Park, J. W. (2006) Antibody targeting of long-circulating lipidic nanoparticles does not increase tumor localization but does increase internalization in animal models. *Cancer Research 66*, 6732-6740.

(12) Bartlett, D. W., Su, H., Hildebrandt, I. J., Weber, W. A., and Davis, M. E. (2007) Impact of tumor-specific targeting on the biodistribution and efficacy of siRNA nanoparticles measured by multimodality in vivo imaging. *Proceedings of the National Academy of Sciences of the United States of America 104*, 15549-15554.

(13) Choi, C. H. J., Alabi, C. A., Webster, P., and Davis, M. E. (2010) Mechanism of active targeting in solid tumors with transferrin-containing gold nanoparticles. *Proceedings of the National Academy of Sciences of the United States of America 107*, 1235-1240.

(14) Slamon, D. J., Leyland-Jones, B., Shak, S., Fuchs, H., Paton, V., Bajamonde, A., Fleming, T., Eiermann, W., Wolter, J., Pegram, M., Baselga, J., and Norton, L. (2001) Use of chemotherapy plus a monoclonal antibody against HER2 for metastatic breast cancer that overexpresses HER2. *New Engl J Med 344*, 783-792.

(15) Smith, I., Procter, M., D Gelber, R., Guillaume, S., Feyereislova, A., Dowsett, M., Goldhirsch, A., Untch, M., Mariani, G., Baselga, J., Kaufmann, M., Cameron, D., Bell, R., Bergh, J., Coleman, R., Wardley, A., Harbeck, N., Lopez, R. I., Mallmann, P., Gelmon, K., Wilcken, N., Wist, E., Rovira, P. S., and Piccart-Gebhart, M. (2007) 2-year follow-up of trastuzumab after adjuvant chemotherapy in HER2-positive breast cancer: a randomised controlled trial. *Lancet 369*, 29-36.

(16) Slamon, D. J., Clark, G. M., Wong, S. G., Levin, W. J., Ullrich, A., and Mcguire, W. L. (1987) Human-Breast Cancer - Correlation of Relapse and Survival with Amplification of the Her-2 Neu Oncogene. *Science 235*, 177-182.

(17) Slamon, D. J., Godolphin, W., Jones, L. A., Holt, J. A., Wong, S. G., Keith, D. E., Levin, W. J., Stuart, S. G., Udove, J., Ullrich, A., and Press, M. F. (1989) Studies of the Her-2/Neu Proto-Oncogene in Human-Breast and Ovarian-Cancer. *Science 244*, 707-712.

(18) Cobleigh, M. A., Vogel, C. L., Tripathy, D., Robert, N. J., Scholl, S., Fehrenbacher, L., Wolter, J. M., Paton, V., Shak, S., Lieberman, G., and Slamon, D. J. (1999) Multinational study of the efficacy and safety of humanized anti-HER2 monoclonal antibody in women who have HER2-overexpressing metastatic breast cancer that has progressed after chemotherapy for metastatic disease. *Journal of Clinical Oncology 17*, 2639-2648.

(19) Vogel, C. L., Cobleigh, M. A., Tripathy, D., Gutheil, J. C., Harris, L. N., Fehrenbacher, L., Slamon, D. J., Murphy, M., Novotny, W. F., Burchmore, M., Shak, S., Stewart, S. J., and Press, M. (2002) Efficacy and safety of trastuzumab as a single agent in first-line treatment of HER2-overexpressing metastatic breast cancer. *Journal of Clinical Oncology 20*, 719-726.

(20) Nahta, R., Yu, D. H., Hung, M. C., Hortobagyi, G. N., and Esteva, F. J. (2006) Mechanisms of disease: understanding resistance to HER2-targeted therapy in human breast cancer. *Nat Clin Pract Oncol 3*, 269-280.

(21) Pohlmann, P. R., Mayer, I. A., and Mernaugh, R. (2009) Resistance to Trastuzumab in Breast Cancer. *Clinical Cancer Research 15*, 7479-7491.

(22) Casi, G., and Neri, D. (2012) Antibody-drug conjugates: Basic concepts, examples and future perspectives. *Journal of Controlled Release 161*, 422-428.

(23) Adair, J. R., Howard, P. W., Hartley, J. A., Williams, D. G., and Chester, K. A. (2012) Antibody-drug conjugates - a perfect synergy. *Expert Opin Biol Th 12*, 1191-1206.

(24) Phillips, G. D. L., Li, G. M., Dugger, D. L., Crocker, L. M., Parsons, K. L., Mai, E., Blattler, W. A., Lambert, J. M., Chari, R. V. J., Lutz, R. J., Wong, W. L. T., Jacobson, F. S., Koeppen, H., Schwall, R. H., Kenkare-Mitra, S. R., Spencer, S. D., and Sliwkowski, M. X. (2008) Targeting HER2-Positive Breast Cancer with Trastuzumab-DM1, an Antibody-Cytotoxic Drug Conjugate. *Cancer Research 68*, 9280-9290.

(25) Verma, S., Miles, D., Gianni, L., Krop, I. E., Welslau, M., Baselga, J., Pegram, M., Oh, D. Y., Dieras, V., Guardino, E., Fang, L., Lu, M. W., Olsen, S., and Blackwell, K. (2012) Trastuzumab emtansine for HER2-positive advanced breast cancer. *The New England Journal of Medicine 367*, 1783-1791.

(26) Drummond, D. C., Noble, C. O., Guo, Z., Hayes, M. E., Connolly-Ingram, C., Gabriel, B. S., Hann, B., Liu, B., Park, J. W., Hong, K., Benz, C. C., Marks, J. D., and Kirpotin, D. B. (2010) Development of a highly stable and targetable

nanoliposomal formulation of topotecan. *Journal of Controlled Release 141*, 13-21.

(27) Yang, T., Choi, M. K., Cui, F. D., Kim, J. S., Chung, S. J., Shim, C. K., and Kim, D. D. (2007) Preparation and evaluation of paclitaxel-loaded PEGylated immunoliposome. *Journal of Controlled Release 120*, 169-177.

(28) Hong, M. H., Zhu, S. J., Jiang, Y. Y., Tang, G. T., and Pei, Y. Y. (2009) Efficient tumor targeting of hydroxycamptothecin loaded PEGylated niosomes modified with transferrin. *Journal of Controlled Release 133*, 96-102.

(29) Cheng, W. W. K., and Allen, T. M. (2008) Targeted delivery of anti-CD19 liposomal doxorubicin in B-cell lymphoma: A comparison of whole monoclonal antibody, Fab' fragments and single chain Fv. *Journal of Controlled Release 126*, 50-58.

(30) Supko, J. G., and Malspeis, L. (1993) Pharmacokinetics of the 9-Amino and 10,11-Methylenedioxy Derivatives of Camptothecin in Mice. *Cancer Research 53*, 3062-3069.

(31) Gakhar, G., Wight-Carter, M., Andrews, G., Olson, S., and Nguyen, T. A. (2009) Hydronephrosis and urine retention in estrogen-implanted athymic nude mice. *Veterinary Pathology 46*, 505-508.

Part II

Targeted Delivery of siRNA

Chapter V

Stability Optimization of CDP/siRNA Delivery System

5.1 Abstract

siRNA holds great promise as a cancer therapeutic, however its delivery to the site of interest has proven to be challenging. In the past years, our research lab has developed a targeted nanoparticle delivery system for siRNA based on β-cyclodextrin-containing polymers (CDP). The attachment of polyethylene glycol (PEG) onto the nanoparticles for steric stabilization is achieved via inclusion complex formation between adamantine (AD) and cyclodextrin cups in CDP using AD-PEG conjugate. This siRNA delivery system has shown to be effective in humans in a phase I trial. However, it demonstrates rapid clearance rate in *in vivo*. In this chapter, CDP/siRNA delivery system is further characterized and optimized for stability. The lessons learnt here will be used in the development of a new siRNA delivery system, MAD/siRNA. CDP/siRNA nanoparticles were observed by cryo-EM to be spherical and between 40 to 80 nm in size. 5 kDa PEG chain lengths was found to be optimal for particle stability by salt stability studies *in vitro*. *In vitro* salt stability studies indicate that adding multivalently attached PEG (AD_2-PEG and AD_3-PEG) or lowering surface charge of nanoparticles (AD-Glu-PEG and AD-Glu-Glu-PEG) was able to confer extra stability to the particles. In *in vivo* studies, particles stabilized with multivalently attached PEG resulted in prolonged circulation compared to other groups including naked siRNA and particles stabilized with AD-PEG, AD-Glu-PEG or AD-Glu-Glu-PEG.

5.2 Introduction

The discovery of the RNA interference (RNAi) pathway by Fire and Mello (*1*) has led to great interest in its application in the field of cancer therapy due to its ability to trigger post-transcriptional sequence specific gene silencing. Central to this pathway is the small interfering RNA (siRNA) that can potentially cleave and degrade any mRNA sequence and thus eliminate its protein products.

However, the delivery of intact and therapeutically significant amount of siRNA to the site of interest has proven to be challenging. Targeted delivery of siRNA via nano-scaled vehicles holds great promise for cancer therapy due to its ability to (i) carry a large payload (siRNA), (ii) protect this payload from degradation, (iii) preferentially accumulate in tumor tissues via the enhanced permeability and retention (EPR) effect and (iv) enhance cellular uptake via targeting.

In the past years, our research lab has developed a targeted nanoparticle delivery system for siRNA based on β-cyclodextrin-containing polymers (CDP), named CALAA-01 (*2, 3*). CALAA-01 is composed of anionic siRNA condensed by cationic CDP to form nanoparticles via electrostatic interactions. The cationic CDP is formed by copolymerization of β-cyclodextrin with dimethylsuberimidate (DMS). This nanoparticle is stabilized by the presence of a steric PEG layer on its surface. The attachment of polyethylene glycol (PEG) onto the nanoparticles is attained by the formation of an inclusion complex of adamantine (AD) with the cyclodextrin in the polymer via an AD-PEG conjugate. Targeting is achieved by attaching ligands, such as human transferrin

protein on the distal end of AD-PEG conjugate to form AD-PEG-Transferrin (Scheme 5.1).

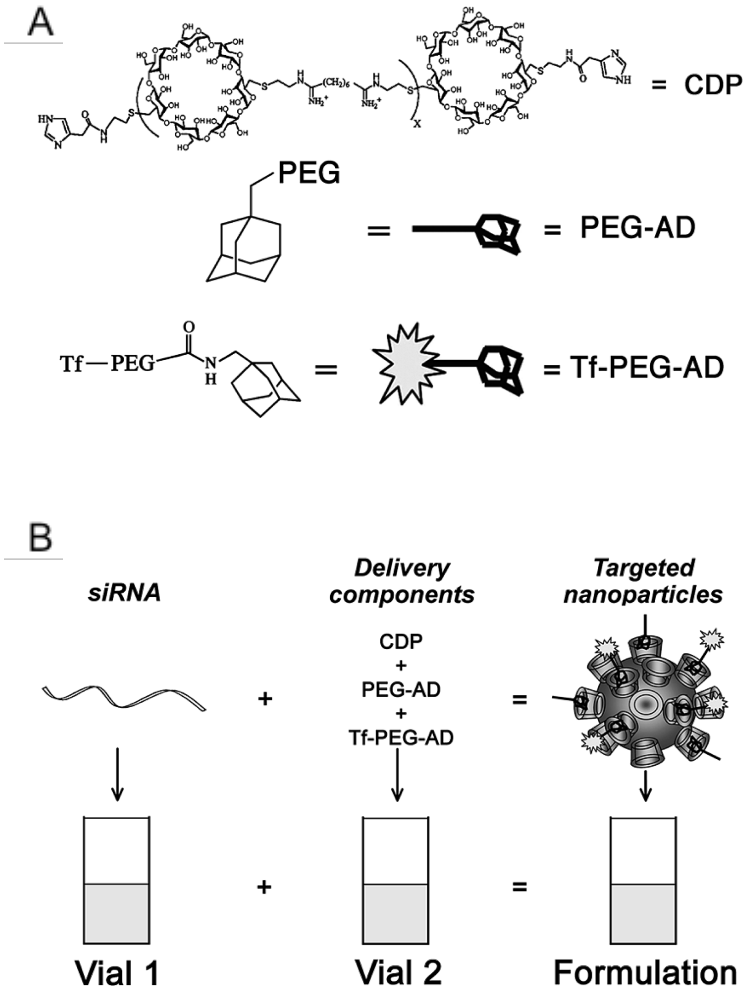

Scheme 5.1 Schematic of targeted siRNA delivery system CALAA-01. (A) Delivery components are β-cyclodextrin-containing polymer (CDP), adamantane polyethylene glycol conjugate (AD-PEG), and Transferrin targeting ligand conjugated to the distal end of PEG-AD (Tf-PEG-AD). (B) When the two vials are mixed together, the targeted nanoparticles form via self-assembly of the four components (*4*).

This delivery system for siRNA has reached phase I clinical trial and evidence for sequence specific gene silencing has been shown (*3*). Yet this system has shown rapid clearance rate in *in vivo* imaging and in non-human primate pharmacokinetic studies (*5, 6*) resulting in limited amount of nanoparticles reaching the solid tumor site via the EPR effect. This rapid clearance has been observed in other cationic polymer-based siRNA delivery systems (*7, 8*). The mechanisms of the fast clearance have been attributed to instability of the particles that lead to aggregation, as well as particle disassembly at the kidney site due to the presence of the negatively charged glomerular basement membrane resulting in competing electrostatic interactions (*9*).

Before proceeding to develop another system for siRNA delivery, in this chapter, we attempt to further characterize and optimize this CDP/siRNA delivery system. This is done by understanding the particle morphology, the effect of PEG chain length and multivalency and particle surface charge on the particle stability and performance in both *in vitro* and *in vivo* conditions. The insights gained can be applied to the design of the new MAP/siRNA delivery system in the following chapter and to cationic polymer-based siRNA delivery systems in general.

5.3 Experimental

5.3.1 General

All commercially purchased reagents and solvents including anhydrous and HPLC grade were used without further purification. Discrete PEG chemicals were obtained from Quanta Biodesign (Powell, OH). Chemicals containing PEG longer than 1 kDa were either purchased from JenKem Technology USA (Allen, TX) or from Laysan bio (Arab, AL). Female NCr nude mice were purchased from Taconic (Oxnard, CA). All other reagents were purchased from Sigma (St Louis, MO).

^{1}H and ^{13}C spectra were recorded on either a 500 MHz or 600 MHz spectrometer (Inova, Varian). Mass spectrometry was carried out using a LCQ ion trap mass spectrometer (Finnigan, Thermo) by direct infusion electrospray ionization or MALDI-TOF mass spectrometer (Voyager DE^{TM}-PRO, Applied Biosystems).

Absorbance and fluorescence measurements were taken on a microplate reader (Infinite 200, Tecan).

All animals were treated as per National Institute of Health Guidelines for Animal Care and approved by the California Institute of Technology Institutional Animal Care and Use Committee.

5.3.2 Cryo-Electron Microscopy

Cryo-electron microscopy (cryo-EM) was used to visualize nanoparticle morphology. Glow discharged Quantifoil holey carbon grid (SPI Supplies) was loaded

into an automated climate-controlled plunge-freezer (Vitrobot, FEI) and 3 μl of sample was applied. Grid was blotted, drained, plunged into liquid ethane, transferred and stored in liquid nitrogen. Samples were visualized under cryogenic temperatures with transmission electron microscope (Tecnai T12, FEI) equipped with a cryo-specimen holder. Acceleration voltage was set at 120 kV.

5.3.3 Synthesis of AD-PEG with Different PEG Lengths

100 mg (0.08 μM) of PEG1kDa and 68 mg (0.41 mM) of adamantanemethylamine were dissolved in 4 ml of DCM. The reaction mixture was stirred for 4 h at room temperature before removing the solvent by rotary evaporator. It was then reconstituted in water and centrifuged to remove any insoluble material. The supernatant was recovered, filtered with a 0.2 μm filter (Amicon) and lyophilized to yield 90 mg of product (87%). MALDI (m/z): 1264 [M+H]. Other PEG lengths, 2, 5 and 10 kDa were synthesized in the same way.

5.3.4 Synthesis of Multivalent AD-PEG

1. AD-dPEG$_4$-BOC

315 mg (1.64 mM) of EDC and 16.7 mg (0.14 mM) of DMAP was added to 500 mg (1.37 mM) of N-t-boc-amido-dPEG$_4$-acid dissolved in 8 mL of anhydrous DCM in a 25 mL 2-neck round bottom flask. 271 mg (1.64 mM) of adamantane methylamine dissolved in 2 mL of anhydrous DCM was then added and the reaction was stirred under

argon at room temperature overnight. The reaction mixture was concentrated on rotary evaporator and Prep TLC was run to isolate the desired product using DCM:MeOH (90:10) as the mobile phase. 550 mg of product was obtained after concentrating on rotary evaporator and drying in vacuum (78%). LC/MS (m/z): 513.3 $[M+H]^+$.

2. AD-dPEG-NH_2 (HCl salt)

3.2 mL of 6 N HCl in MeOH was added dropwise to 550 mg (1.07 mM) of AD-$dPEG_4$-BOC dissolved in 3.2 mL of MeOH. This reaction was stirred for 6 h in an ice bath. Solvent and excess HCl was removed by rotary evaporator and dried under vacuum overnight to yield an amber colored viscous material (100%). ^{1}H NMR ($(CD_3)_2SO$) δ 7.90 (m, 2H), 7.63 (d, 1H), 3.40-3.69 (m, PEG Hs), 1.38-1.87 (m, AD Hs). ESI/MS (m/z): 449.0 $[M+Na]^+$.

3. AD-Glu(Bn)-BOC

300 mg (1.8 mM) of adamantane methylamine was dissolved in 4 mL of anhydrous DCM prior to the addition of 200 mg (0.46 mM) NHS-Glu(Bn)-BOC. This mixture was allowed to react overnight at room temperature under constant stirring. The desired product was isolated by running a flash column using DCM/methanol (98:2) as the mobile phase. The product was concentrated and dried on rotary evaporator to yield a colorless viscous liquid (81%). ^{1}H NMR ($(CD_3)_2SO$) δ 7.57 (m, 1H), 7.34 (m, 5H), 6.88 (d, 2H), 5.06 (s, 2H), 4.40 (m, 1H), 1.35-1.87 (m, AD and BOC Hs). ESI/MS (m/z): 507.3 $[M+Na]^+$.

4. AD-Glu(Bn)-NH_2 (TFA salt)

4 mL of 25% of TFA/DCM was added dropwise to 180 mg (0.37 mM) of AD-Glu(Bn)-BOC was dissolved in DCM. This reaction was stirred for 6 h in an ice bath. Solvent and excess TFA was removed by rotary evaporator and dried under vacuum overnight to yield a viscous liquid (100%). ^{1}H NMR ($(CD_3)_2SO$) δ 8.25 (m, 1H), 8.11 (s, 2H) 7.34 (m, 5H), 5.09 (s, 2H), 4.40 (m, 1H), 1.35-1.87 (m, AD Hs). ESI/MS (m/z): 385.1 $[M+H]^+$.

5. AD-Glu(Bn)-PEG5kDa

185 mg (0.37 mM) of AD-Glu(Bn)-NH_2 (TFA salt) was dissolved in 6 mL of DCM. 100 µl of TEA and 500 mg (0.09 mM) of PEG5kDa-SCM was subsequently added and the reaction mixture was stirred overnight at room temperature. Solvents were removed on rotary evaporator and vacuum prior to reconstituting the product in water. Insoluble material was filtered away with a 0.1µm PTFE syringe filter (Whatman). The resultant solution was dialyzed against water 3 times using a 3 kDa MWCO centrifuge filter device (Amicon). The product was lyophilized to give 413 mg of white fluffy powder (78%). ^{1}H NMR ($(CD_3)_2SO$) δ 7.90 (m, 1H), 7.61 (d, 1H), 7.33 (m, 5H), 5.06 (s, 2H), 4.40 (m, 1H), 3.23-3.69 (m, PEG Hs), 1.38-1.87 (m, AD Hs). MALDI (m/z): 5900 $[M+H]^+$.

6. AD-Glu-PEG5kDa

To a 25 mL round bottom flask containing 6 mL of MeOH was charged 190 mg (0.03 mM) of AD-Glu(Bn)-PEG5kDa and 14 mg of Pearlman's catalyst (20% $Pd(OH)_2/C$). Argon was used to vent the system of air prior to the insertion of a syringe

linked to a hydrogen filled balloon. Argon was then flashed out with one balloon volume of hydrogen. The reaction proceeded for 24 h under constant stirring and hydrogen balloon was refilled on demand. Catalyst was filtered away from the reaction with a 0.1 µm PTFE syringe filter prior to dialyzing with a 3 kDa MWCO centrifuge filter device 3 times against water. The product was then lyophilized to yield 150 mg of white fluffy material (82%). ^{1}H NMR ($(CD_3)_2SO$) δ 7.90 (m, 1H), 7.61 (d, 1H), 4.40 (m, 1H), 3.23-3.69 (m, PEG Hs), 1.38-1.87 (m, AD Hs). MALDI (m/z): 5800 $[M+H]^+$.

7. AD_2-PEG5kDa

150 mg (0.03mM) of AD-Glu-PEG5kDa was dried under vacuum for 3 h in a 25 mL round bottom flask prior to the addition of 1 mL of anhydrous DCM. 22 mg (0.11 mM) of EDC and 4.7 mg (0.03 mM) of DMAP were subsequently added followed by the addition of 46.5 mg (0.11 mM) of AD-dPEG$_4$-NH$_2$ (HCl salt) dissolved in 1 mL of anhydrous DCM and 40 µl TEA. The reaction was stirred overnight under argon at room temperature. Precipitate was filtered away using a 0.1 µm PTFE syringe filter. Solvent was then removed via rotary evaporator and vacuum followed by reconstitution of the product in water. Insoluble material was filtered away with a 0.1 µm PTFE syringe filter and the product was dialyzed against water 3 times using a 3kDa MWCO centrifuge filter device (Amicon). The product was lyophilized to yield 148 mg of very light amber-colored fluffy material (94%). ^{1}H NMR ($(CD_3)_2SO$) δ 7.90 (m, 1H), 7.61 (d, 1H), 4.40 (m, 1H), 3.23-3.69 (m, PEG Hs), 1.38-1.87 (m, AD Hs), 1.94x increase in Hs due to AD (from integration analysis). MALDI (m/z): 6150 $[M+H]^+$.

5.3.5 Synthesis of Negatively Charged AD-PEG

1. AD-Glu-PEG5kDa

AD-Glu-PEG5kDa was synthesized as per section 6 under 5.3.2 Synthesis of multivalent AD-PEG.

2. OH-Glu(Bn)-Glu(Bn)-BOC

1.22 g (2.81 mM) of BOC-Glu(Bn)-NHS was added to 1 g (4.21 mM) of H-Glu(Bn)-OH dissolved in 3.09 ml (28.1 mM) TEA and 42 ml of ACN/H2O (5:1). This mixture was allowed to react overnight at room temperature under constant stirring. ACN and TEA were removed via rotary evaporator after which precipitation was observed. Liquid-liquid extraction was performed with 3x 30 ml chloroform (with an additional 30 ml of water). The organic phase was collected, dried with $MgSO_4$, filtered, concentrated on rotary evaporator and dried under vacuum at 30 ^oC overnight to give a quantitative yield of white viscous liquid. ESI/MS (m/z): 579.2 $[M+Na]^+$.

3. AD-Glu(Bn)-Glu(Bn)-BOC

0.78 g (1.40 mM) of BOC-Glu(Bn)-Glu(Bn)-OH was dissolved in 5 ml of dry THF and transferred to a flask purged with and under Argon. 0.30 g (1.47mM) of DCC, 0.23 g (1.40 mM) of adamantane methylamine and 0.20 g (1.47 mM) of HOBt in 0.49 ml (2.80 mM) of DIPEA each in 1 ml of dry THF were added to the above reaction under argon at 0 ^oC. The reaction mixture was warmed to room temperature and reacted under constant stirring overnight. Insoluble urea side product was filtered. Filtrate was dried on rotary evaporator and crystallized with hot MeOH. Crystals were grown for 24 h at

room temperature and consequently filtered and washed with cold MeOH to yield 0.42 g of white crystals (43%). ESI/MS (m/z): 726.5 $[M+Na]^+$.

4. AD-Glu(Bn)-Glu(Bn)-NH_2 (TFA salt)

0.75 ml of TFA was added drop-wise to 150 mg (0.21 mM) of BOC-Glu(Bn)-Glu(Bn)-AD dissolved in 2.25 ml of DCM at 0 ^oC. Reaction was performed under constant stirring in ice bath for 5 h after which it was slowly warmed to room temperature, dried on rotary evaporator and under vacuum overnight to give quantitative yield of a clear viscous liquid. ESI/MS (m/z): 604.4 $[M+H]^+$.

5. AD-Glu(Bn)-Glu(Bn)-PEG5kDa

102 mg (0.14 mM) of AD-Glu(Bn)-Glu(Bn)-NH_2 was dissolved in 3 ml of dry DCM. 150 µl of TEA and 180 mg (0.04 mM) of NHS-PEG5kDa were subsequently added. The reaction was stirred at room temperature overnight. Solvent was removed on rotary evaporator and dried under vacuum overnight. This was reconstituted in water, insoluble material was filtered via a 0.2 µm PVDF filter (Whatman) and the filtrate was dialyzed three times against water with a 3 kDa MWCO centrifuge filter device (Amicon). The supernatant was lyophilized to yield 158 mg of product (79%). ^1H NMR ($(CD_3)_2SO$) δ 8.10 (m, 1H), 7.65-7.75 (d, 2H), 7.33 (m, 10H), 5.06 (s, 4H), 4.40 (m, 2H), 3.23-3.69 (m, PEG Hs), 1.35-1.87 (m, AD Hs). MALDI (m/z): 6400 $[M+H]^+$.

6. AD-Glu-Glu-PEG5kDa

To a 25 mL round bottom flask containing 5 mL of MeOH was charged 150 mg (0.02 mM) of AD-Glu(Bn)-Glu(Bn)-PEG5kDa and 20 mg of Pearlman's catalyst (20%

$Pd(OH)_2/C$). Argon was used to vent the system of oxygen prior to the insertion of a syringe linked to a hydrogen filled balloon. Argon was then flashed out with one balloon volume of hydrogen. The reaction proceeded for 24 h under constant stirring and hydrogen balloon was refilled on demand. Catalyst was filtered away from the reaction with a 0.1 μm PTFE syringe filter prior to dialyzing with a 3 kDa MWCO centrifuge filter device (Amicon) 3 times against water. The product was then lyophilized to yield 121 mg of white fluffy material (83%). ^{1}H NMR ($(CD_3)_2SO$) δ 8.10 (m, 1H), 7.65-7.75 (d, 2H), 4.40 (m, 2H), 3.23-3.69 (m, PEG Hs), 1.35-1.87 (m, AD Hs). MALDI (m/z): 6200 $[M+H]^+$.

5.3.6 *In Vitro* and *In Vivo* Characterization

1. Particle formulation

A solution of AD-PEG was added to a solution of CDP at a 1:1 AD-PEG/β-CD (mol/mol) ratio in water. This mixture was allowed to sit at room temperature for 30 min for the complexation of AD-PEG into β-cyclodextrin cups. It was then added to an equal volume of siRNA in water at a charge ratio of 3 (+/-) (3 positive charges from CDP for every negative charge from siRNA) and mixed by pipetting. After 30 min, tests and characterizations were performed. The formulations of particles stabilized with different PEG were conducted in the same manner.

2. Nanoparticle size and surface charge

Particle size and zeta potential measurements were determined by dynamic light scattering (DLS) using a ZetaPALS instrument (Brookhaven Instruments, Holtsville, NY). Effective hydrodynamic diameter was recorded and averaged from 10 runs at 1 min each. Zeta potential measurements were collected for three sets of 10 runs at a target residual of 0.012, and the results were averaged.

3. Salt stability studies

Particle size was recorded for 5 runs at 1 min each on a DLS ZetaPALS instrument (Brookhaven Instruments, Holtsville, NY). Measurement was stopped to allow the addition of a 10x PBS solution to the particle formulation such that the resulting particle formulations contain 1x PBS. Measurements were subsequently restarted and 10 successive runs of 1min each were recorded to study the effect of salt addition on particle stability.

To emulate PEG dissociation from nanoparticles, particle formulations were subjected to filtration with a 100 kDa MWCO (ca. 10 nm cut off) centrifuge membrane filter (Amicon) for 8 min at 2,000 g. Filtrations were performed for either 1, 4 or 12 times. Retentate was recovered, salt was added and any aggregation was tracked by DLS.

4. Pharmacokinetic studies

CDP/siRNA formulation was prepared at 1 mg siRNA/ml containing 20% siCy3 (fluorescent siRNA) at charge ratio of 3 (+/-) and injected at 5 mg siRNA/kg mice. To prepare for blood collection, hind legs of female BALC/c mice were shaved to expose the

saphenous veins. Particle formulations were injected via tail vein. Time measurements began as soon as the injections were complete. After 2 and 4 min, blood was collected from the saphenous vein into EDTA containing vials (Microvette CB 300 EDTA, Sarstedt). Time points 7 and 9 min were collected from the alternate leg. Samples were immediately centrifuged at 10,000 g, 4 ^{o}C for 15 min and supernatant removed and analyzed by measuring the fluorescence of siCy3 at 530 nm excitation and 570 nm emission wavelengths. Standard curves were generated from known concentrations of siCy3 in the same environment.

5.4 Results and Discussion

5.4.1 Particle Morphology

The CDP/siRNA delivery system has been well characterized (*2*). However, no clear images of particle morphology were obtained.

Transmission electron microscopy (TEM) was first used to visualize the nanoparticles. Due to the low electron density of the constituents, uranyl acetate stain was added to assist in the visualization of the particles. This negative heavy metal stain is designed to give more contrast to the image by staining the particle surroundings. However, the background appeared inhomogeneous and it was hard to distinguish between staining and drying effects from the nanoparticles. As well, particle staining and drying is likely to affect the observed particle morphology.

Therefore, cryo-electron microscopy (cryo-EM) was employed since it does not require sample staining or drying and thus is able to generate images of particle morphology in its natural environment. Figure 5.1A shows a representative cryo-EM image of CDP/siRNA/AD-PEG particle formulation. Particles are spherical discreet entities with diameters of between 40 to 80 nm. This size correlates well with that determined from DLS measurements. To further verify the particle structure, AD-PEG-Au (5 nm gold particles, PEG length 1 kDa) was added to a formulation of CDP/siRNA/AD-PEG. Figure 5.1B shows a particle surrounded with 5 nm Au nanoparticles. This indicates that some of the added AD-PEG-Au has displaced the AD-PEG from the β-cyclodextrin cups on the surface of the particle. These images serve as visual validation to our understanding of the structure of CDP/siRNA/AD-PEG particles.

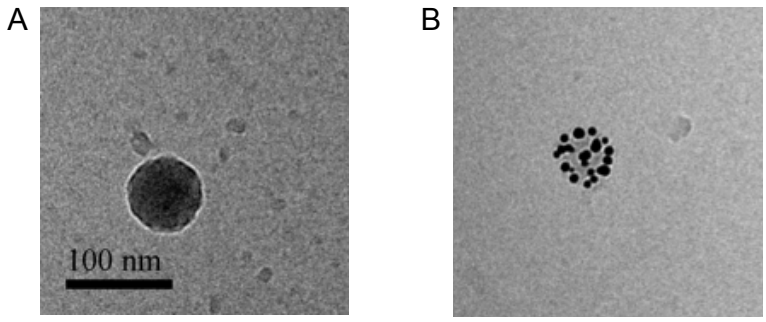

Figure 5.1 Cryo-electron microscopy images of (A) CDP/siRNA/AD-PEG formulation at charge ratio 3 (+/-), (B) CDP/siRNA/AD-PEG formulation at charge ratio 3 (+/-) with added AD-PEG-Au.

5.4.2 Effect of PEG Length Variation on Particle Stability

AD-PEG is used for the stabilization of CDP/siRNA nanoparticles via surface steric hindrance effect. Currently the system uses AD-PEG with PEG chain length of 5 kDa. No studies on whether additional PEG length may stabilize the particle further, or if shorter PEG lengths would be sufficient have been conducted.

Hence, a series of AD-PEG at different PEG chain lengths were synthesized and the abilities of each in stabilizing CDP/siRNA nanoparticles at physiological salt concentrations were evaluated via a dynamic light scattering (DLS) based kinetic study. Figure 5.2 shows that in general, as PEG chain length increased, detectable aggregation decreased. It is interesting to note however, that nanoparticles stabilized with PEG chains of 10 kDa showed slightly more aggregation than that stabilized with 5 kDa. Hence, PEG length of 5 kDa is verified to show the best salt stabilization performance and will continue to be used.

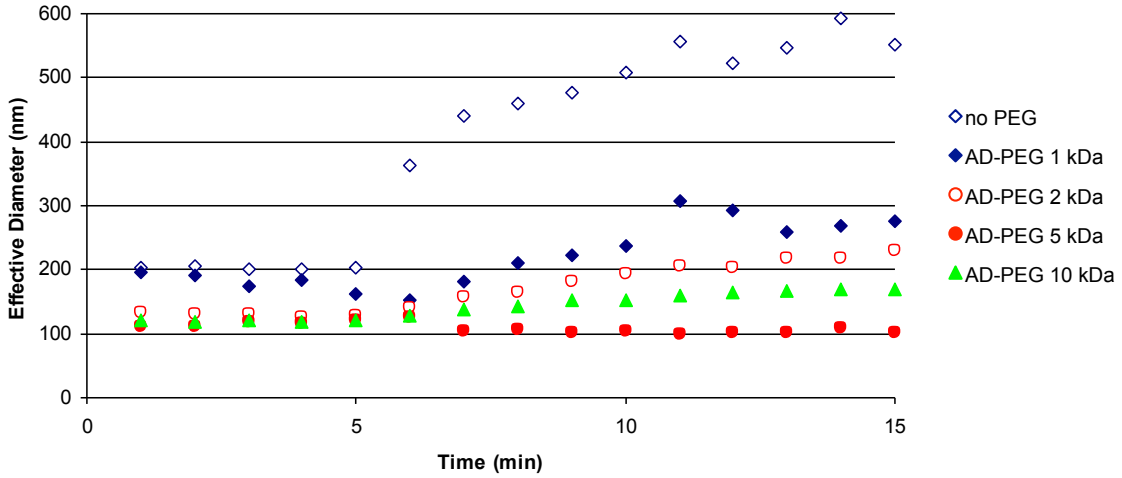

Figure 5.2 Salt stability of CDP/siRNA nanoparticles stabilized by PEG chains of various lengths. Formulated at charge ratio 3 (+/-), filtered once via 100 kDa membrane filter, 10x PBS was added at time 5 min such that the resulting solution was in 1x PBS.

5.4.3 Effect of Multivalency and Surface Charge on Particle Stability

Multivalent interactions have been shown to decrease dissociation constant, K_D dramatically between targeting ligands and receptors (*10, 11*). Therefore, multivalently attached PEG on CDP/siRNA nanoparticles through the non-covalent interactions between AD and β-cyclodextrin cups could also show a significant reduction in K_D. A stronger binding between AD-PEG and CDP/siRNA nanoparticle would confer greater particle stability. To achieve this, AD-PEG, AD_2-PEG and AD_3-PEG were synthesized and particles formulated with each were characterized by *in vitro* studies as well as by pharmacokinetic studies in mice.

As well, positively charged particles have been proven to trigger higher clearance rate than negatively charged particles. This is likely due to the presence of many negatively charged constituents in blood which the positively charged particles can bind to (*12*). Zeta potential measurements of the current CDP/siRNA/AD-PEG system reveal particle surface charge of ca. 5 mV. This means that the particle surface is slightly positive. To tune the surface charge to slightly negative, negatively charged groups can be incorporated into the AD-PEG constituent. One such group is glutamate (Glu), which has an additional carboxylic acid side chain with a pKa of 4.1 and thus exists in its negatively charged form at physiological pH. AD-PEG, AD-Glu-PEG and AD-Glu-Glu-PEG were synthesized and particles formulated with each were characterized by *in vitro* and *in vivo* studies.

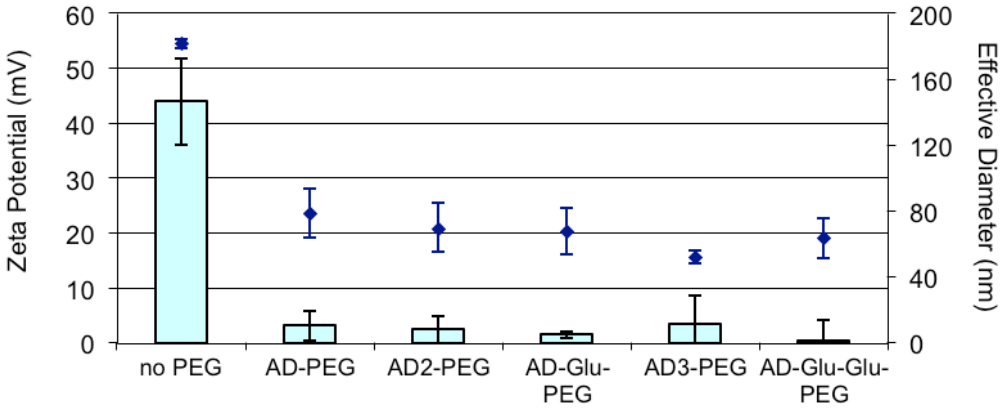

Figure 5.3 Zeta potential and effective hydrodynamic diameter of CDP/siRNA nanoparticles stabilized by different PEG chains. Formulated at charge ratio of 3 (+/-), filtered via 100 kDa membrane filter; zeta potential (bar), effective diameter (scatter).

CDP/siRNA nanoparticles stabilized with no PEG, AD-PEG, AD_2-PEG, AD_3-PEG, AD-Glu-PEG or AD-Glu-Glu-PEG were characterized for particle size and surface charge (Figure 5.3). It was found that without PEG, particle surface charge or zeta potential is at ca. 45 mV. When PEG was added, these particles exhibited a near neutral zeta potential. This implies that the PEG layer effectively reduced the particle zeta potential by masking the surface charge. The zeta potentials of CDP/siRNA nanoparticles stabilized with AD-Glu-PEG or AD-Glu-Glu-PEG were less than that with AD-PEG, AD_2-PEG or AD_3-PEG due to the negative charge present in AD-Glu-PEG and AD-Glu-Glu-PEG. The effective hydrodynamic diameters of particles stabilized with the different PEG chains were in the desirable sub 100 nm range.

Particle stability in physiological salt conditions can be used as a prediction for its stability *in vivo*. Stable nanoparticles would remain as discreet entities while unstable nanoparticles would aggregate. In here, we use DLS as a guide for particle stability by measuring and recording any size changes after the addition of salt. CDP/siRNA nanoparticles are stabilized by the presence of a PEG layer on its surface, therefore, instability caused by the removal of this steric layer would lead to aggregations in salt conditions. The removal of this steric PEG layer was emulated by the filtration of CDP/siRNA nanoparticles. The molecular size cut off for the filter was chosen to be 100 kDa, which is ca. 10 nm. This means that only unbound components including PEG, CDP or siRNA would flow through, while intact nanoparticles would remain in the retentate.

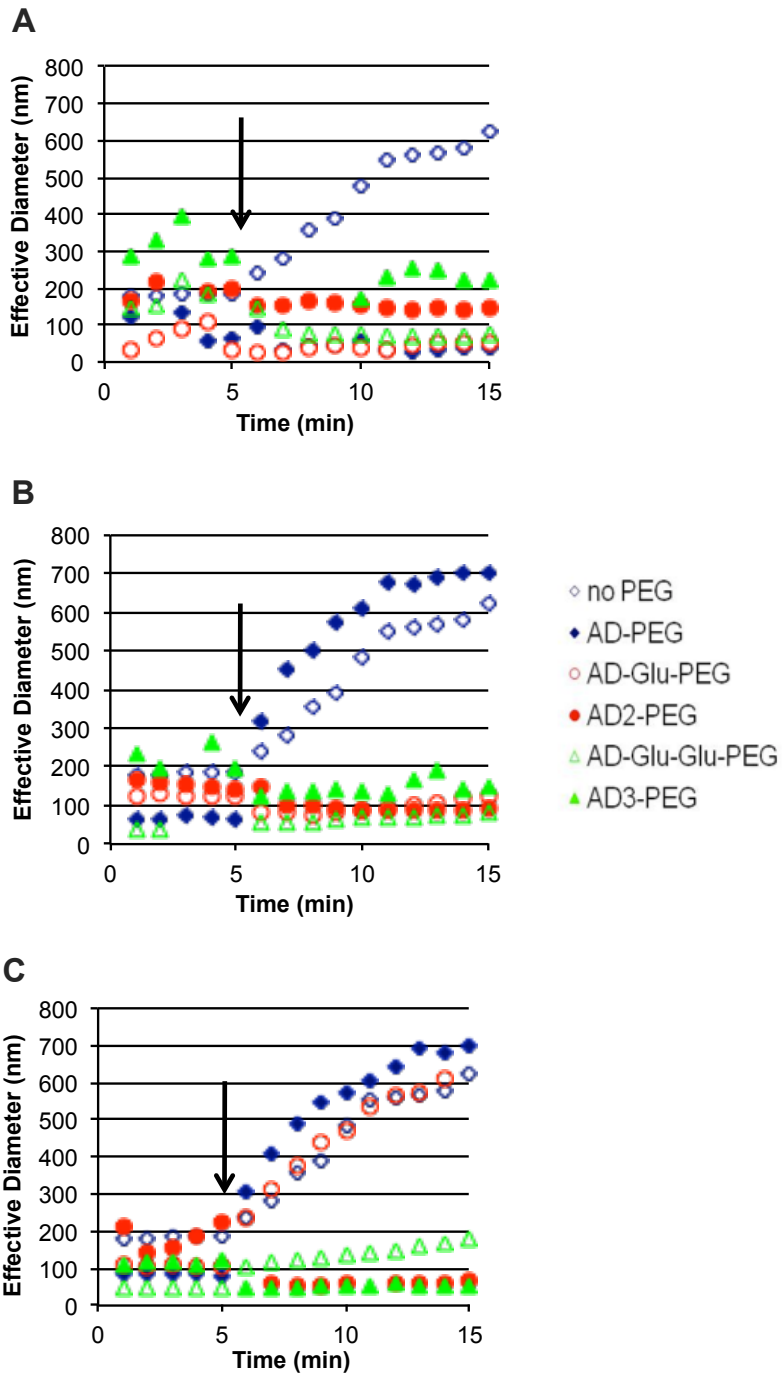

Figure 5.4 Salt stability of CDP/siRNA nanoparticles stabilized by different PEG chains. Formulated at charge ratio 3 (+/-), filtered via 100 kDa membrane filter, PBS was added at time 5 min such that the resulting solution was in 1x PBS. (A) After 1 filtration (B) After 4 filtrations (C) After 12 filtrations.

Figure 5.4 shows the effect of filtration on particle stability. After one filtration, all formulations containing PEG resulted in particle stabilization in salt conditions (Figure 5.4A). However, after 4 filtrations, formulations containing AD-PEG showed dramatic aggregation after salt addition, while formulations containing AD_2-PEG, AD-Glu-PEG, AD_3-PEG and AD-Glu-Glu-PEG remained stable. This implies that the amount of AD-PEG falling off the particle due to filtration exceeded that required for stabilization while sufficient amounts of AD_2-PEG, AD-Glu-PEG, AD_3-PEG or AD-Glu-Glu-PEG remained on the surface of the nanoparticles. After 12 filtrations, nanoparticles stabilized with AD_2-PEG or AD_3-PEG remained stable, particles stabilized with AD-Glu-Glu were moderately stable, while all the others aggregated under salt conditions. Combined, these results indicate that multivalently attached PEG is capable of improving particle stability as observed for particles stabilized with AD_2-PEG and AD_3-PEG. As well, the addition of negative charge confers stability as seen for particles stabilized with AD-Glu-PEG and AD-Glu-Glu-PEG.

From the encouraging salt stability results, pharmacokinetics of CDP/siRNA nanoparticles formulated with AD_2-PEG, AD-Glu-PEG, AD_3-PEG and AD-Glu-Glu-PEG were evaluated in mice models and compared with that formulated with no PEG and with AD-PEG. BALB/c mice were injected with particle formulations containing 20% siCy3 (fluorescently labeled siRNA) via tail vein injection and blood was collected from saphenous vein at various time points.

Figure 5.5 shows the pharmacokinetic data for the nanoparticles stabilized with various PEG groups. Free siRNA, particles stabilized with AD-PEG, AD-Glu-PEG or AD-Glu-Glu-PEG all show similar fast *in vivo* circulation profiles. While particles

stabilized with AD_2-PEG or AD_3-PEG demonstrate dramatically longer *in vivo* circulation profiles. After 10 min of injection, the fraction of siCy3 remaining in blood in formulations containing AD_2-PEG or AD_3-PEG were over ten times greater than that with no PEG, with AD-PEG, AD-Glu-PEG or AD-Glu-Glu-PEG. It is interesting to note that although particles stabilized with AD-Glu-Glu-PEG showed good stability in *in vitro* conditions, in *in vivo*, the effect of this extra stability was not observed. This is perhaps because the strength of binding between PEG onto cyclodextrin cups is more important than having a more negative charge on the surface of the nanoparticles for longer circulations *in vivo*.

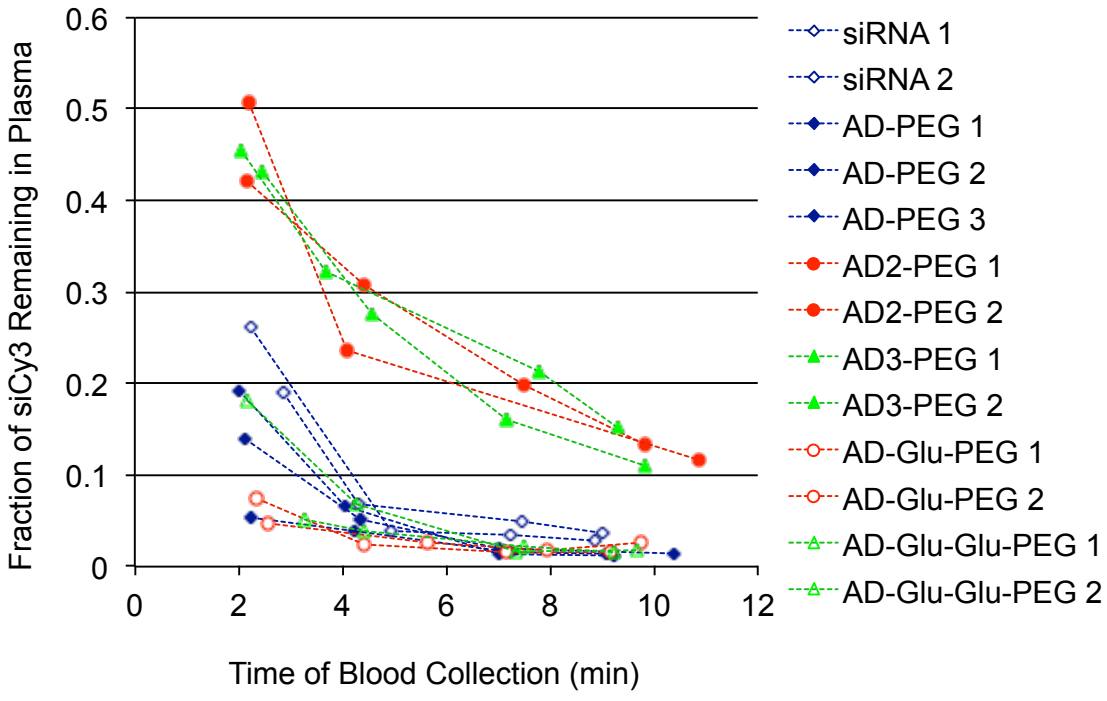

Figure 5.5 Pharmacokinetics of CDP/siRNA nanoparticles stabilized with different PEG chains in BALB/c mice. Formulated with 20% siCy3, charge ratio 3(+/-), 5 mg siRNA/kg mouse injection, dashed lines join data for each individual mouse.

5.5 Conclusions

In this chapter, the current siRNA delivery system developed by the Davis lab was further characterized and optimized. First, particle morphology was observed by cryo-EM to show that particles are between 40 to 80 nm in size. PEG compounds capable of multivalent attachment onto cyclodextrin cups (AD_2-PEG and AD_3-PEG) and capable of lowering the zeta potential of the nanoparticle system (AD-Glu-PEG and AD-Glu-Glu-PEG) were synthesized. *In vitro* salt stability studies indicate that adding multivalently attached PEG or lowering surface charge of the nanoparticles were capable of conferring extra stability. In pharmacokinetic studies, particles stabilized with multivalently attached PEG demonstrated prolonged *in vivo* circulation compared to all other groups including particles with a more negative charge.

5.6 References

(1) Fire, A., Xu, S. Q., Montgomery, M. K., Kostas, S. A., Driver, S. E., and Mello, C. C. (1998) Potent and specific genetic interference by double-stranded RNA in Caenorhabditis elegans. *Nature 391*, 806-811.

(2) Davis, M. E. (2009) The First Targeted Delivery of siRNA in Humans via a Self-Assembling, Cyclodextrin Polymer-Based Nanoparticle: From Concept to Clinic. *Molecular Pharmaceutics 6*, 659-668.

(3) Davis, M. E., Zuckerman, J. E., Choi, C. H. J., Seligson, D., Tolcher, A., Alabi, C. A., Yen, Y., Heidel, J. D., and Ribas, A. (2010) Evidence of RNAi in humans from systemically administered siRNA via targeted nanoparticles. *Nature 464*, 1067-1071.

(4) Davis, M. E. (2009) The First Targeted Delivery of siRNA in Humans via a Self-Assembling, Cyclodextrin Polymer-Based Nanoparticle: From Concept to Clinic. *Mol Pharmaceut 6*, 659-668.

(5) Bartlett, D. W., Su, H., Hildebrandt, I. J., Weber, W. A., and Davis, M. E. (2007) Impact of tumor-specific targeting on the biodistribution and efficacy of siRNA nanoparticles measured by multimodality in vivo imaging. *Proceedings of the National Academy of Sciences of the United States of America 104*, 15549-15554.

(6) Heidel, J. D., Yu, Z. P., Liu, J. Y. C., Rele, S. M., Liang, Y. C., Zeidan, R. K., Kornbrust, D. J., and Davis, M. E. (2007) Administration in non-human

primates of escalating intravenous doses of targeted nanoparticles containing ribonucleotide reductase subunit M2 siRNA. *Proceedings of the National Academy of Sciences of the United States of America 104*, 5715-5721.

(7) Malek, A., Merkel, O., Fink, L., Czubayko, F., Kissel, T., and Aigner, A. (2009) In vivo pharmacokinetics, tissue distribution and underlying mechanisms of various PEI(-PEG)/siRNA complexes. *Toxicology and Applied Pharmacology 236*, 97-108.

(8) Merkel, O. M., Librizzi, D., Pfestroff, A., Schurrat, T., Buyens, K., Sanders, N. N., De Smedt, S. C., Behe, M., and Kissel, T. (2009) Stability of siRNA polyplexes from poly(ethylenimine) and poly(ethylenimine)-g-poly(ethylene glycol) under in vivo conditions: Effects on pharmacokinetics and biodistribution measured by Fluorescence Fluctuation Spectroscopy and Single Photon Emission Computed Tomography (SPECT) imaging. *Journal of Controlled Release 138*, 148-159.

(9) Zuckerman, J. E., Choi, C. H. J., Han, H., and Davis, M. E. (2012) Polycation-siRNA nanoparticles can disassemble at the kidney glomerular basement membrane. *Proceedings of the National Academy of Sciences of the United States of America 109*, 3137-3142.

(10) Hong, S., Leroueil, P. R., Majoros, I. J., Orr, B. G., Baker, J. R., and Holl, M. M. B. (2007) The binding avidity of a nanoparticle-based multivalent targeted drug delivery platform. *Chem Biol 14*, 107-115.

(11) Choi, C. H. J., Alabi, C. A., Webster, P., and Davis, M. E. (2010) Mechanism of active targeting in solid tumors with transferrin-containing gold nanoparticles. *Proceedings of the National Academy of Sciences of the United States of America 107*, 1235-1240.

(12) Tabata, Y., Kawai, T., Murakami, Y., and Ikada, Y. (1997) Electric charge influence of dextran derivatives on their tumor accumulation after intravenous injection. *Drug Deliv 4*, 213-221.

Chapter VI

Synthesis and Characterization of Targeted MAD/siRNA Delivery System

6.1 Abstract

The use of siRNA as a cancer therapeutic possesses great potential. However, the delivery of sufficient amount of therapeutically active siRNA to the solid tumor site has proven to be challenging. Our lab has developed a siRNA delivery system based on cyclodextrin-containing polymers named CALAA-01. This has shown effectiveness in clinical trials, yet, it suffers from its fast *in vivo* clearance. In here, a new delivery platform involving boronic acid-diol complexation is used for siRNA delivery. A copolymer of mucic acid and dimethylsuberimidate (DMS), named MAD was synthesized and used to condense the anionic siRNA into nanoparticles. The condensed nanoparticles were stabilized by placing a PEG layer onto the particle surface using boronic acid-diol complexation where boronic acid PEG (BA-PEG) form reversible covalent bonding with vicinal diol groups on the MAD backbone. Targeting was achieved by conjugating the distal end of the BA-PEG with a targeting agent, in this case, a Herceptin antibody. Through transfection studies, MAD/siRNA nanoparticles were found to effectively enter cells and demonstrate low cellular toxicity. It was seen by gel electrophoresis studies that charge ratios of 1.5 (+/-) for MAD-2 and MAD-4 were sufficient to encapsulate all siRNA. Different BA-PEG were synthesized and tested for their effectiveness in stabilization of the MAD/siRNA nanoparticles. It was found that nitroPBA-PEG provided the most stabilization. MAD/siRNA nanoparticles stabilized with nitroPBA-PEG show a diameter of ca. 130 nm and a surface charge of ca. -4 mV. Pharmacokinetic studies in mice demonstrate improved circulation compared to CALAA-01.

6.2 Introduction

In the past years, our research group has been involved in translating a polymer-based nanoparticle delivery system for siRNA from the lab to the clinic, named CALAA-01 (*1, 2*). CALAA-01 is comprised of anionic siRNA condensed by cationic β-cyclodextrin-containing polymers (CDP) to form a nanoparticle. This nanoparticle is stabilized by a steric polyethylene glycol (PEG) layer and targeted with a human protein transferrin. In phase I studies, evidence for sequence specific gene silencing has been shown (*1*). However, this system (*3, 4*), like many other cationic polymer-based siRNA delivery systems (*5, 6*), shows rapid clearance *in vivo*. It is proposed that particle stability and particle surface charge are the main contributors to this issue.

We have created a new targeted nanoparticle delivery platform involving the use of boronic acid-diol complexation that can be applied to siRNA delivery and potentially prolong its circulation *in vivo*.

We designed the cationic siRNA condensing polymer to be a copolymer of mucic acid and dimethylsuberimidate (DMS), named MAD. Mucic acid, the oxidized form of galactose was selected due to its polyol characteristic and economic reasons. DMS was chosen due to the finding in CDP/siRNA delivery system that it provided the optimal distance between charge centers for transfection efficiency and cell viability (*7*). The condensed MAD/siRNA nanoparticles are stabilized by placing a PEG layer onto the particle surface using boronic acid-diol complexation where boronic acid PEG (BA-PEG) form reversible covalent bonding with vicinal diol groups on the MAD backbone. Targeting is achieved by conjugating the distal end of the BA-PEG with a targeting agent

of choice, for instance, an antibody (Scheme 6.1).

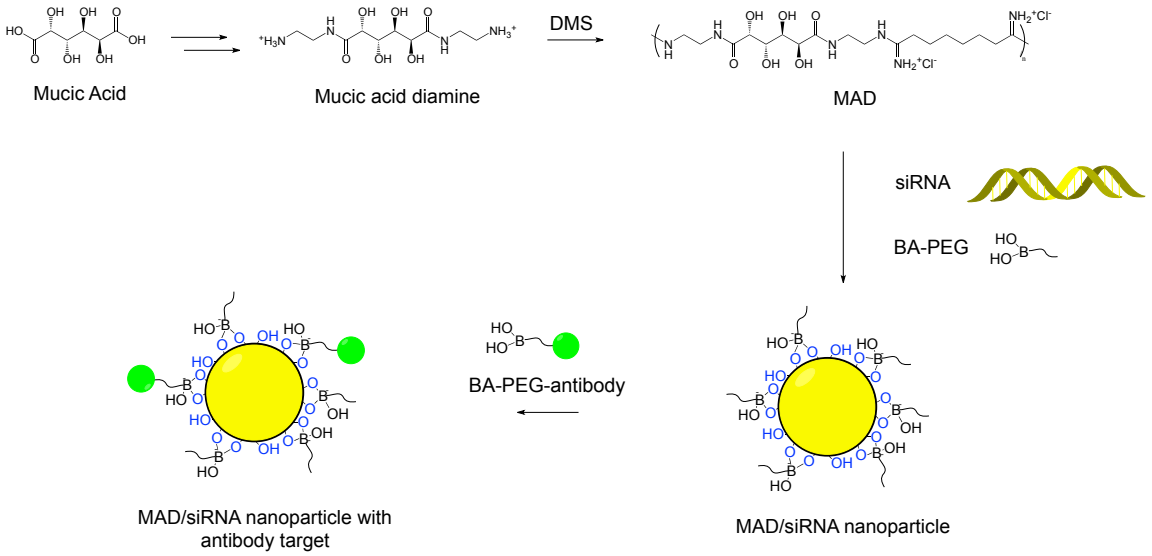

Scheme 6.1 Targeted MAD/siRNA nanoparticle delivery system assembly. MAD, copolymer of mucic acid and polyethylene glycol; (MAD-2 is shown, two methylene units between charge center (amidine) and binding site (polyol)); BA, boronic acid.

The negative charge resulting from boronic acid binding to polyols would bring the particle to a slightly negative surface charge regime. This will minimize electrostatic interactions with blood components and reduce the recognition and clearance by the mononuclear phagocyte system (MPS) (*8*). Hence, this siRNA delivery system could potentially show longer *in vivo* circulation. As well, the synthesis of MAD is straightforward compared to that of CDP. This is more favorable from both research and possible future clinical viewpoints. In addition, the presence of boron leads to the potential for imaging, such as, neutron capture autoradiography using the natural high

abundance of B-10 isotope (19.9%) that is capable of capturing neutrons (*9-11*). Boron neutron capture therapy (BNCT) for solid tumors is also possible. This is where solid tumors containing accumulated boron are irradiated with low-energy neutrons (*12, 13*) to generate high energy radiation that in turn destroys the tumor cells (*14*).

In this chapter, the new MAD/siRNA delivery system was designed, synthesized and characterized. It was evaluated by *in vitro* studies including siRNA encapsulation efficiency via gel electrophoresis, cellular transfection and cell viability. It was also characterized by pharmacokinetic studies in mice.

6.3 Experimental

6.3.1 General

All commercially purchased reagents and solvents including anhydrous and HPLC grade were used without further purification. Dimethylsuberimidate (DMS) was obtained from Thermo Scientific (Rockford, IL). 3-carboxylphenylboronic acid and 3-carboxy 5-nitrophenylboronic acid were purchased from Alfa Aesar (Ward Hill, MA). Amine polyethylene glycol carboxylic acid (NH_2-PEG-CO_2H, MW 5000) was purchased from JenKem Technology USA (Allen, TX). Herceptin® (Trastuzumab) was obtained from Dr. Y. Yen at the City of Hope (Duarte, CA). All other reagents were purchased from Sigma (St Louis, MO).

^{1}H and ^{13}C NMR spectra were recorded on either a 500 MHz or 600 MHz spectrometer (Inova, Varian). Mass spectrometry was carried out using a LCQ ion trap mass spectrometer (Finnigan, Thermo) by direct infusion electrospray ionization or MALDI-TOF mass spectrometer (Voyager DE^{TM}-PRO, Applied Biosystems).

Absorbance and fluorescence measurements were taken on a microplate reader (Infinite 200, Tecan).

6.3.2 Synthesis of MAD (Mucic Acid and DMS Copolymer)

1. Mucic acid dimethyl ester

120 ml of methanol and 0.4 ml of concentrated sulfuric acid were added to 5 g (22.8 mmol) of mucic acid. This mixture was refluxed at 85 ^{o}C overnight under constant

stirring. Solids were filtered, washed with methanol, recrystallized and dried under vacuum overnight to yield 8 g (71%) of mucic acid dimethyl ester. ^{1}H NMR ($(CD_3)_2SO$) δ 4.88-4.91 (d, 2H), 4.78-4.81 (m, 2H), 4.28-4.31 (d, 2H), 3.77-3.78 (d, 2H), 3.63 (s, 6H). ESI/MS (m/z): 261.0 $[M+Na]^+$.

2. Protected mucic acid diamine (with 2 methylene units)

60 ml of methanol, 5.25 g (32.7 mmol) of N-Boc-ethylenediamine and 5.7 ml (32.7 mmol) of N, N-diisopropylethylamine (DIPEA) were added to 3 g (12.6 mmol) of mucic acid dimethyl ester. This reaction mixture was refluxed at 85 ^oC overnight under constant stirring. Solids were filtered, washed with methanol, recrystallized and dried under vacuum to give 4.65 g (75%) of product. ^{1}H NMR ($(CD_3)_2SO$) δ 7.72 (t, 2H), 6.82 (t, 2H), 5.13-5.15 (d, 2H), 4.35-4.38 (d, 2H), 4.08-4.11 (d, 2H), 3.78-3.80 (d, 2H), 2.95-3.15 (m, 8H), 1.36 (s, 18). ESI/MS (m/z): 517.1 $[M+Na]^+$.

3. Mucic acid diamine (with 2 methylene units)

8 g (16.2 mmol) of protected mucic acid diamine was transferred to a flask containing 3 N HCl in methanol (160 ml) and reacted for 6 h at room temperature under constant stirring. Precipitate was filtered, washed with methanol and vacuum dried overnight to yield 5.69 g (96%) of mucic acid diamine. ^{1}H NMR ($(CD_3)_2SO$) δ 7.93-7.99 (m, 8H), 5.31-5.34 (d, 2H), 4.57 (d, 2H), 4.10-4.17 (d, 2H), 3.82 (d, 2H), 3.32-3.38 (m, 4H), 2.82-2.86 (m, 4H). ESI/MS (m/z): 295.1 $[M]^+$.

4. MAD-2 (Mucic Acid DMS copolymer, with 2 methylene units)

To a 1.5 ml Eppendorf tube containing 85.5 mg (0.233 mmol) of mucic acid diamine in 0.8 ml of 0.5 M $NaHCO_3$ was added 63.3 mg (0.233 mmol) of dimethylsuberimidate (DMS). Components were dissolved by vortexing and centrifuging. The resulting mixture was stirred at room temperature for 15 h. 8 ml of water was added and the pH brought to 4 with 1 N HCl. This solution was then dialyzed against water with a 3 kDa MWCO membrane filter device (Amicon) until a constant pH was attained. The supernatant was filtered with a 0.2 μm filter (Acrodisc) and lyophilized to yield 49 mg (33%) of white fluffy powder. ^{1}H NMR ($(CD_3)_2SO$) δ 9.15, 7.92, 5.40, 4.55, 4.16, 3.82, 3.38, 3.29, 2.37, 1.59, 1.28. ^{13}C NMR ($(CD_3)_2SO$) δ 174.88, 168.38, 71.45, 71.22, 42.34, 36.96, 32.74, 28.09, 26.90. GPC Mw = 6800, Mw/Mn = 1.14.

5. MAD-x (Mucic Acid DMS copolymer, with x methylene units)

To synthesize MAD with different number of methylene units between charge center (amidine) and binding site (polyol), alternatives to N-Boc-ethylenediamine were used in section 2. For example, to make MAD-4, N-Boc-butanediamine was used in the reaction. These reactions were conducted in the same manner as for the synthesis of MAD-2.

6. Absolute molecular weight determination of MAD

The absolute determination of molecular weights does not require standards for calibration. This was determined on a GPC system equipped with an Agilent pump, degasser and autosampler, a gel permeation column (TSKgel G3000PWxl-cationic polymer column, Tosoh) connected to a multi-angle laser light scattering (MALS)

detector (DAWN HELEOS, Wyatt) and a refractive index (RI) detector (Optilab rEX, Wyatt). 0.1 M $NaNO_3$ was used as the eluent at a flow rate of 0.7 ml/min. Specific refractive increment, dn/dc was measured by batch injection of various concentrations of MAD dissolved in PBS into Optilab rEX at 0.2 ml/min.

6.3.3 Synthesis of Boronic Acid PEG Linker

1. PBA-PEG-CO_2H (3-amide-PEG5kDa-carboxylic acid phenylboronic acid) and PBA-PEG

To 200 mg (1.21 mM) of 3-carboxyphenylboronic acid dissolved in 5 ml of anhydrous tetrahydrofuran was added 18.7 µl (0.24 mM) of anhydrous dimethylformamide under argon. This reaction vessel was transferred into an ice bath and 195 µl (2.89 mM) of oxalyl chloride was slowly added under argon. Reaction was allowed to proceed under vent and constant stirring for 2 h at room temperature. Solvent and excess reagent were removed under vacuum. 37 mg (0.2 mM) of this dried acyl chloride compound was dissolved in 15 ml of anhydrous dichloromethane under argon. To this was added 500 mg (0.1 mM) of NH_2-PEG5kDa-CO_2H and 52 µl (0.3 mM) of dry DIPEA under argon. After overnight reaction under constant stirring, solvent was removed under vacuum and the dried product was reconstituted in 0.5 N HCl. This solution was passed through a 0.2 µm filter (Acrodisc) and dialyzed against water with a 3 kDa MWCO membrane filter device (Amicon) until constant pH was attained. The supernatant was then filtered with a 0.2 µm filter (Acrodisc) and lyophilized to yield 377 mg (73%) of PBA-PEG-CO_2H. ^1H NMR ($(CD_3)_2SO$) δ 12.52 (s, 1H), 8.39 (t, 1H), 8.22 (s,

1H), 8.14 (s, 2H), 7.88 (d, 1H), 7.82 (d, 1H), 7.39 (t, 1H), 3.99 (s, 2H), 3.35-3.62 (PEG peak). MALDI-TOF (m/z): 5600 g/mol (NH_2-PEG5kDa-CO_2H, 5400 g/mol). The synthesis of PBA-PEG proceeded in the same way except NH_2-PEG5kDa-methoxy was used.

2. nitroPBA-PEG-CO_2H (3-amide-PEG5kDa-carboxylic acid, 5-nitrophenylboronic acid) and nitro-PEG

Synthesis of nitroPBA-PEG-CO_2H was performed in the same way as for PBA-PEG-CO_2H except the starting material was 3-carboxy 5-nitrophenylboronic acid. The reaction yielded 393 mg (76%) of nitroPBA-PEG-CO_2H. ^1H NMR ($(CD_3)_2SO$) δ 12.52 (s, 1H), 8.89 (t, 1H), 8.72 (s, 1H), 8.68 (s, 1H), 8.64 (s, 1H), 8.61 (s, 2H), 3.99 (s, 2H), 3.35-3.62 (PEG peak). MALDI-TOF (m/z): 5600 g/mol (NH_2-PEG5kDa-CO_2H, 5400 g/mol). The synthesis of nitroPBA-PEG proceeded in the same way except NH_2-PEG5kDa-methoxy was used.

3. *pKa determination for PBA*

pKa of PBA was found by measuring the change in absorbance of PBA as it converted from trigonal (in low pH) to tetrahedral (in high pH) conformation. To a solution of 10^{-3} M PBA in 0.1 M PBS, pH 7.4 was titrated 1 N NaOH. pH was recorded and corresponding samples were removed for absorbance measurements at 268 nm.

4. Herceptin-PEG-nitroPBA (Herceptin-PEG5kDa-5-nitrophenylboronic acid)

36 mg (6.4 μM) of nitroPBA-PEG-CO_2H, 12.3 mg (64 μM) of EDC and 11.1 mg (96 μM) of NHS were dissolved in 2.4 ml of 0.1 M MES buffer, pH 6.0. This mixture

was reacted for 15 min on a rotating shaker at room temperature. Excess reactants were dialyzed away with 3 kDa MWCO membrane filter device (Amicon). This activated carboxylic acid PEG compound was added to 20 mg (0.14 mM) of Herceptin in 0.1 M PBS, pH 7.2. Reaction was carried out on a rotating shaker at room temperature for 2 h and then dialyzed 4 times with 50 kDa MWCO membrane filter device (Amicon) against 1x PBS at pH 7.4. MALDI-TOF: average conjugation of 1 to 2 nitroPBA-PEG per antibody.

6.3.4 *In Vitro* Characterization

1. Particle formulation (without PEG)

A solution of MAD was added to a solution of siRNA at a charge ratio of 3 (+/-) (three positive charge from MAD for every negative charge from siRNA) in water and mixed by pipetting. This mixture was allowed to sit at room temperature for 10 min before characterizations were performed. Particle formulations containing MAD-2, MAD-4 or MAD-6 and at different charge ratios were conducted in the same manner.

2. Agarose gel mobility studies

1 w% of agarose gel was made by dissolving 0.5 g of agarose powder in 50 ml of 0.5x TBE buffer. After the addition of 10 µl of ethidium bromide dye, the mixture was heated thoroughly and poured into a cast to set. Particle formulations mixed with loading dye were loaded into the wells. Voltage was applied and the positions of nucleic acids within the wells were visualized under ultraviolet light due to the specific ethidium

bromide binding to nucleic acids. Since the charge from free nucleic acids (anionic) and that from nucleic acids encapsulated by cationic polymers (near neutral) are different, therefore, relative quantification of the nucleic acid encapsulation capacity of polymers at different charge ratios is possible.

3. In vitro transfection

For the transfection of MAD/pDNA nanoparticles into HeLa cells, HeLa cells were seeded at 20,000 cells/well in 24 well plates 48 h prior to transfection and grown in medium supplemented with 10 % fetal bovine serum (FBS). MAD particles were formulated to contain 1 μg of pGL3 in 200 μl of Opti-MEM I at various charge ratios of polymer to pDNA. Growth medium was removed, cells washed with PBS and the above particle formulation added. The cells were incubated at 37 ^{o}C and 5% CO_2 for 5 h before the addition of 800 μl of growth medium supplemented with 10% FBS. 48 h of incubation later, a fraction of the cells were analyzed for cell viability using MTS assay. The remaining cells were lysed in 100 μl of 1x Luciferase Cell Culture Lysis Reagent. Luciferase activity was determined by adding 100 μl of Luciferase Assay Reagent to 10 μl of cell lysate and the bioluminescence was quantified using a Monolight luminometer. Luciferase activity was subsequently reported as relative light units (RLU) per 10,000 cells.

For the cotransfection of MAD/pDNA and/or siRNA particles into HeLa Cells, HeLa cells were seeded at 20,000 cells/well in 24 well plates 48 h prior to transfection and grown in medium supplemented with 10% FBS. MAD particles were formulated to contain 1 μg of pGL3 and 50 nM of siGL3 in 200 μl of Opti-MEM I at a charge ratio of 5

(+/-). Particles containing only pGL3 or pGL3 and siCON were used as controls. Growth medium was removed, cells washed with PBS and the above particle formulation added. Cells were subsequently incubated at 37 ^{o}C and 5% CO_2 for 5 h before the addition of 800 µl of growth medium supplemented with 10% FBS. 48 h of incubation later, cells for assayed for viability and luciferase activity (as above).

For the transfection of MAP/siGL3 into HeLa-LUC cells, HeLa-LUC, cells (containing the gene for firefly luciferase protein) were seeded at 20,000 cells/well in 24 well plates 48 h prior to transfection and grown in medium supplemented with 10% FBS. MAD particles were formulated to contain 0, 50 and 100 nM of siGL3 in 200 µl of Opti-MEM I at a charge ratio of 5 (+/-). Particles containing only pGL3 or pGL3 and siCON were used as controls. Growth medium was removed, cells washed with PBS and the above particle formulation added. The cells were subsequently incubated at 37 ^{o}C and 5% CO_2 for 5 h before the addition of 800 µl of growth medium supplemented with 10% FBS. 48 h of incubation later, cells for assayed for viability and luciferase activity (as above).

4. Particle formulation (with PEG)

A solution of PBA-PEG was added to a solution of MAD at 3 (+/-) charge ratio (three positive charge from MAD for every negative charge from siRNA) in phosphate buffer at pH 7.4. This mixture was allowed to sit at room temperature for 10 min for the complexation of PBA-PEG with the diol-containing MAD. This was then added to an equal volume of siRNA in water and mixed by pipetting. After 10 min, characterizations

were performed. The formulations of particles stabilized with nitroPBA-PEG and at different charge ratios were conducted in the same manner.

5. Nanoparticle size and surface charge

Particle size and zeta potential measurements were determined by dynamic light scattering (DLS) using a ZetaPALS instrument (Brookhaven Instruments, Holtsville, NY). Effective hydrodynamic diameter was recorded and averaged from 10 runs at 1 min each. Zeta potential measurements were collected for three sets of 10 runs at a target residual of 0.012, and the results were averaged.

6. Salt Stability Studies

Particle size was recorded for 5 runs at 1 min each on a DLS ZetaPALS instrument (Brookhaven Instruments, Holtsville, NY). Measurement was stopped to allow the addition of a 10x PBS solution to the particle formulation such that the resulting particle formulations contain 1x PBS. Measurements were subsequently restarted and 10 successive runs of 1 min each were recorded to study the effect of salt addition on particle stability.

6.3.5 *In Vivo* Characterization

1. Pharmacokinetic Studies

MAD/siRNA nanoparticles stabilized with nitroPBA-PEG was prepared at 1 mg siRNA/ml containing 20% siCy3 (fluorescent siRNA) in 0.9 wt% NaCl at a charge ratio of 3 (+/-) and injected at 5 mg siRNA/kg mice into female BALB/c mice. To prepare for

blood collection, hind legs of mice were shaved to expose the saphenous veins. Particle formulations were injected via tail vein. Time measurement began as soon as the injection was complete. After 2 and 4 min, blood was collected from the saphenous vein into EDTA containing vials (Microvette CB 300 EDTA, Sarstedt). Time points 7 and 9 min were collected from the alternate leg. Samples were immediately centrifuged at 10,000 g, 4 ^{o}C for 15 min and supernatant removed and analyzed by measuring the fluorescence of siCy3 at 530 nm excitation and 570 nm emission wavelengths. Standard curves were generated from known concentrations of siCy3 in the same environment.

6.4 Results and Discussion

6.4.1 Synthesis of MAD (Mucic Acid and DMS Copolymer)

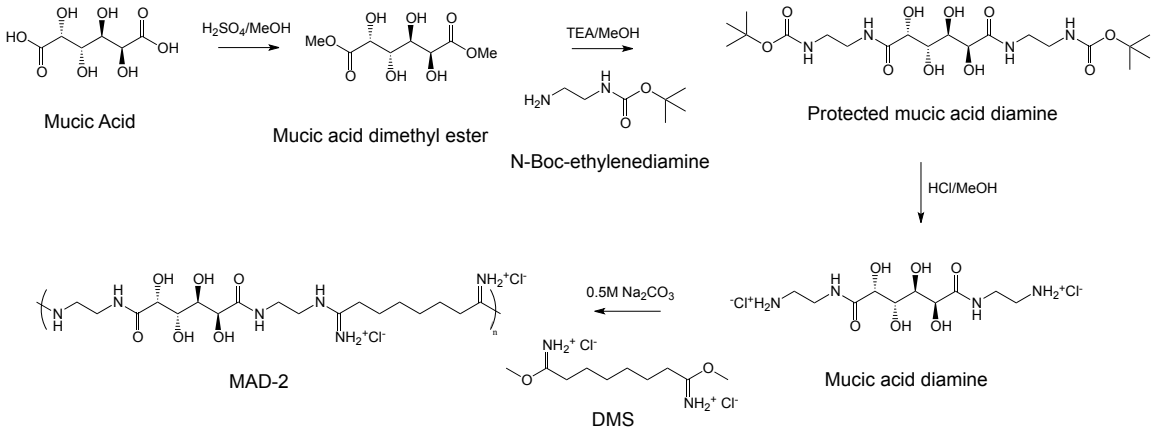

Scheme 6.2 Synthesis of MAD-2 (copolymer of mucic acid and DMS, with 2 methylene units between charge center and binding site).

The synthesis methodology for MAD is outlined in Scheme 6.2. Mucic acid was modified to contain reactive methyl ester groups on both ends, this was then conjugated with either N-boc-ethylenediamine, N-boc-butanediamine, or N-boc-hexanediamine to form mucic acid containing either 2, 4 or 6 methylene groups between the charge center (amidine) and the binding site (polyol) respectively (Scheme 6.3). Mucic acid diamine was then polymerized with DMS to form MAD. Any unreacted reagents were removed by dialysis. The synthesis for MAD was straightforward and no difficulties were encountered. Figure 6.1 shows a representative proton NMR for MAD.

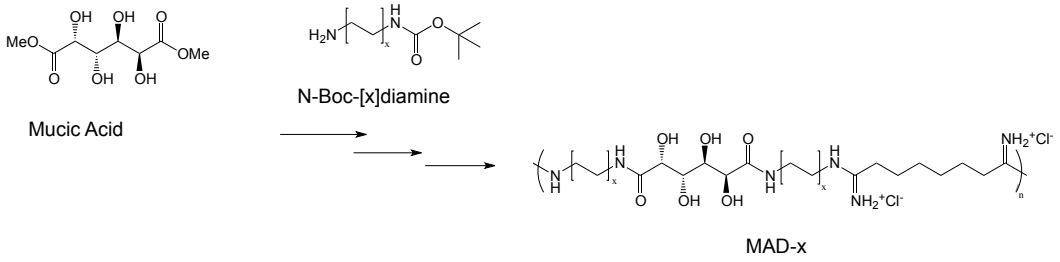

Scheme 6.3 Synthesis of MAD-x (copolymer of mucic acid and DMS), where x is number of methylene units separating binding site and charge center.

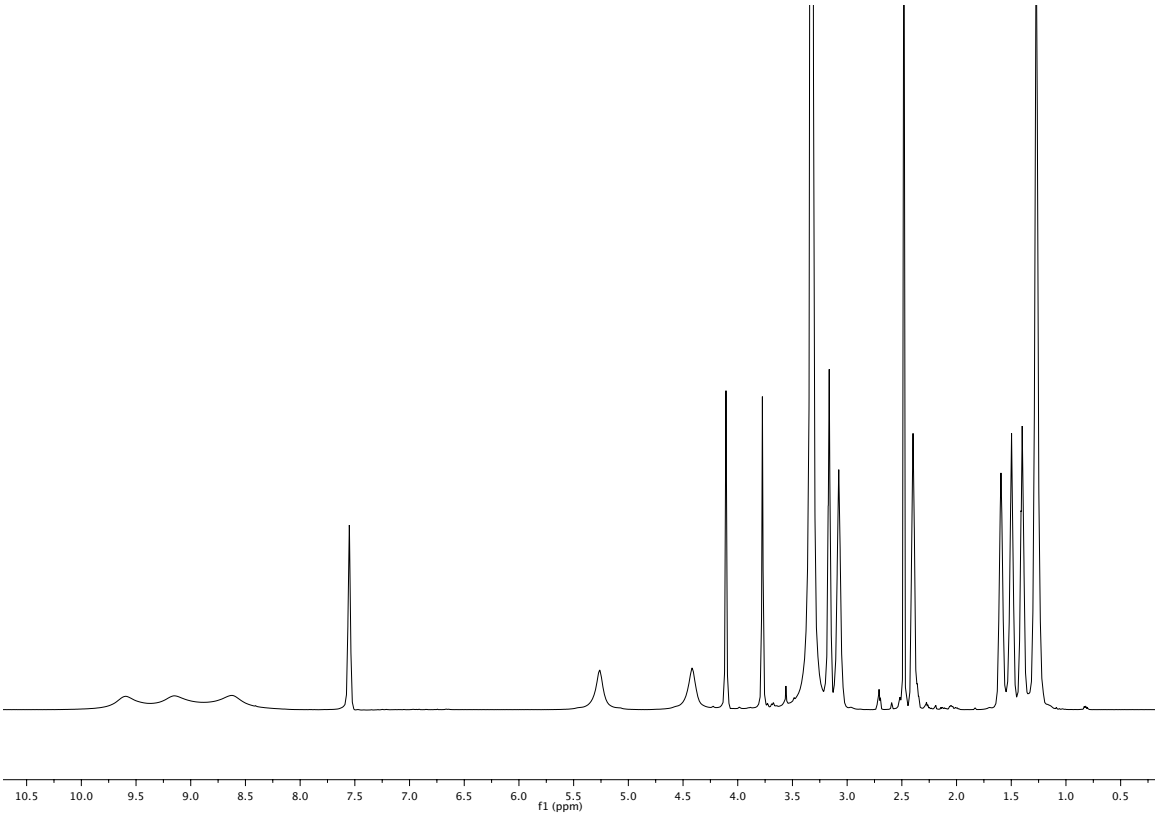

Figure 6.1 ^{1}H spectrum of MAD-6 in DMSO-*d6*.

The absolute molecular weights of MAD were measured using multi-angle laser light scattering (MALS) and refractive index (RI) detections. A refractive index

increment (dn/dc) value of 0.169 ml/g was found for the MAD-2. This dn/dc value along with MALS and RI data were used to determine the number average molecular weight (Mn), weight average molecular weight (Mw) and polydispersity (Mw/Mn) of MAP (Table 6.1).

	Mw (Da)	Mn (Da)	Polydispersity	Ave Molecular Weight	# of repeats
MAD-2	6804	5962	1.14	6.4 kDa	11-13
MAD-4	6982	6174	1.13	6.6 kDa	11-13
MAD-6	8086	7373	1.1	7.7 kDa	12-13

Table 6.1 Characterization of MAD. MAD-x, x represent number of methylene groups; Average molecular weight determined as (Mw+Mn)/2; Mw, weight average molecular weight; Mn, number average molecular weight. Polydispersity determined as Mw/Mn.

6.4.2 Synthesis of Boronic Acid PEG Linker

This is similar to that in chapter II, section 2.4.2.

Briefly, to prepare a stabilized and targeted nanoparticle, the covalent, reversible binding property between boronic acids and MAD (diol-containing) was used. The pKa of phenylboronic acid (PBA) is high at 8.8. To decrease the pKa, PBAs with electron withdrawing groups on the phenyl ring were employed to increase the acidity of the boron atom. Commercially available 3-carboxyPBA and 3-carboxy 5-nitroPBA were converted into acyl chlorides using oxalyl chloride (Scheme 6.4). These acyl chloride species were then reacted with NH_2-PEG to form PBA-PEG and nitroPBA-PEG respectively. The addition of bases DMF and DIPEA were required for the synthesis

reactions to proceed. However, the presence of these bases resulted in tetrahedral adduct formations with acidic PBA. To remove these adducts, work up in 0.5 N HCl with subsequent equilibration to neutral pH by dialysis against water was carried out.

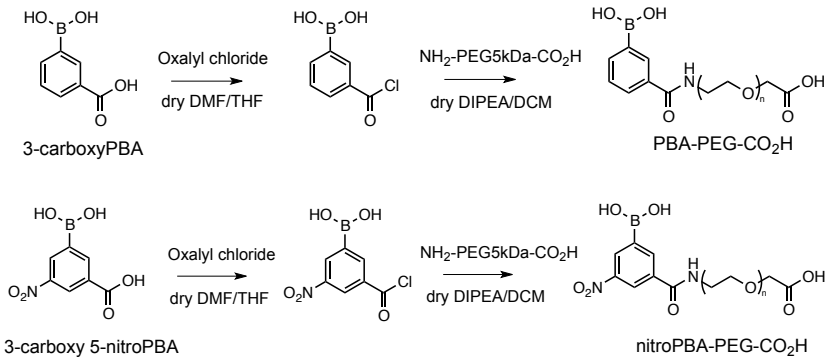

Scheme 6.4 Synthesis of PBA-PEG and nitroPBA-PEG.

pKa values of the modified PBAs were determined by absorbance changes due to conformational change of PBA from trigonal to tetrahedral form as pH increased (Table 6.2). PBA with electron withdrawing groups resulted in lower pKa's, with nitroPBA-PEG having the lowest pKa of 6.8. Thus, at physiological pH, most of the PBA was present in the reactive anionic tetrahedral form. Because of the low pKa value for nitroPBA-PEG, it was chosen to stabilize the MAD/siRNA nanoparticles.

	pKa
PBA	8.8
PBA-PEG-CO_2H	8.3
nitroPBA-PEG-CO_2H	6.8

Table 6.2 pKa values of different PBAs (phenylboronic acids).

Targeting is achieved by conjugating Herceptin to nitroPBA-PEG-CO_2H via EDC coupling (Scheme 6.5). An average of 1 to 2 PEGs were attached per Herceptin antibody.

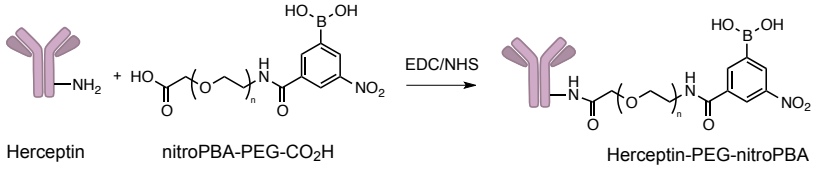

Scheme 6.5 Synthesis of Herceptin-PEG-nitroPBA.

6.4.3 *In Vitro* Characterization

Gel electrophoresis was used to evaluate the siRNA encapsulation capabilities of MAD. Free siRNA (anionic) would travel towards the cathode, while encapsulated siRNA (near neutral) would remain in the wells. Figure 6.2 shows the siRNA encapsulation abilities of MAD-2, MAD-4 and MAD-6 at various charge ratios. For MAD-2 and MAD-4, charge ratios of 1.5 (+/-) were sufficient to encapsulate all the siRNA, while for MAD-6, a higher charge ratio of 3 (+/-) was required. Therefore, we choose MAD-2 and MAD-4 to advance to further testings. It is noted that for CDP, the siRNA condensing polymer in CALAA-01, full siRNA encapsulation was observed at charge ratio of 3 (+/-) (*15*).

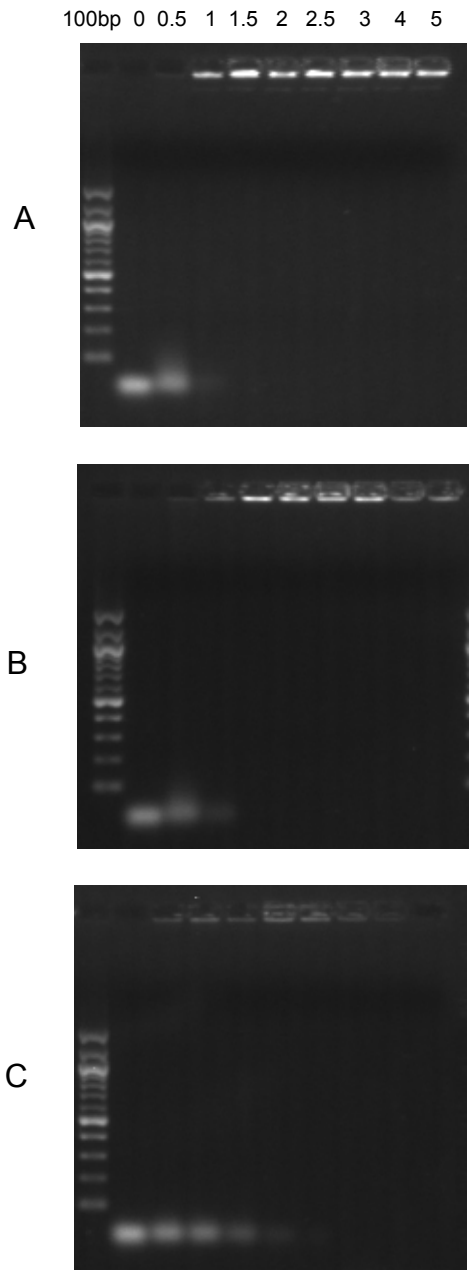

Figure 6.2 Electrophoretic gel mobility shift assay for MAD/siRNA. siRNA condensed with (A) MAD-2 (B) MAD-4 or (C) MAD-6. From left to right, 100 bp ladder, free siRNA, particles formulated at 0.5, 1, 1.5, 2, 2.5, 3, 4 and 5 (+/-) charge ratios.

To test the efficiency and toxicity of MAD for the transfection of nucleic acids into cells, pGL3, a plasmid containing the firefly luciferase gene was condensed by MAD at various charge ratios and transfected into HeLa cells, a cell line capable of translating pGL3 into the luminescent luciferase protein. Figure 6.3 illustrates the resultant luciferase protein activity and cell viability. There were greater than 2 orders of magnitude increases in luciferase activity when charge ratios of between 1.5 and 10 (+/-) were used compared to the control. This result suggests that MAD is capable of delivering nucleic acids into cells. Cell viability is good for charge ratios of up to 5 (+/-) indicating that MAD is relatively non-toxic to the cells.

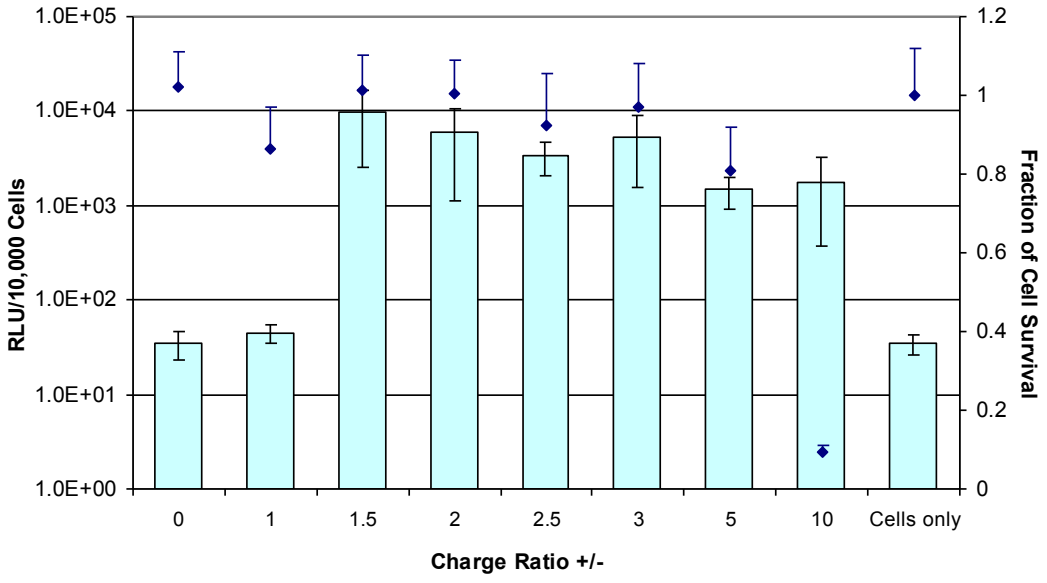

Figure 6.3 Transfection of MAD-2/pGL3 into HeLa cells at various charge ratios; relative light units (RLU) per 10,000 cells (bar), fraction of cell survival (scatter).

In order to assess the ability of MAD in delivering siRNA, cotransfection of pGL3 and siGL3 into HeLa cells was conducted to see any silencing of luciferase gene induced by siGL3. pGL3 or pGL3 and control siRNA (siCON) serve as controls for this study. Figure 6.4 indicate that the cotransfection of pGL3 and siGL3 resulted in nearly 50% reduction in luciferase signal. This suggests that pGL3 and siGL3 are co-delivered into the cell.

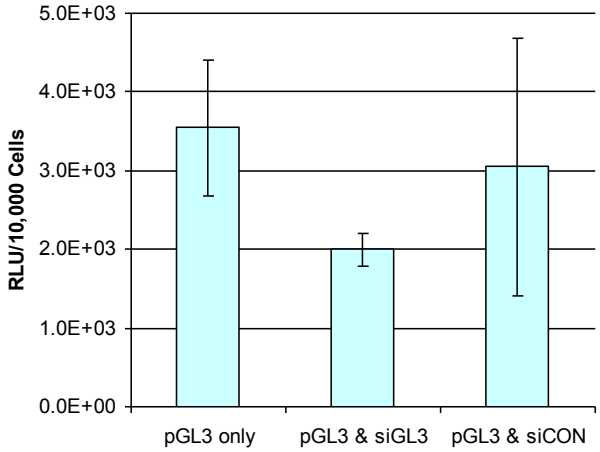

Figure 6.4 Cotransfection of pGL3 and siGL3 by MAD-2 into HeLa cells.

Another transfection method to evaluate the capability of MAD in delivering siRNA into cells is the transfection of siGL3 into HeLa-LUC cells, a cell containing the gene for luciferase protein. From Figure 6.5, it can be seen that with increasing siGL3 concentration, the luciferase activities were reduced. This suggests knockdown of luciferase gene by siGL3 and thus indicates that siGL3 has been successfully delivered internally into the cell.

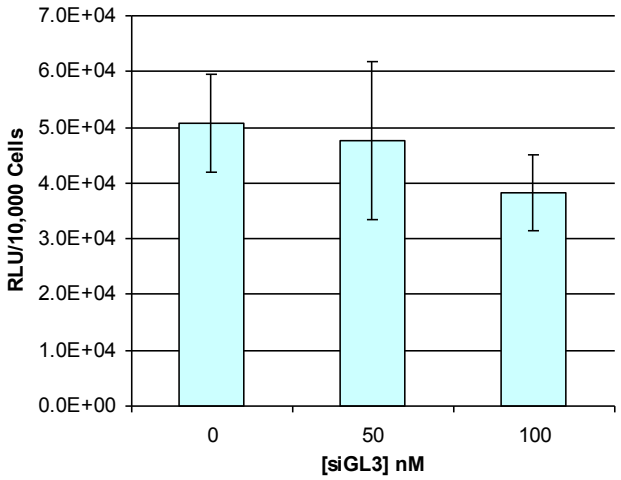

Figure 6.5 Transfection of MAD-2/siGL3 at various concentrations into HeLa-LUC cells.

Now that we have shown that MAD is capable of siRNA encapsulation at low charge ratios and demonstrate good transfection and low cellular toxicity, we proceed to add BA-PEG to form stabilized nanoparticles.

The effect of PBA-PEG and nitroPBA-PEG on nanoparticle formation and stability were examined. The use of PBA-PEG formed MAD/siRNA particles of 150-300 nm in size. MAD-4 resulted in smaller nanoparticles than when MAD-2 was used. However, upon the addition of salt, all particles aggregated indicating that PBA-PEG was incapable of providing sufficient stability to the nanoparticles. When nitroPBA-PEG was used, particles at all charge ratios tested, 1 and 3 (+/-), demonstrated stabilized nanoparticles in salt conditions. The difference in particle stability conferred by PBA-

PEG and nitroPBA-PEG indicates the importance of the modification of boronic acid to possess stronger binding to polyols.

For siRNA condensed with MAD-4 without the presence of stabilizing agent PEG, a particle size of 640 nm was observed with a high zeta potential of ca. 32 mV (Figure 6.6). When nitroPBA-PEG was added to stabilize the particle, the diameter reduced to ca. 130 nm with a negative surface charge of ca. -4 mV. This negative charge is a result of the binding between boronic acid and diols. When 0.25 mol% Herceptin conjugated nitroPBA-PEG was introduced, interestingly, the particle size reduced further to 82 nm while the zeta potential remained similar.

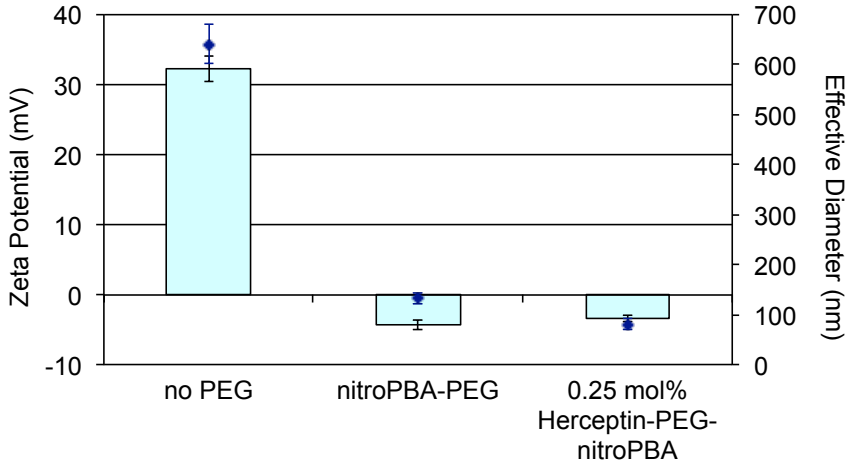

Figure 6.6 Zeta potential and effective hydrodynamic diameter of MAD-4/siRNA nanoparticles stabilized by different PEG chains. Formulated at charge ratio of 3 (+/-), zeta potential (bar), effective diameter (scatter).

Figure 6.7 provides the salt stability data for MAD-4/siRNA nanoparticles with various PEG groups attached. Without the presence of stabilizing agent PEG, the particles aggregated. When nitroPBA-PEG was present, particles remained stable in salt conditions.

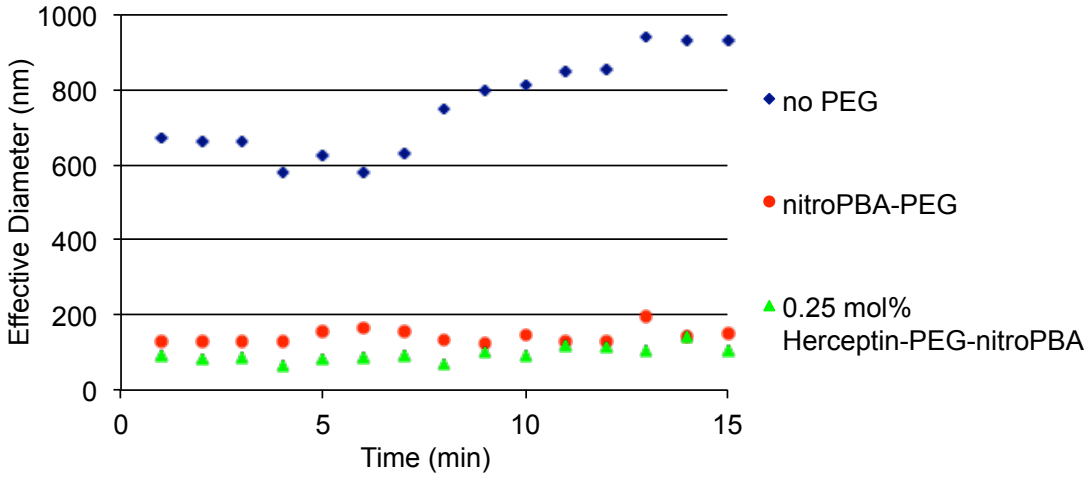

Figure 6.7 Salt stability of MAD-4/siRNA nanoparticles stabilized with no PEG, nitroPBA-PEG and 0.25 mol% Herceptin-PEG-nitroPBA. Formulated at charge ratio 3 (+/-), 10x PBS was added at time 5 min such that the resulting solution was in 1x PBS.

6.4.4 *In Vivo* Characterization

Based on the promising *in vitro* results, the best nanoparticle formulation composed of siRNA condensed by MAD-4 and stabilized with nitroPBA-PEG at charge ratio of 3 (+/-) proceeded to animal pharmacokinetic evaluation. BALB/c mice were injected with particle formulations containing 20% siCy3 (fluorescently labeled siRNA) via tail vein injection and blood was collected from saphenous vein at various time points.

Figure 6.8 shows the pharmacokinetic data for MAD-4/siRNA nanoparticles stabilized with nitroPBA-PEG. It can be seen that at 2 min post injection, there was significantly more siCy3 remaining for MAD-4/siRNA nanoparticles than that for CDP/siRNA nanoparticles (CALAA-01). However, by 7 min both groups show similar fast *in vivo* clearance.

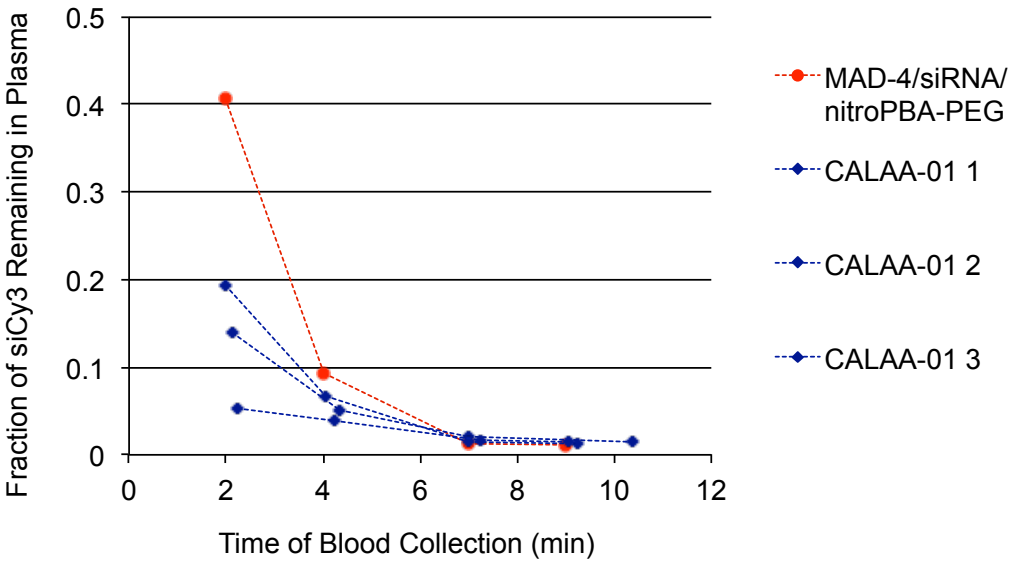

Figure 6.8 Pharmacokinetics of MAD-4/siRNA nanoparticles stabilized with nitroPBA-PEG in BALB/c mice, compared with that of CALAA-01 (CDP/siRNA nanoparticles stabilized with AD-PEG). Formulated with 20% siCy3, charge ratio 3 (+/-), 5 mg siRNA/kg mouse injection, dashed lines join data for each individual mouse.

6.5 Conclusions

An example for the use of boronic acid-diol complexation in the targeted delivery of siRNA via nanoscaled vehicles was presented. A copolymer of mucic acid and dimethylsuberimidate (DMS), named MAD, was synthesized and used to condense the anionic siRNA into nanoparticles. The condensed nanoparticles were stabilized by placing a PEG layer onto the particle surface using boronic acid-diol complexation where boronic acid PEG (BA-PEG) form reversible covalent bonding with vicinal diol groups on the MAD backbone. Targeting was achieved by conjugating the distal end of the BA-PEG with a targeting agent, in this case, a Herceptin antibody. MAD/siRNA nanoparticles were found to effectively enter cells by transfection studies and show low cellular toxicity. It was found by gel electrophoresis studies that charge ratios of 1.5 (+/-) for MAD-2 and MAD-4 were sufficient to encapsulate all siRNA. MAD/siRNA nanoparticles stabilized with nitroPBA-PEG were formulated with a diameter of ca. 130 nm and a surface charge of ca. -4 mV. Pharmacokinetic studies in mice demonstrate improved circulation compared to CALAA-01.

6.6 References

(1) Davis, M. E., Zuckerman, J. E., Choi, C. H. J., Seligson, D., Tolcher, A., Alabi, C. A., Yen, Y., Heidel, J. D., and Ribas, A. (2010) Evidence of RNAi in humans from systemically administered siRNA via targeted nanoparticles. *Nature 464*, 1067-1071.

(2) Davis, M. E. (2009) The First Targeted Delivery of siRNA in Humans via a Self-Assembling, Cyclodextrin Polymer-Based Nanoparticle: From Concept to Clinic. *Molecular Pharmaceutics 6*, 659-668.

(3) Bartlett, D. W., Su, H., Hildebrandt, I. J., Weber, W. A., and Davis, M. E. (2007) Impact of tumor-specific targeting on the biodistribution and efficacy of siRNA nanoparticles measured by multimodality in vivo imaging. *Proceedings of the National Academy of Sciences of the United States of America 104*, 15549-15554.

(4) Heidel, J. D., Yu, Z. P., Liu, J. Y. C., Rele, S. M., Liang, Y. C., Zeidan, R. K., Kornbrust, D. J., and Davis, M. E. (2007) Administration in non-human primates of escalating intravenous doses of targeted nanoparticles containing ribonucleotide reductase subunit M2 siRNA. *Proceedings of the National Academy of Sciences of the United States of America 104*, 5715-5721.

(5) Malek, A., Merkel, O., Fink, L., Czubayko, F., Kissel, T., and Aigner, A. (2009) In vivo pharmacokinetics, tissue distribution and underlying mechanisms of

various PEI(-PEG)/siRNA complexes. *Toxicology and applied pharmacology 236*, 97-108.

(6) Merkel, O. M., Librizzi, D., Pfestroff, A., Schurrat, T., Buyens, K., Sanders, N. N., De Smedt, S. C., Behe, M., and Kissel, T. (2009) Stability of siRNA polyplexes from poly(ethylenimine) and poly(ethylenimine)-g-poly(ethylene glycol) under in vivo conditions: Effects on pharmacokinetics and biodistribution measured by Fluorescence Fluctuation Spectroscopy and Single Photon Emission Computed Tomography (SPECT) imaging. *Journal of Controlled Release 138*, 148-159.

(7) Reineke, T. M., and Davis, M. E. (2003) Structural effects of carbohydrate-containing polycations on gene delivery. 1. Carbohydrate size and its distance from charge centers. *Bioconjugate Chemistry 14*, 247-254.

(8) Xiao, K., Li, Y., Luo, J., Lee, J. S., Xiao, W., Gonik, A. M., Agarwal, R. G., and Lam, K. S. (2011) The effect of surface charge on in vivo biodistribution of PEG-oligocholic acid based micellar nanoparticles. *Biomaterials 32*, 3435-3446.

(9) Altieri, S., Bortolussi, S., Bruschi, P., Chiari, P., Fossati, F., Stella, S., Prati, U., Roveda, L., Zonta, A., Zonta, C., Ferrari, C., Clerici, A., Nano, R., and Pinelli, T. (2008) Neutron autoradiography imaging of selective boron uptake in human metastatic tumours. *Appl Radiat Isotopes 66*, 1850-1855.

(10) Mikado, S., Yanagie, H., Yasuda, N., Higashi, S., Ikushima, I., Mizumachi, R., Murata, Y., Morishita, Y., Nishimura, R., Shinohara, A., Ogura, K., Sugiyama, H.,

Iikura, H., Ando, H., Ishimoto, M., Takamoto, S., Eriguchi, M., Takahashi, H., and Kimura, M. (2009) Application of neutron capture autoradiography to Boron Delivery seeking techniques for selective accumulation of boron compounds to tumor with intra-arterial administration of boron entrapped water-in-oil-in-water emulsion. *Nucl Instrum Meth A 605*, 171-174.

(11) Ogura, K., Yanagie, H., Eriguchi, M., Lehmann, E. H., Kuhne, G., Bayon, G., and Kobayashi, H. (2004) Neutron capture autoradio graphic study of the biodistribution of B-10 in tumor-bearing mice. *Appl Radiat Isotopes 61*, 585-590.

(12) Smith, D. R., Chandra, S., Barth, R. F., Yang, W. L., Joel, D. D., and Coderre, J. A. (2001) Quantitative imaging and microlocalization of boron-10 in brain tumors and infiltrating tumor cells by SIMS ion microscopy: Relevance to neutron capture therapy. *Cancer Research 61*, 8179-8187.

(13) Wittig, A., Michel, J., Moss, R. L., Stecher-Rasmussen, F., Arlinghaus, H. F., Bendel, P., Mauri, P. L., Altieri, S., Hilger, R., Salvadori, P. A., Menichetti, L., Zamenhof, R., and Sauerwein, W. A. G. (2008) Boron analysis and boron imaging in biological materials for Boron Neutron Capture Therapy (BNCT). *Crit Rev Oncol Hemat 68*, 66-90.

(14) Coderre, J. A., and Morris, G. M. (1999) The radiation biology of boron neutron capture therapy. *Radiat Res 151*, 1-18.

(15) Bartlett, D. W., and Davis, M. E. (2007) Physicochemical and biological characterization of targeted, nucleic acid-containing nanoparticles. *Bioconjugate chemistry 18*, 456-468.

Chapter VII

Future Directions and Recommendations

In the previous chapters, it has been shown that boronic acid-diol complexation can be used in the targeted delivery of both camptothecin (CPT) and siRNA. Thus the purpose of this thesis has been fulfilled. Yet, as with all scientific endeavors, the more we learn about a system, the more question arises. In the following, I will provide some future directions and recommendations for the targeted, polymeric delivery of CPT and siRNA via boronic acid-diol complexation.

First, this delivery platform utilizes boronic acid-diol complexation for targeting (MAP-CPT and MAD/siRNA) and stabilization purposes (MAD/siRNA) by tethering PEG modified at the distal end with a boronic acid and complexing this with diol-containing groups on the surface of the nanoparticles. However, there are sugars, including glucose present *in vivo* that could compete for binding with boronic acids. This could potentially lead to PEG chains falling off of the particle and thus reduce the targeting capability and/or stability of the nanoparticles. It is proposed that studies in quantifying the amount of boronic acid that remains on the surface of the nanoparticles as a function of time as they circulate *in vivo* be conducted. If boronic acids are found to be falling off of the particles and are binding to unspecific sugar groups, effects of this behavior on the delivery system and in the host should be investigated.

To increase the binding constant of boronic acid to diols, a series of phenylboronic acids (PBA) with electron withdrawing groups on the phenyl ring has been synthesized. This effectively increased the binding constant between MAP and PBA by over 70 times. Another way of increasing the binding constant is by introducing multivalent interactions. Nanoparticles possessing multiple targeting agents on its surface and can multivalently bind to receptors have been shown to have significantly lower

dissociation constants, K_D (*1, 2*). In Chapter V, we examined the effect of multivalency in the PEG stabilization of CDP/siRNA nanoparticles. It was found that CDP/siRNA nanoparticles stabilized with multivalently attached PEG, AD_2-PEG or AD_3-PEG, demonstrated enhanced stability in both *in vitro* and *in vivo* conditions. Therefore, another method of increasing the binding constant between boronic acids and diols is to multivalently attach boronic acid groups, for instance, $(PBA)_2$-PEG onto the surface of the nanoparticles. This would result in potentially less off targeting affect due to PEG falling off of the nanoparticle in the MAP-CPT and MAD/siRNA systems; and increasing the nanoparticle stability in the MAD/siRNA system.

The design of our delivery platform is modular such that in theory any targeting agent can be placed on the surface of the nanoparticles. Those include whole antibodies other than Herceptin, antibody fragments such as $F(ab')_2$ and Sc-Fv, proteins including human transferrin, and peptides. MAP can be conjugated to other small molecule hydrophobic drugs. As well, sugars other than mucic acid can be used in the synthesis of the hydrophilic polymer for small hydrophobic drug delivery and in the synthesis of cationic siRNA condensing polymer.

7.1 References

(1) Hong, S., Leroueil, P. R., Majoros, I. J., Orr, B. G., Baker, J. R., and Holl, M. M. B. (2007) The binding avidity of a nanoparticle-based multivalent targeted drug delivery platform. *Chem Biol 14*, 107-115.

(2) Choi, C. H. J., Alabi, C. A., Webster, P., and Davis, M. E. (2010) Mechanism of active targeting in solid tumors with transferrin-containing gold nanoparticles. *Proceedings of the National Academy of Sciences of the United States of America 107*, 1235-1240.